TABLE OF CONTENTS

NASA Contractor Report 3210

Two Dimensional Aerodynamic Interference Effects on Oscillating Airfoils With Flaps in Ventilated Subsonic Wind Tunnels

Joseph Fromme, Michael Golberg, and John Werth

GRANT NSG-2140
DECEMBER 1979

NASA

NASA Contractor Report 3210

Two Dimensional Aerodynamic Interference Effects on Oscillating Airfoils With Flaps in Ventilated Subsonic Wind Tunnels

Joseph Fromme, Michael Golberg,
and John Werth
University of Nevada
Las Vegas, Nevada

Prepared for
Ames Research Center
under Grant NSG-2140

National Aeronautics
and Space Administration

Scientific and Technical
Information Branch

1979

SUMMARY

The numerical computation of unsteady airloads acting upon thin airfoils with multiple leading and trailing edge controls in two dimensional ventilated subsonic wind tunnels is studied. The foundation of the computational method is strengthened with a new and more powerful mathematical existence and convergence theory for solving Cauchy singular integral equations of the first kind, and the method of convergence acceleration by extrapolation to the limit is introduced to analyze airfoils with flaps. New results are presented for steady and unsteady flow, including the effect of acoustic resonance between ventilated wind tunnel walls and airfoils with oscillating flaps.

TABLE OF CONTENTS

LIST OF FIGURES

LIST OF TABLES

LIST OF SYMBOLS

This section provides a partial list of frequently occurring symbols and their names. Places of first occurrence or definition are given by section number denoted with §, by equation number enclosed in parentheses, etc. In a few instances the same symbol is used for different meanings but it will be clear from the context which is correct. Any consistent system of physical units may be employed, although most quantities are nondimensional.

Symbol	Name	Place
$[A_{mn}]$, $[\hat{A}_{mn}]$	Aerodynamic work matrices.	§7
a	Point of discontinuity.	(5.26)
a_{mN}	N point collocation coefficients.	§6
a_k, $\hat{a}_k$, δa_k	Collocation coefficients, their numerically computed values, and their error.	§10
$\underline{a}$, $\hat{\underline{a}}$, δa	Vectors of a_k, $\hat{a}_k$ and δa_k.	§10
b	Airfoil semichord.	§2
C	Complex constant.	§10
Ci	Cosine integral.	(12.8)
$\mathbb{C}$, $\mathbb{C}^N$	Set of complex numbers, and Nth Cartesian product.	§10
$[C^N_{mn}]$, C^N	N point collocation matrix.	§§6, 10
C_L, C_M	Lift and pitching moment coefficients.	§7
C_{L_m}, C_{M_m}, $\hat{C}_{L_m}$, $\hat{C}_{M_m}$	Lift and pitching moment coefficients due to displacements h_n and $\hat{h}_n$.	§7
c_∞	Ambient speed of sound.	§2
$\bar{c}$	Mean aerodynamic chord.	(7.2)
$[D^\alpha_{mn}]$, $[D^\gamma_{mn}]$	Differentiating matrices.	(5.40)
$d\eta$, $d\beta$	Stieltjes measures.	Theorem 10.1
E_N	Quadrature error.	§5
e	Element index. Also 2.71828...	§8
F	Interference function.	(4.17)
F_1, F_2	Functions in kernel.	(12.2)

Symbol	Name	Place
F_{nk}	Integrand.	(5.27)ff.
$(f,\hat{f})$	Fourier transform pairs.	(3.2)
G_o, G_1	Analytic functions.	(12.19)
$[G^{\alpha}_{mn}]$, $[G^{\gamma}_{mn}]$	Transformation matrices.	(5.35)
H_1, H_2	Arbitrary Hilbert spaces	§5
H, H^{-1}, H^*	Akheizer-Bland transform, its inverse and adjoint.	§5
$[H_{mn}]$, $[\hat{H}_{mn}]$	Transformation matrices between deflection bases.	(7.22)
$\{h_n\}$, $\{\hat{h}_n\}$	Displacement bases.	§7
h_{mn}, $h_{mn}(e)$	Displacement nodal values, and element displacement nodal values.	§8
h	Airfoil profile or displacement function.	Figure 1
I1, I2, I3	TWODI solution parameters.	§9.4
i	Imaginary unit. Also integer index.	§2
J_n	Bessel function of the first kind.	§12
K, ΔK	Kernel and interference kernel. The integral operator corresponding to K is denoted by T.	§§3, 4
$\tilde{K}$	Non unitary part of K. The integral operator corresponding to $\tilde{K}$ is denoted by K.	§10.1
K_1, K_2	Non unitary parts of T.	§10.1
K_L, K_c	Logarithmic and continuous parts of the kernel K, and the integral operator T.	(6.10), §10
K_N	Downwash collocation operators.	(10.4)
k	Reduced frequency based on semichord.	§2
k_n	The nth resonant reduced frequency.	(14.1)
L	Lift.	(7.2)
L^2_α, L^2_γ, L^2_h	Hilbert spaces for downwash, pressure and displacement.	§§5, 7
L_N	N point collocation operator.	(10.3)
ℓ_k	Lagrange interpolation polynomial.	(10.3)
ℓ	Length.	(2.9_2)
M	Free stream Mach number, pitching moment.	§2, (7.2)

Symbol	Name	Place
N_e	Number of chordwise elements.	§8.2
N_h	Number of displacement modes.	§8.1
N_x	Number of displacement nodes.	§8.1
N_δ	Number of hinges.	§8.1
p	Aerodynamic pressure.	(2.3)
Δp, Δp_n	Pressure jump, pressure jump due to h_n.	(2.5_2), §7.2
Q_N	Quadrature operator. Also operator of orthogonal projection.	§10.1, §11.2
q_n, $\dot{q}_n$	Generalized coordinates.	§7
R_1, R_2	TWODI solution parameters.	§9.4
r_N	Residual downwash.	(6.5)
S, S'	Function defined by infinite series, and its derivative.	(3.11_1)
s_n	Coefficient in S.	(3.11_2)
s	Fourier transform variable.	(3.2)
T	Integral operator of generalized airfoil integral equation.	(6.1)
t	Time.	§2
u	Variable of integration.	(12.6)
V1,...,VN	Real or integer numbers.	§9.4
v_n	Normal component of velocity	(2.9_2)
v_p	Porosity resistence velocity	(2.10_1)
v_∞	Free stream velocity	§2
W_i^N	Quadrature weights.	§5
$[W_{mn}]$	Downwash transformation matrix.	(7.40)
w, w_n	Downwash, downwash due to h_n.	§§2, 7
w_R	Residual downwash.	(11.2)
w_s, w_c	Singular and continuous parts of downwash	(11.19)

Symbol	Name	Place
x	Streamwise coordinate.	Figure 1
x_{CP}	Center of pressure as a fraction of chord, measured from leading edge.	(7.5)
x_m	Collocation points.	(6.6)
x_i^N	The ith zero of α_N. Also collocation points.	(5.6_1), (6.12)
Y_n	Bessel function of the second kind.	(12.14)
z_n^j	The jth order extrapolate from α_n.	(11.50)
z	Vertical coordinate.	Figure 1
α	Limit of $\{\alpha_n\}_1^\infty$. Also angle of attack. Also extrapolation coefficient.	§11.5, Table 12, (11.54)
$\{\alpha_n\}$	Downwash (α-angle of attack) basis functions.	(5.4)
β	Co Mach number, $\beta = \sqrt{1-M^2}$. Also extrapolation coefficient.	(3.3_1), (11.54)
β_k	Integral.	Theorem 10.1
γ	Ventilation parameter. Also extrapolation coefficient.	(3.11_5), (11.54)
$\{\gamma_n\}$	Pressure (γ-vorticity) basis functions.	(5.4_2)
δ	Flap rotation angle.	Table 7
δ_{mn}	Kronecker delta.	(5.7)
$\delta\phi_n$	Difference between mathematically exact and computational values of ϕ_n.	§10.2
ϵ	Real number. Also set containment symbol.	§§4, 5
ϵ_n	Error.	§11.5
ζ	Leakage angle for porous wall tunnel.	(4.7)
ζ_n	Frequency ratio.	(3.11_3)
η	Tunnel height to airfoil chord ratio.	Figure 1
θ, θ_a, θ_η	Angular variables.	(5.26)ff., §13
λ_n	Eigenvalues. Also quadrature weights.	(3.11), §10
μ	Mass effect (slotted wall) ventilation coefficient.	(2.9_3)
ν	Viscous effect (porous wall) ventilation coefficient.	(2.10_2)
ξ	Streamwise coordinate.	§3
ξ_i^N	The ith zero of Y_N. Also quadrature points.	(5.6_2), (6.12)

Symbol	Name	Place
τ_N	Operator of orthogonal projection.	(11.30)
ρ_∞	Free stream fluid density.	§2
σ	Fourier transform parameter. Also constant in convergence analysis.	(3.4_2), (10.19)
σ_n	Asymptotic coefficients.	(11.46)
τ	Similarity parameter. Also convergence and error analysis parameter.	(4.18), §10.2
τ_N	Convergence and error analysis parameter.	Lemma 10.1
ϕ	Perturbation velocity potential	(2.2)
ψ	Pressure factor.	(3.15)
ψ_o	Approximation to ϕ.	(11.2)
ψ_N, ψ_N^C	Collocation approximation to ψ.	(10.5), (11.27)
$\hat{\psi}_N$	Computed value of ψ_N.	(10.13)
$\tilde{\psi}_N$	Approximation to ϕ.	(11.11)
ψ_N^G	Galerkin approximation to ϕ.	(11.27)
ψ_N^R	Approximation to ϕ_R.	(11.5)
ψ_N^s	Picard iterate of ψ_N^G.	(11.31)
ψ_R	Residual pressure factor.	(11.3)
Ω	Domain of wind tunnel problem.	(3.1)
Ω_e	Element domain along chord.	(8.6)
ω	Frequency, rad/s.	Figure 1
$\|.\|$	Operator norm.	(5.16)
$\|.\|_2^Q$	Quadrature norm.	(10.20)
$\|.\|_i$	Vector norms; i=1, 2, α, β.	§5
$<.,.>_i$	Inner products; i=1, 2, α, β.	§5
$<x>$	Jump function.	(5.25)

§1. Introduction[1]

The theory of aerodynamic interference is necessary to extrapolate wind tunnel test data to free flight conditions. Analytically the wind tunnel problem is more difficult than the free air problem because of the presence of the wind tunnel walls, although computationally it may be checked against known free air results. However, the physical validity of wind tunnel interference theories must be established by the more stringent comparison with experimental data for both the free air and wind tunnel conditions.

Physically the nature of wind tunnel flow is highly complex so that considerable simplification of the theory is necessary in order to produce useful results. Most existing wind tunnel theories, see e.g., [1], [2], [3], [4][2], are based on far field effects under the assumption of inviscid linear potential flow. Clearly viscosity plays a major role in boundary layer and wall effects, as do nonlinearities in transonic flow. Although significant progress has been made in the general field of computational fluid mechanics in the past decade, the inclusion of viscosity and nonlinearities entails an order of magnitude more computational expense than the linear inviscid theories.

In shock free flow over moderately thin airfoils, good correlation with experiment can be obtained using linear potential flow theory, and there remain open significant research problems of practical importance. Among these are the proper form or forms of the boundary condition at ventilated tunnel walls, the efficient computation of unsteady airloads especially when flaps are present, and effects of acoustic resonance between oscillating airfoils and ventilated wind tunnel walls.

In this report we discuss the problem of predicting unsteady airloads on thin airfoils in two dimensional subsonic flow through ventilated wind tunnels. Our previous work [5], [6] is extended to include the problem of multiple leading and trailing edge controls, and to permit porous wind tunnel walls in steady flow. This work is based on the method of orthogonal polynomial pairs discovered originally by N.I. Akheizer [7] in the Soviet Union in 1945 and developed independently but later by S.R. Bland and his coworkers for the practical solution of airfoil problems [8], [9],

---

[1]The authors wish to acknowledge the valuable help of Dr. Sanford Davis, Ms. Thelma Grinnell and Messrs. Charles Doughty, Paul Kriner and Steven Sedlacek.

[2]Numbers in square brackets refer to the bibliography found in the REFERENCES in order of first citation, and may also give the page, section or chapter of interest.

[10]. In section 2 below we set down the underlying partial differential equations and boundary conditions. Section 3 describes Bland's kernel of the integral equation relating downwash to pressure for unsteady flow in slotted wall tunnels and section 4 describes the kernel for porous wall tunnels in steady flow. Sections 5 and 6 review the theory of airfoil polynomials and Bland's collocation method. Although this is slightly repetitious of earlier work, we have simplified the notation somewhat and unified certain other concepts. Sections 7 and 8 discuss the calculation of airloads and the method of representation of airfoil profiles possessing multiple leading and trailing edge controls. Section 9 and the APPENDIX present instructions for the use of the computer program TWODI and a sample interactive input/output scenario. Sections 10 and 11 present a comprehensive analysis of convergence of collocation and other computational methods and of the method of extrapolation used to accelerate numerical convergence in the case of flaps. Section 12 shows how computational efficiency can be further improved by identifying the singularities in the kernel and integrating them separately. Sections 13, 14 and the APPENDIX present numerical results for steady flow in porous wall tunnels and for steady and unsteady flow over airfoils with flaps in ventilated tunnels for frequency ranges which include resonance between the oscillating airfoil and the wind tunnel walls. In section 15, we offer our conclusions based on the present study and recommendations for future research.

§2. Basic equations

Consider a thin nearly planar airfoil undergoing simple harmonic motion at frequency ω rad/sec about the center plane of a two dimensional ventilated wind tunnel (Figure 1). The flow is considered to be inviscid and strictly subsonic, and to be a small disturbance from the free stream flow.

We point out that free air conditions are included as an important special case upon taking the walls to be infinitely far apart ($\eta \to \infty$).

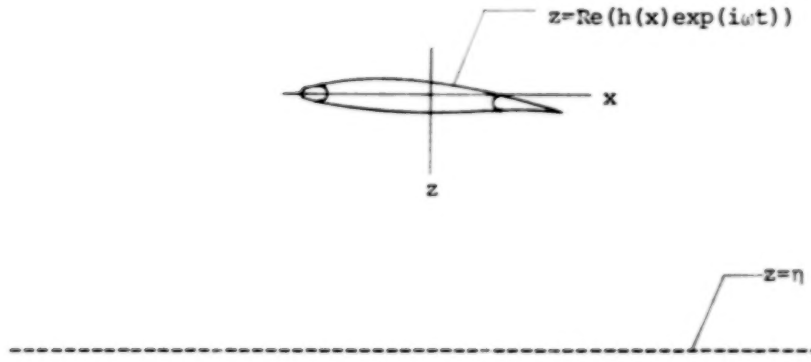

Figure 1. Coordinate system and sign conventions

In this study we are particularly interested in unsteady interference effects on airfoils with flaps but, in general, we may allow the deflection amplitude function h to represent upper, lower or mean airfoil profiles as well as arbitrary aeroelastic shapes, including rigid body and control surface deflections.

Deflection is measured positive downward so that positive streamwise derivatives correspond to positive angles of attack. Lift will be measured positive upward, and pitching moment will be measured about the quarter chord, positive in the direction of increasing angle of attack (nose up).

Except where specifically stated to the contrary, all quantities are dimensionless. Lengths are nondimensionalized by the airfoil semichord b, pressures by the free stream dynamic pressure $\frac{1}{2}\rho_\infty v_\infty^2$ and, with the notable exception of Mach number, velocities are nondimensionalized by the free stream velocity v_∞. Following customary practice, streamwise coordinates are measured positive downstream, having value -1 at the leading edge and +1 at the trailing edge.

Denote by w the downwash amplitude nondimensionalized by the free stream velocity,

$$w(x) = (\frac{d}{dx} + ik)h(x), \tag{2.1}$$

where $k=\omega b/v_\infty$ is the reduced frequency based on semichord. Denote by ϕ the perturbation velocity potential nondimensionalized by bv_∞ and denote by p the perturbation pressure nondimensionalized by $\frac{1}{2}\rho_\infty v_\infty^2$. Then the perturbation velocity potential satisfies the unsteady wave equation

$$\nabla^2\phi - M^2(\frac{\partial}{\partial x} + ik)^2\phi = 0 \tag{2.2}$$

where $M=v_\infty/c_\infty$ is the free stream Mach number (for simplicity we omit the subscript on M). The pressure is related to the velocity potential by

$$p = -2(\frac{\partial}{\partial x} + ik)\ \phi. \tag{2.3}$$

When the boundary conditions at the upper and lower walls are the same, both the pressure and velocity potential can be shown to be antisymmetric functions of z; i.e.,

$$p(x,-z) = -p(x,z),\ \phi(x,-z) = -\phi(x,z). \tag{2.4}$$

Since the pressure is assumed to be continuous everywhere in the flow field except across the airfoil where it is permitted to be discontinuous (vortex surface) and since the pressure is assumed to be continuous at the trailing edge (Kutta condition), we may write

$$p(x,0) = 0, \qquad |x|>1, \tag{2.5$_1$}$$

$$p(x,0) = -\frac{1}{2}\Delta p(x), \quad |x|<1, \tag{2.5$_2$}$$

$$p(x,0) = 0, \qquad x = 1, \tag{2.5$_3$}$$

where Δp is the lifting pressure jump across the airfoil.

At the surface of the airfoil, the flow must be tangent to the surface. Thus,

$$\frac{\partial \phi}{\partial z}\Big|_{z=0} = w(x), \qquad |x|<1. \tag{2.6}$$

The purely kinematical boundary condition (2.6) is exactly equivalent to the assertion that zero mass can flow through the surface of the airfoil. The corresponding statement for a <u>closed wall</u> wind tunnel is

$$\frac{\partial \phi}{\partial z}\Big|_{z=\pm\eta} = 0, \qquad |x|<\infty, \tag{2.7$_1$}$$

which in view of (2.3), is equivalent to

$$\frac{\partial p}{\partial z}\Big|_{z=\pm\eta} = 0, \qquad |x|<\infty. \tag{2.7$_2$}$$

An <u>open jet</u> boundary is derined mathematically as one on which the perturbation pressure is zero (see, e.g., [1, p.47] or [2, p.41]),

$$p\big|_{z=\pm\eta} = 0, \qquad |x|<\infty. \tag{2.8$_1$}$$

An alternate formulation which is equivalent to (2.8$_1$),

$$\phi\big|_{z=\pm\eta} = 0, \qquad |x|<\infty, \tag{2.8$_3$}$$

is obtained by integrating (2.3).

We point out that an open jet boundary differs from free air because in the latter case the pressure perturbation due to the presence of a model will vanish in general only at infinity.

It has been known since the time of Prandtl [11] (see also Glauert [4, p.43], Garner et al [1, p.5] and Kraft [12,p.1]) that the closed wall and open jet boundary conditions (2.7) and (2.8) cause opposite interference effects in the sense that closed walls produce more lift than free air and open jets produce less. The desire to exploit these opposing effects to enable an interference free tunnel and to avoid the problem of choking has led to the construction of ventilated wind tunnels at various facilities.

The physical flow at a ventilated wind tunnel is quite complex and depends, among other things, upon viscous and boundary layer phenomena as well as the detail construction of the walls themselves. However, at some distance away from the wall, the localized effects of individual slots or holes by which the tunnel is ventilated will blend into a more homogeneous effect, thereby permitting the introduction of homogeneous boundary conditions.

Two types of homogeneous boundary conditions have been proposed, the so-called slotted wall boundary condition and the porous wall boundary condition. The slotted wall boundary is physically based on an accelerative or mass effect whereas the porous wall boundary condition is based on a viscous effect. However, this simple distinction seems not to be generally made. Therefore, to emphasize the underlying principles of mechanics involved, we shall adopt in the sequel the more descriptive terms mass effect and viscous effect.

The mass effect boundary condition may be developed heuristically as follows. Recall that Euler's vector equation for conservation of linear momentum in a perfect fluid is

$$\text{(physical dimensions)} \qquad -\underline{\nabla} p = \rho \underline{a}. \tag{2.9$_1$}$$

If one applies this law across a ventilated wind tunnel wall over a distance ℓ such that local effects at the wall may be neglected, there results

$$\text{(physical dimensions)} \qquad \frac{p_{\text{tunnel}} - p_{\text{plenum}}}{\ell} = \rho \frac{dv_n}{dt}, \tag{2.9$_2$}$$

where the pressure gradient has been approximated by a finite difference quotient and where v_n is the average velocity component normal to the wall. Neglecting the difference between the plenum chamber pressure and the free stream atmospheric pressure (this assumption can be removed [13]), and nondimensionalizing all quantities

gives

$$p \pm \mu \frac{\partial p}{\partial z} = 0, \qquad z = \pm\eta, \tag{2.9$_3$}$$

where

$$\mu = \ell/b.$$

Regarding the length ratio μ as an empirically determined quantity in order to account for only part of the wall being closed, we may call μ the mass effect ventilation coefficient and we call (2.9$_3$) the mass effect boundary condition. An alternate form of (2.9$_3$) that is often used, especially in steady flow, is

$$\phi \pm \mu \frac{\partial \phi}{\partial z} = 0, \qquad z = \pm\eta. \tag{2.9$_4$}$$

The mass effect boundary condition (2.9$_3$) was apparently first proposed by Davis and Moore [14] in 1953. Although their basic analysis does not seem to preclude application to other forms of wall ventilation, they were primarily interested in slotted wall tunnels and called (2.9$_3$) the slotted wall boundary condition.

Formulas for estimating the mass effect ventilation coefficient μ for slotted wall tunnels in terms of the slot geometry are given by Davis and Moore [14], Guderley [15], Baldwin, Turner and Knechtel [16], Chen and Mears [17] (see [13]), Goethert [2], Garner et al [1], Pindzola and Lo [18], Barnwell [13] and others.

Recently, Barnwell [19] has concluded that better agreement with experiment using the boundary condition (2.9) is obtained if μ is determined by correlation with experiment rather than if it is calculated using existing theories based on slot geometry, etc.

The viscous effect boundary condition is based on the assumption that the wall is porous in the sense that the mass flow rate through the wall is proportional to the difference in pressure between the inside of the wind tunnel and the plenum chamber; i.e.,

(physical dimensions) $$p_{tunnel} - p_{plenum} = \rho v_p v_n, \tag{2.10$_1$}$$

where v_p is a physical constant having dimensions of velocity and which depends upon

the porosity of the wall and the properties of the fluid in the wind tunnel (usually air).

If v_p is nondimensionalized by the free stream velocity according to

$$\nu = \frac{v_p}{v_\infty} = \frac{p_{tunnel} - p_{plenum}}{\rho v_n v_\infty}, \qquad (2.10_2)$$

and if the difference between the plenum chamber pressure and the free stream atmospheric pressure is again neglected, then it can be shown that the viscous effect boundary condition in the form

$$p = \pm 2\nu \frac{\partial \phi}{\partial z}, \qquad z = \pm\eta \qquad (2.10_3)$$

follows. The dimensionless quantity ν is called the viscous effect ventilation coefficient. A convenient alternate form of (2.10_3) is

$$\left(\frac{\partial}{\partial x} + ik\right)p \pm \nu \frac{\partial p}{\partial z} = 0, \quad z = \pm\eta. \qquad (2.10_4)$$

The boundary condition described by (2.10) clearly represents a viscous mechanism in the sense that force in the form of pressure is proportional to velocity. Sometimes this is loosely referred to as Darcy's law [20] à la soil mechanics but that does not seem to be an appropriate attribution in the present context. Such a viscous effect boundary condition for wind tunnels was proposed apparently first by Goodman [21] in 1950 for steady flow. Further investigations along this line have been made by Baldwin, Turner and Knechtel [16], Woods [22] and [23], Drake [24] and [25], Parkinson and Lim [26], Ebihara [27], Mokry [28], Kraft and Lo [29] and others. Woods and Drake considered walls with finite length porous sections and Drake considered unsteady flow but gave no numerical results for subsonic flow.

In connection with Barnwell's conclusions cited above concerning the difficulty of obtaining good agreement with experimental data using the so-called slotted wall (mass effect) boundary condition, we note that experimental evidence exists [26] which indicates that the viscous effect boundary condition is more realistic for slotted wall tunnels with narrow slots (see also [28,p.48]).

A complete understanding of the mass effect and viscous effect boundary conditions has yet to be achieved. On the theoretical side, this is partly because the

kernel of the integral equation relating downwash and pressure has not been explicitly calculated for the latter. However, a computationally tractable form of the kernel for the unsteady mass effect boundary condition was presented by Bland [8] in 1968. This is discussed briefly in section 3 below and further information may be found in [5] and [9]. Extensive calculations using Bland's kernel were first given in 1978 by us [5] and a rigorous existence and convergence theory for the numerical solution method was established. While the bulk of our present analysis centers around Bland's kernel, we present in section 4 an analysis of the kernel for the viscous effect boundary condition for purely porous wind tunnel walls. In section 13 we present calculations for steady airloads using the viscous effect boundary condition over the full range of the Mach number, height to chord ratio and ventilation coefficient ν.

Most of the existing wind tunnel interference theory is founded on the incomplete point of view that the effect of the boundary conditions at the wall can be determined by knowing the far flowfield characteristics of the airfoil. While this viewpoint has produced useful and simple engineering approximations to angle of attack and Mach number "corrections", it suffers by neglecting the truly coupled nature of interference between the walls and the model. Thus, any rational theory of wind tunnel interference must be based on an appropriate boundary value problem in which this coupling is explicitly present. The analysis used in this report is based on an integral equation method which correctly accounts for such coupling.

Whether the governing boundary value problem is solved directly via partial differential equations or by reduction to an integral equation is just a matter of computational method. However, whereas integral equations are more difficult to formulate, they enjoy the advantage that the dimension of the space in which the problem must be solved is reduced by one. This undoubtedly accounts for integral equations being a frequent method of choice in subsonic and supersonic flow, and there is now evidence [29] to suggest that in transonic flow as well, integral equation methods may be an order of magnitude faster than PDE methods.

§3. Øland's integral equation

Based on the preceding discussion, the boundary value problem for flow in a ventilated wind tunnel with the mass effect boundary condition may be completely formulated on the lower (or upper) half of the infinite strip

$$\Omega = \{(x,z) \mid \ |x|<\infty \ \& \ 0\leq z\leq \eta\} \tag{3.1}$$

using equations (2.1)-(2.3), (2.5), (2.6) and (2.9_3). Introducing streamwise Fourier transform pairs

$$\hat{f}(s,z) = \frac{1}{\sqrt{2\pi}}\int_{-\infty}^{\infty} e^{-isx} f(x,z)dx, \tag{3.2$_1$}$$

$$f(x,z) = \frac{1}{\sqrt{2\pi}}\int_{-\infty}^{\infty} e^{isx} \hat{f}(s,z)ds, \tag{3.2$_2$}$$

with the property that

$$\left(\frac{\partial \hat{f}}{\partial x}\right) = is\hat{f}, \tag{3.2$_3$}$$

it follows that

$$\frac{d^2\hat{p}}{dz^2} - \beta^2\left(s-\frac{Mk}{1-M}\right)\left(s+\frac{Mk}{1+M}\right)\hat{p} = 0, \ 0\leq z\leq \eta, \tag{3.3$_1$}$$

$$\hat{p} = -\frac{1}{2\sqrt{2\pi}}\int_{-1}^{1} e^{-is\xi}\Delta p(\xi)d\xi, \ z = 0, \tag{3.3$_2$}$$

$$\mu\frac{d\hat{p}}{dz} + \hat{p} = 0, \qquad z = \eta, \tag{3.3$_3$}$$

which can be solved, giving

$$\hat{p}(s,z) = \frac{1}{2\sqrt{2\pi}}\frac{\beta\mu\sigma\cosh\beta(\eta-z)\sigma + \sinh\beta(\eta-z)\sigma}{\beta\mu\sigma\cosh\beta\eta\sigma + \sinh\beta\eta\sigma}\int_{-1}^{1} e^{-is\xi}\Delta p(\xi)d\xi, \tag{3.4$_1$}$$

where

$$\sigma(s) = \sqrt{(s-\frac{Mk}{1-M})(s+\frac{Mk}{1+M})}. \qquad (3.4_2)$$

Equation (2.6) for the downwash may be restated as

$$w(x) = \frac{1}{\sqrt{2\pi}} \int_{-\infty}^{\infty} e^{isx} (\frac{\partial \hat{\phi}}{\partial y})_{y=0} ds, \qquad (3.5)$$

and from equation (2.3) it follows that

$$\hat{\phi} = \frac{i}{2(s+k)} \hat{p}. \qquad (3.6)$$

Combining equations (3.4_1), (3.5) and (3.6) results in

$$w(x) = \frac{1}{\pi} \int_{-\infty}^{\infty} \int_{-1}^{1} \frac{\beta \Delta p(\xi)}{4} e^{is(x-\xi)} \frac{i\sigma(s)}{2(s+k)} \frac{\beta\mu\sigma \sinh \beta\eta\sigma + \cosh \beta\eta\sigma}{\beta\mu\sigma \cosh \beta\eta\sigma + \sinh \beta\eta\sigma} d\xi ds. \qquad (3.7)$$

Equation (3.7) may be interpreted as an integral equation of the form

$$w(x) = \frac{\beta}{4\pi} \int_{-1}^{1} K(x-\xi) \Delta p(\xi) d\xi, \qquad (3.8)$$

where the kernel is given by

$$K(x,k,M,\eta,\mu) = \int_{-\infty}^{\infty} e^{isx} \frac{i\sigma(s)}{2(s+k)} \frac{\beta\mu\sigma \sinh \beta\eta\sigma + \cosh \beta\eta\sigma}{\beta\mu\sigma \cosh \beta\eta\sigma + \sinh \beta\eta\sigma} ds. \qquad (3.9)$$

The inverse Fourier transform (3.9) was evaluated by Bland [8] following an extensive analysis. He showed that

$$\begin{aligned} K(x,k,M,\eta,\mu) = {} & \frac{1}{x} - \frac{ik}{\beta^2} \log |x| + \frac{\pi}{2\beta} (1+\operatorname{sgn}(x)) \frac{1+\mu k \tanh k\eta}{\mu + \frac{1}{k} \tanh k\eta} \exp(-ikx) \\ & - \frac{\pi}{\beta\eta} [\operatorname{sgn}(x) S'(\frac{|x|}{\beta\eta}) - \frac{ik\eta}{\beta} S(\frac{|x|}{\beta\eta})] \exp \frac{ikM^2x}{\beta^2} \\ & + \frac{\pi}{2\beta\eta} [\operatorname{csch} \frac{\pi x}{2\beta\eta} - \frac{2\beta\eta}{\pi x} + (\exp \frac{ikM^2x}{\beta^2} - 1) \operatorname{csch} \frac{\pi x}{2\beta\eta}] \\ & - \frac{ik}{\beta^2} [\log(\frac{1}{x} \tanh \frac{\pi x}{4\beta\eta}) - (\exp \frac{ikM^2x}{\beta^2} - 1) \log \tanh \frac{\pi|x|}{4\beta\eta}], \end{aligned} \qquad (3.10)$$

where

$$S(\delta) = \sum_{n=1}^{\infty} \{\frac{s_n}{\hat{\lambda}_n} \exp(-\hat{\lambda}_n\delta) - \frac{1}{\pi(n-\frac{1}{2})} \exp[-(n-\frac{1}{2})\pi\delta]\} \tag{3.11$_1$}$$

$$s_n = \frac{1}{[1 + \frac{\gamma}{1+(\gamma\lambda_n)^2}][1 + (\frac{k\eta}{\lambda_n})^2]}, \tag{3.11$_2$}$$

$$\hat{\lambda}_n = \lambda_n\sqrt{1-\zeta_n^2},\ \zeta_n = \frac{Mk\eta}{\beta\lambda_n}, \tag{3.11$_3$}$$

$$\tan\lambda_n + \gamma\lambda_n = 0, \tag{3.11$_4$}$$

$$\gamma = \frac{\mu}{\eta}\ . \tag{3.11$_5$}$$

Equation (3.8) is recognized as a Fredholm integral equation of the first kind. Its kernel, given by (3.10), identifies it further as a Cauchy singular equation because of the dominant $\frac{1}{x}$ singularity. The remainder of the kernel consists of a weaker, integrable logarithmic singularity followed by a continuous part.

It is well-known (see, e.g. [5,p.11]) that solutions of such Cauchy singular integral equations are not unique unless the auxiliary Kutta condition, given in strong form by (2.5$_3$) or in weak form by

$$\lim_{x\to 1^-}|\Delta p(x)| < \infty, \tag{3.12$_1$}$$

is imposed. Then it follows also that solutions for Δp possess inverse square root singularities at the leading edge

$$\lim_{x\to -1^+}|\sqrt{1+x}\ \Delta p(x)| < \infty \tag{3.12$_2$}$$

and square root singularities

$$\lim_{x\to 1^-}|\frac{\Delta p(x)}{\sqrt{1-x}}| < \infty \tag{3.12$_3$}$$

at the trailing edge.

In the case of steady flow in free air, Bland's kernel (3.10) reduces to the classical Prandtl-Glauert vortex kernel

$$K(x,0,M,\infty,.) = \frac{1}{x} \tag{3.13}$$

which consists of the Cauchy singularity alone. In this case, the Söhngen inversion formula [30] (see also [31], [32] and [5, §§2,9]) holds, and (3.8) has the closed form solution

$$(k=0,\ \eta=\infty) \qquad \Delta p(x) = \frac{8}{4\pi}\sqrt{\frac{1-x}{1+x}}\int_{-1}^{1}\sqrt{\frac{1+\xi}{1-\xi}}\,\frac{1}{\xi-x}\,w(\xi)d\xi. \tag{3.14}$$

In view of the above considerations concerning uniqueness, leading and trailing edge singularities and the Söhngen inversion formula, Bland changed the unknown in (3.8) from the pressure jump Δp to the pressure factor ψ according to

$$\Delta p(x) = \frac{4}{\beta}\sqrt{\frac{1-x}{1+x}}\,\psi(x). \tag{3.15}$$

Then (3.8) becomes

$$w(x) = \frac{1}{\pi}\int_{-1}^{1}\sqrt{\frac{1-\xi}{1+\xi}}\,K(x-\xi)\psi(\xi)d\xi, \tag{3.16}$$

where K is still given by (3.10). The theoretical advantage of (3.16) over (3.8) is that (3.16) has a unique solution with the correct leading and trailing edge singularities. Without the auxiliary Kutta condition, (3.8) does not have a unique solution and is thus not well posed [33,Ch.III,§6.2]. Since this reformulation of the airfoil integral equation into a well posed problem was first made by S.R. Bland [8], [9], we shall refer to (3.16) as Bland's integral equation.

§4. Extension to porous wall wind tunnels

In a porous wall wind tunnel, the predominant mechanism by which ventilation is resisted is viscosity. The governing boundary value problem is given by equations (2.1)-(2.6) together with the viscous effect boundary condition (2.10_4). Taking streamwise Fourier transforms as in section 3 gives the two point boundary value problem

$$\frac{d^2\hat{p}}{dz^2} - \beta^2\sigma^2\hat{p} = 0, \quad 0\leq z\leq \eta, \tag{4.1$_1$}$$

$$\hat{p} = -\frac{1}{2\sqrt{2\pi}}\int_{-1}^{1} e^{-is\xi}\Delta p(\xi)d\xi, \quad z = 0, \tag{4.1$_2$}$$

$$\nu\frac{d\hat{p}}{dz} + i(s+k)\hat{p} = 0, \quad z = \eta. \tag{4.1$_3$}$$

Solving (4.1) gives

$$\hat{p}(s,z) = -\frac{1}{2\sqrt{2\pi}}\frac{\beta\nu\sigma\cosh\beta(\eta-z)\sigma + i(s+k)\sinh\beta(\eta-z)\sigma}{\beta\nu\sigma\cosh\beta\eta\sigma + i(s+k)\sinh\beta\eta\sigma}\int_{-1}^{1} e^{-is\xi}\Delta p(\xi)d\xi, \tag{4.2}$$

and relating $\hat{p}$ to the downwash using (3.5) and (3.6) results in

$$w(x) = \frac{1}{\pi}\int_{-\infty}^{\infty}\int_{-1}^{1}\frac{\beta\Delta p(\xi)}{4}e^{is(x-\xi)}\frac{i\sigma(s)}{2(s+k)}\frac{\beta\nu\sigma\sinh\beta\eta\sigma + i(s+k)\cosh\beta\eta\sigma}{\beta\nu\sigma\cosh\beta\eta\sigma + i(s+k)\sinh\beta\eta\sigma}d\xi ds. \tag{4.3}$$

Equation (4.3) may be interpreted as an extension of Bland's integral equation (3.16) to the viscous effect boundary condition (2.10_4). The kernel is given by

$$K(x,M,k,\eta,\nu) = \int_{-\infty}^{\infty} e^{isx}\frac{i\sigma(s)}{2(s+k)}\frac{\beta\nu\sigma\sinh\beta\eta\sigma + i(s+k)\cosh\beta\eta\sigma}{\beta\nu\sigma\cosh\beta\eta\sigma + i(s+k)\sinh\beta\eta\sigma}ds, \tag{4.4}$$

and depends upon Mach number, reduced frequency, height to chord ratio and the viscous effect ventilation coefficient.

Technically, both (3.9) and (4.4) are inverse Fourier transforms in the distributional sense [34]. For this reason, their numerical computation is not straightforward. However, for steady flow the kernel in (4.4) can be obtained easily in closed form.

Setting $k = 0$ in (4.4) gives

$$K(x,M,\eta,\nu) = \frac{i}{2}\int_{-\infty}^{\infty} e^{isx}\,\frac{\beta\nu\,\sinh\beta\eta s + i\,\cosh\beta\eta s}{\beta\nu\,\cosh\beta\eta s + i\,\sinh\beta\eta s}\,ds, \tag{4.5}$$

and introducing a compressible leakage angle ζ defined by

$$\tan\zeta = \frac{1}{\beta\nu} \tag{4.7}$$

results in

$$K(x,M,\eta,\nu) = \frac{i}{2}\int_{-\infty}^{\infty} e^{isx}\tanh(\beta\eta s+i\zeta)ds. \tag{4.7}$$

For infinite height to chord ratio, $\eta = \infty$, and we observe that (4.7) reduces to

$$K(x) = \frac{i}{2}\int_{-\infty}^{\infty} e^{isx}\,\mathrm{sgn}(s)ds = \frac{1}{x}, \tag{4.8}$$

which is the known classical result for steady compressible flow in a free atmosphere.

The integrals in (4.5), (4.7) and (4.8) do not exist as ordinary Lebesgue (nor Riemann) integrals; instead they must be regarded as distributions. However, if we write

$$K(x,M,\eta,\nu) = \frac{1}{x} + \Delta K(x,M,\eta,\nu), \tag{4.9}$$

then the inverse Fourier transform,

$$\Delta K(x,M,\eta,\nu) = \frac{i}{2}\int_{-\infty}^{\infty} e^{isx}(\tanh(\beta\nu s+i\zeta)-\mathrm{sgn}(s))ds, \tag{4.10}$$

for the incremental part ΔK of the kernel exists as the Cauchy principal value of an ordinary Legesgue integral. Splitting the integral (4.10) into two parts, we obtain

$$\Delta K(x,M,\eta,\nu) = i\lim_{\varepsilon\to 0}\left(\int_{-\infty}^{-\varepsilon} e^{isx}\,\frac{e^{2(\beta\eta s+i\zeta)}}{1+e^{2(\beta\eta s+i\zeta)}}\,ds - \int_{\varepsilon}^{\infty} e^{isx}\,\frac{e^{-2(\beta\eta s+i\zeta)}}{1+e^{-2(\beta\eta s+i\zeta)}}ds\right),$$

and expanding the denominators into geometric series gives

$$\Delta K(x,M,\eta,\nu) = i\lim_{\varepsilon\to 0}\int_{-\infty}^{-\varepsilon}\sum_{n=1}^{\infty}(-1)^{n+1}\,e^{(2n\beta\eta+ix)s+2n\zeta i}ds$$

$$- i\lim_{\varepsilon\to 0}\int_{\varepsilon}^{\infty}\sum_{n=1}^{\infty}(-1)^{n+1}\,e^{(-2n\beta\eta+ix)s-2n\zeta i}ds.$$

For $s \neq 0$, these series are bounded by an absolutely integrable function, so by the dominated convergence theorem, integration and summation can be interchanged. Upon taking the limit as $\varepsilon \to 0$,

$$\Delta K(x,M,\eta,v) = \frac{i}{2\beta\eta} \sum_{n=1}^{\infty} (-1)^{n-1} \left(\frac{e^{2n\zeta i}}{n+\frac{ix}{2\beta\eta}} - \frac{e^{-2n\zeta i}}{n-\frac{ix}{2\beta\eta}} \right), \tag{4.11$_1$}$$

which may be written as the imaginary part of a complex series

$$\Delta K(x,M,\eta,v) = \frac{1}{\beta\eta} \operatorname{Im} \sum_{n=1}^{\infty} \frac{(-e^{2i\zeta})^n}{n-\frac{ix}{2\beta\eta}}, \tag{4.11$_2$}$$

or as a real series

$$\Delta K(x,M,\eta,v) = \frac{1}{\beta\eta} \sum_{n=1}^{\infty} (-1)^n \frac{n \sin 2n\zeta - \frac{x}{2\beta\eta} \cos 2n\zeta}{n^2 + (\frac{x}{2\beta\eta})^2}. \tag{4.11$_3$}$$

The last series is the sum of two series which may be summed in closed form [35, Nos. 561, 562]. Thus, we obtain the incremental part of the kernel in closed form as

$$\Delta K(x,M,\eta,v) = \frac{1}{\beta\eta} \left(\frac{\exp(\frac{\zeta x}{\beta\eta})}{\frac{2}{\pi} \sinh \frac{\pi x}{2\beta\eta}} - \frac{\beta\eta}{x} \right). \tag{4.12}$$

Adding the Cauchy singularity gives the complete kernel,

$$K(x,M,\eta,v) = \frac{1}{\beta\eta} \frac{\exp(\frac{\zeta x}{\beta\eta})}{\frac{2}{\pi} \sinh \frac{\pi x}{2\beta\eta}}. \tag{4.13}$$

We point out that, physically, ΔK represents the interference effect due to the presence of the wind tunnel walls since

$$\lim_{\eta \to \infty} \Delta K(x,M,\eta,v) = 0.$$

Thus, we are justified in referring to ΔK as <u>the interference kernel for steady flow</u>. Also, we observe that for a closed wall, (4.13) reduces to

$$K(x,M,\eta,\infty) = \frac{\pi}{2\beta\eta} \operatorname{csch} \frac{\pi x}{2\beta\eta}, \tag{4.14}$$

which is a result originally given by Runyan, Woolston and Rainey [36, Appendix] (see also Bland [9, p. 839]).

The parametric behavior of the interference kernel and the complete kernel can be displayed explicitly by writing

$$\beta\eta\Delta K(x,M,\eta,\nu) = F(\zeta,\tau), \tag{4.15}$$

$$\beta\eta K(x,M,\eta,\nu) = \frac{1}{\tau} + F(\zeta,\tau), \tag{4.16}$$

where

$$F(\zeta,\tau) = \frac{\exp(\zeta\tau)}{\frac{2}{\pi}\sinh\frac{\pi}{2}\tau} - \frac{1}{\tau} \tag{4.17}$$

is a function of two parameters ζ and τ given by

$$\zeta = \tan^{-1}\frac{1}{\beta\nu},\quad \tau = \frac{x}{\beta\eta}. \tag{4.18}$$

Thus, our analysis reduces the original four parameters

$$x,M,\eta,\nu$$

to only three

$$\beta\eta,\ \frac{x}{\beta\eta},\ \beta\nu\,.$$

The parameters

$$\beta\eta,\ \beta\nu$$

could be expected from the Lorentz compressibility contraction (as pointed out by Küssner for unsteady flow (and by Glauert and Prandtl for steady flow)). The parameter

$$\frac{x}{\beta\eta}$$

could be expected from the previous result (4.14) for closed wall tunnels and represents the ratio of the chordwise influence distance to the contracted height to chord ratio. These results were originally derived by Ebihara [27] using the method of images in conjunction with compressibility corrections to steady incompressible flow (see also Mokry [28]).

The ease of obtaining the interference kernel in terms of elementary functions can be attributed to the relative simplicity of steady flow. For unsteady flow, it seems unlikely that the inverse Fourier transform (4.4) would admit such a pat result. If the singularities were removed, however, the interference kernel for unsteady flow in a wind tunnel with porous walls might be expressible as an ordinary integral. This integral, once it were obtained, could be attacked via infinite series or via numerical integration. For analytic functions, the Laguerre-Gaussian

quadrature rule [37] is convergent in the sense that weights W_i^N and nodes x_i^N are tabulated [38] such that

$$\int_0^\infty e^{-x} f(x)dx = \lim_{N\to\infty} \sum_{i=1}^{N} W_i^N f(x_i^N).$$

On the other hand, the uniformly convergent series presented in (4.11) are not rapidly convergent. We have found that three decimal accuracy requires tens of thousands of terms; such behavior, even with convergence acceleration, is quite pronounced in the numerical computation of Bland's kernel (3.10)-(3.11). This poses the interesting question: from the standpoint of computational efficiency, is it better to calculate the continuous part of the kernel as an infinite series as has been customary in the past, or is it better to compute it as a Fourier transform?

For future reference, we present tabulated values of the interference kernel and of the complete kernel in Tables 1 and 2. Two features may be noted. First, it is easy to show from (4.17) that

$$\lim_{\tau\to 0} F(\zeta,\tau) = \zeta. \tag{4.19}$$

Second, we observe that

$$\lim_{|\tau|\to\infty} F(\zeta,\tau) = 0 \text{ if } 0\le\zeta<\frac{\pi}{2}, \tag{4.20$_1$}$$

$$\lim_{\tau\to-\infty} F(\frac{\pi}{2},\tau) = 0, \tag{4.20$_2$}$$

$$\lim_{\tau\to\infty} F(\frac{\pi}{2},\tau) = \pi. \tag{4.20$_3$}$$

Figures 2 and 3 depict the parametric behavior of the interference kernel and of the complete kernel for variable porosity tunnels. In Figure 2, it is seen that for $\zeta = 0$ (the closed wall case), the interference kernel is an odd function of streamwise distance. Thus, upstream and downstream distances produce opposing interference effects. However, the interference downwash, given by

$$\frac{1}{\pi}\int_{-1}^{1} \sqrt{\frac{1-\xi}{1+\xi}}\, \Delta K(x-\xi,M,\eta,\nu)\psi(\xi)d\xi,$$

is skewed upstream by the singularity factor

$$\sqrt{\frac{1-\xi}{1+\xi}}$$

so that upstream pressures have a greater effect on downwash than downstream pressures.

Also the interference kernel modifies the complete kernel so that the same pressure produces less downwash than in the free atmosphere. Reversing the argument, the same downwash in a closed wind tunnel corresponds to more pressure than in free air. As ventilation occurs, the leakage angle

$$\zeta = \tan^{-1}\left(\frac{1}{\beta v}\right)$$

increases. This skews the interference kernel to the right as shown in Figure 2 and increases the magnitude of the complete kernel as shown in Figure 3. Thus, increasing the ventilation causes upstream pressures to have a relatively greater interference effect than downstream pressures, and causes the same pressure to produce more downwash than in a closed tunnel. Again reversing the argument the kernels shown in Figures 2 and 3 indicate that as the ventilation increases, the airloads will decrease for the same downwash.

Table 1. Steady interference kernel $\beta\eta\Delta K$ for variable porosity wind tunnels

$\tau=\frac{x}{\beta\eta}$	$\zeta=0^0$	$\zeta=15^0$	$\zeta=30^0$	$\zeta=45^0$	$\zeta=60^0$	$\zeta=75^0$	$\zeta=90^0$
-8.00	.124989	.124999	.125000	.125000	.125000	.125000	.125000
-7.00	.142804	.142849	.142856	.142857	.142857	.142857	.142857
-6.00	.166413	.166614	.166656	.166664	.166666	.166667	.166667
-5.00	.198780	.199671	.199911	.199976	.199994	.199998	.200000
-4.00	.244133	.247941	.249278	.249746	.249911	.249969	.249989
-3.00	.305109	.320465	.327466	.330658	.332114	.332777	.333080
-2.50	.338078	.367819	.383275	.391308	.395483	.397652	.398780
-2.00	.363985	.419427	.452270	.471725	.483251	.490078	.494122
-1.50	.366207	.463787	.529767	.574166	.604207	.624492	.638189
-1.00	.317431	.474650	.595656	.688791	.760473	.815644	.858108
-.50	.191725	.413590	.608233	.778995	.928805	1.06023	1.17554
0	0	.261799	.523599	.785398	1.04720	1.30900	1.57080
.50	-.191725	.061169	.349431	.678006	1.05254	1.47944	1.96605
1.00	-.317431	-.113161	.152240	.497066	.945087	1.52719	2.28349
1.50	-.366207	-.221694	-.007674	.309284	.778689	1.47387	2.50340
2.00	-.363985	-.270395	-.112406	.154295	.604510	1.36451	2.64747
2.50	-.338078	-.280850	-.170735	.041147	.448845	1.23333	2.74281
3.00	-.305109	-.271430	-.197562	-.035548	.319792	1.09915	2.80851
4.00	-.244133	-.233282	-.202359	-.114239	.136872	.852451	2.89160
5.00	-.198780	-.195485	-.183282	-.138102	.029176	.648516	2.94159
6.00	-.166413	-.165447	-.160800	-.138445	-.030906	.486406	2.97493
7.00	-.142804	-.142528	-.140798	-.129990	-.062435	.359791	2.99874
8.00	-.124989	-.124911	-.124278	-.119133	-.077359	.261871	3.01659

Table 2. Steady complete kernel $\beta\eta K$ for variable porosity wind tunnels

$\tau=\frac{x}{\beta\eta}$	$\zeta=0^0$	$\zeta=15^0$	$\zeta=30^0$	$\zeta=45^0$	$\zeta=60^0$	$\zeta=75^0$	$\zeta=90^0$
-8.00	-.000011	-.000001	-.000000	-.000000	-.000000	-.000000	-.000000
-7.00	-.000053	-.000008	-.000001	-.000000	-.000000	-.000000	-.000000
-6.00	-.000254	-.000053	-.000011	-.000002	-.000000	-.000000	-.000000
-5.00	-.001220	-.000329	-.000089	-.000024	-.000006	-.000002	-.000000
-4.00	-.005867	-.002059	-.000722	-.000254	-.000089	-.000031	-.000011
-3.00	-.028224	-.012868	-.005867	-.002675	-.001220	-.000556	-.000254
-2.50	-.061922	-.032181	-.016725	-.008692	-.004517	-.002348	-.001220
-2.00	-.136015	-.080573	-.047730	-.028275	-.016749	-.009922	-.005878
-1.50	-.300460	-.202880	-.136991	-.092501	-.062459	-.042175	-.028478
-1.00	-.682569	-.525350	-.404344	-.311209	-.239527	-.184356	-.141892
-.50	-1.80828	-1.58641	-1.39177	-1.22101	-1.07120	-.939766	-.824462
0	$\pm\infty$	$\pm\infty$	$\pm\infty$	$\pm\infty$	$\pm\infty$	$\pm\infty$	$\pm\infty$
.50	1.80828	2.06117	2.34943	2.67801	3.05254	3.05254	3.96605
1.00	.682569	.886839	1.15224	1.49707	1.94509	2.52719	3.28349
1.50	.300460	.444973	.658993	.975950	1.44536	2.14053	3.17007
2.00	.136015	.229605	.387594	.654295	1.10451	1.86451	3.14747
2.50	.061922	.119150	.229265	.441147	.848845	1.63333	3.14281
3.00	.028224	.061903	.135771	.297785	.653126	1.43249	3.14185
4.00	.005867	.016718	.047641	.135761	.386872	1.10245	3.14160
5.00	.001220	.004515	.016718	.061898	.229176	.848516	3.14159
6.00	.000254	.001220	.005867	.028222	.135761	.653073	3.14159
7.00	.000053	.000329	.002059	.012867	.080422	.502648	3.14159
8.00	.000011	.000089	.000722	.005867	.047641	.386871	3.14159

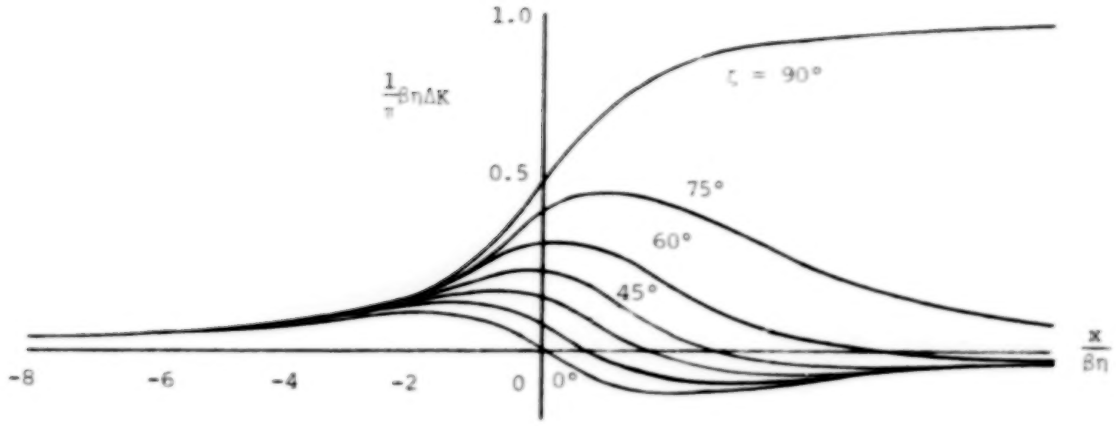

Figure 2. Steady interference kernel for variable porosity wind tunnels

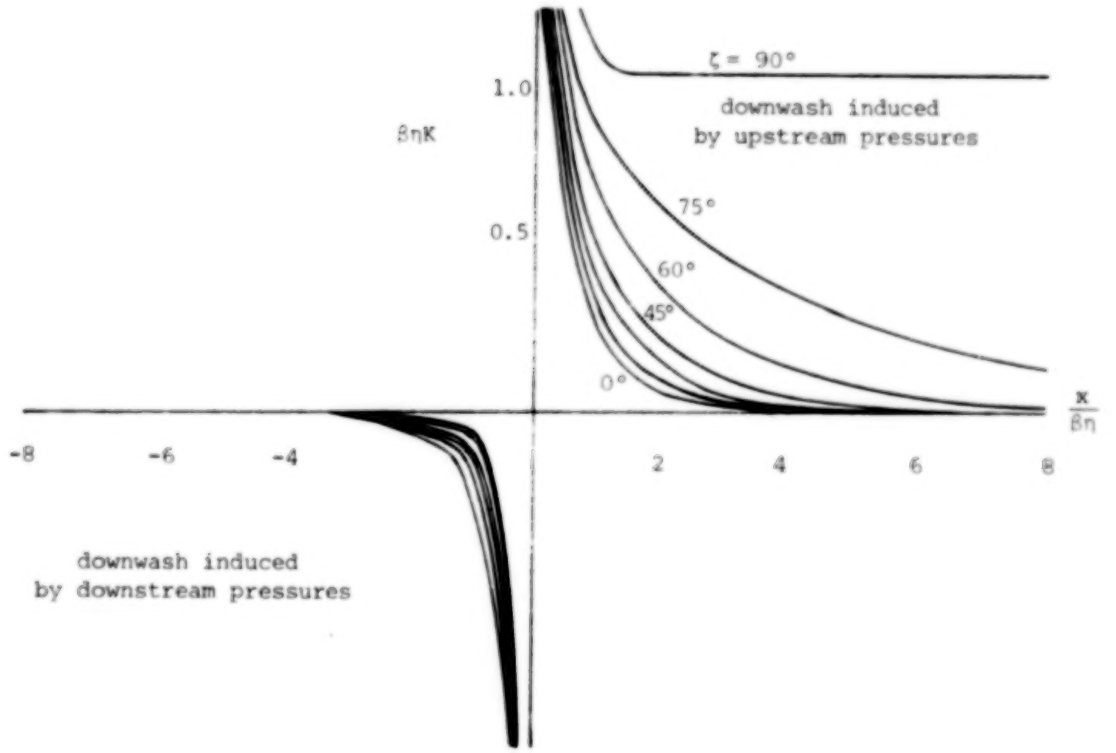

Figure 3. Steady complete kernel for variable porosity wind tunnels

§5. Fourier theory of airfoil polynomials

In our previous work [5], two sets of orthogonal polynomials were used in the solution of Bland's integral equation. These polynomials are computationally well suited for unsteady flow in ventilated wind tunnels, probably because the airloads for subcritical Mach numbers and nonresonant frequencies are well-behaved parametric extensions of the steady free air case which they solve so elegantly in closed form. From a theoretical viewpoint, they have unique mathematical properties which provide efficient use of the abstract geometrical structure of the underlying Hilbert spaces of downwash and pressure functions. This section briefly summarizes some of their features. For additional information, see Bland [8] and [9], Ivanoff [7, Ch. 2], or Fromme and Golberg [5].

Consider the case of steady flow in free air. A completely symmetrical theory between downwash and pressure will now be presented for this special case. To do this, (3.14) and (3.16) are viewed as a solution pair

$$\frac{1}{\pi}\int_{-1}^{1}\sqrt{\frac{1-\xi}{1+\xi}}\;\frac{1}{x-\xi}\;\psi(\xi)\,d\xi = w(x), \tag{5.1$_1$}$$

$$\frac{1}{\pi}\int_{-1}^{1}\sqrt{\frac{1+\xi}{1-\xi}}\;\frac{1}{\xi-x}\;w(\xi)\,d\xi = \psi(x). \tag{5.1$_2$}$$

This may be written more briefly in operator notation as

$$H\,\psi = w, \tag{5.2$_1$}$$

$$H^{-1}\,w = \psi. \tag{5.2$_2$}$$

A sequence of linearly independent solution pairs to (5.2) is given by

$$H\,\gamma_n = \alpha_n,\quad n = 1,\ldots,\infty, \tag{5.3$_1$}$$

$$H^{-1}\,\alpha_n = \gamma_n,\quad n = 1,\ldots,\infty, \tag{5.3$_2$}$$

where

$$\alpha_n(x) = \frac{1}{\sqrt{\pi}}\,\frac{\cos\left((n-\frac{1}{2})\cos^{-1}x\right)}{\cos\left(\frac{1}{2}\cos^{-1}x\right)}, \tag{5.4$_1$}$$

$$\gamma_n(x) = \frac{1}{\sqrt{\pi}}\,\frac{\sin\left((n-\frac{1}{2})\cos^{-1}x\right)}{\sin\left(\frac{1}{2}\cos^{-1}x\right)}. \tag{5.4$_2$}$$

These functions satisfy the following recursion formulas

$$\alpha_1(x) = \frac{1}{\sqrt{\pi}},\ \alpha_2(x) = \frac{1}{\sqrt{\pi}}(-1+2x),\ldots,\ \alpha_{n+2}(x) = 2x\,\alpha_{n+1}(x)-\alpha_n(x), \tag{5.5$_1$}$$

$$\gamma_1(x) = \frac{1}{\sqrt{\pi}},\ \gamma_2(x) = \frac{1}{\sqrt{\pi}}(1+2x),\ldots,\ \gamma_{n+2}(x) = 2x\,\gamma_{n+1}(x)-\gamma_n(x), \tag{5.5$_2$}$$

and are therefore polynomials. We call α_n and γ_n the nth downwash and pressure polynomials, respectively. Collectively they are called airfoil polynomials. Their n-1 zeros are given by

$$\alpha_n(x_i^n) = 0;\ x_i^n = -\cos\frac{2i\pi}{2n-1};\ i = 1,\ldots,n-1;\ n\geq 2, \tag{5.6$_1$}$$

$$\gamma_n(\xi_i^n) = 0;\ \xi_i^n = \cos\frac{2i\pi}{2n-1};\ i = 1,\ldots,n-1;\ n\geq 2, \tag{5.6$_2$}$$

and are interdigitated according to

$$-1 < \xi_{n-1}^n < x_1^n < \ldots < \xi_1^n < x_{n-1}^n < 1. \tag{5.6$_3$}$$

One of the more striking properties of the airfoil polynomials is that they are orthogonal with respect to reciprocal weight functions with leading and trailing edge singularities:

$$\int_{-1}^{1}\sqrt{\frac{1+x}{1-x}}\,\alpha_m(x)\alpha_n(x)dx = \delta_{mn}, \tag{5.7$_1$}$$

$$\int_{-1}^{1}\sqrt{\frac{1-x}{1+x}}\,\gamma_m(x)\gamma_n(x)dx = \delta_{mn}. \tag{5.7$_2$}$$

This leads to two generalized Fourier series representations, one for downwash, the other for pressure. To see this, define two complex Hilbert spaces

$$L_\alpha^2 = \{f:[-1,1]\to\mathbb{C}\mid \int_{-1}^{1}\sqrt{\frac{1+x}{1-x}}\,|f(x)|^2dx<\infty\}, \tag{5.8$_1$}$$

$$L_\gamma^2 = \{f:[-1,1]\to\mathbb{C}\mid \int_{-1}^{1}\sqrt{\frac{1-x}{1+x}}\,|f(x)|^2dx<\infty\}, \tag{5.8$_2$}$$

called downwash space and pressure space, with respective inner products

$$\langle f,g\rangle_\alpha = \int_{-1}^{1} \sqrt{\frac{1+x}{1-x}}\, f(x)\bar{g}(x)\,dx, \tag{5.9$_1$}$$

$$\langle f,g\rangle_\gamma = \int_{-1}^{1} \sqrt{\frac{1-x}{1+x}}\, f(x)\bar{g}(x)\,dx, \tag{5.9$_2$}$$

and norms

$$\|f\|_\alpha = \sqrt{\langle f,f\rangle_\alpha}, \tag{5.10$_1$}$$

$$\|f\|_\gamma = \sqrt{\langle f,f\rangle_\gamma}. \tag{5.10$_2$}$$

It can be shown that $\{\alpha_n\}$ and $\{\gamma_n\}$ are complete orthonormal bases for L^2_α and L^2_γ, respectively. Therefore, an arbitrary function in either space can be represented by generalized Fourier series using airfoil polynomials; i.e.,

$$f\in L^2_\alpha \Rightarrow f = \sum_{m=1}^{\infty} \langle f,\alpha_m\rangle_\alpha\, \alpha_m, \tag{5.11$_1$}$$

$$f\in L^2_\gamma \Rightarrow f = \sum_{m=1}^{\infty} \langle f,\gamma_m\rangle_\gamma\, \gamma_m. \tag{5.11$_2$}$$

Referring to the solution pair given by (5.1), we see that for steady flow in free air,

$$w\in L^2_\alpha \Rightarrow \phi\in L^2_\gamma \;\&\; \phi = \sum_{m=1}^{\infty} \langle w,\alpha_m\rangle_\alpha\, \gamma_m, \tag{5.12$_1$}$$

$$\phi\in L^2_\gamma \Rightarrow w\in L^2_\alpha \;\&\; w = \sum_{m=1}^{\infty} \langle \phi,\gamma_m\rangle_\gamma\, \alpha_m. \tag{5.12$_2$}$$

Thus, in this fundamental special case, the pressure Fourier coefficients and the downwash Fourier coefficients are exactly equal; i.e.,

$$\langle \phi,\gamma_m\rangle_\gamma = \langle w,\alpha_m\rangle_\alpha, \tag{5.13}$$

thereby providing an elegant and computationally powerful reformulation of the Söhngen inversion formula.

Another way of viewing the result (5.13) is that if ϕ and w satisfy (5.1), then

they have the same length, or norm, in their respective space; i.e.,

$$H\phi = w \Rightarrow \|\phi\|_\gamma = \|w\|_\alpha \tag{5.14}$$

In general, if T is a linear transformation between two Hilbert spaces H_1 and H_2,

$$T: H_1 \to H_2, \tag{5.15}$$

and if we define the operator norm of T as

$$\|T\| = \sup_{\|x\|_1=1} \|Tx\|_2 \tag{5.16}$$

where $\|.\|_i$ is the norm on H_i, i=1,2, and if

$$\|T\| = 1, \tag{5.17}$$

then we say T is an <u>isometry</u>. By (5.13), H is an isometry; i.e.,

$$\|H\| = 1, \ \|H^{-1}\| = 1. \tag{5.18}$$

An isometry is an abstract generalization of a length preserving transformation and enjoys generalized properties of orthogonal, or unitary finite dimensional transformations. If T is defined in general as above, then the <u>adjoint</u> of T is the operator

$$T^*: H_2 \to H_1 \tag{5.19}$$

such that

$$\langle T^*x, y\rangle_1 = \langle x, Ty\rangle_2 \tag{5.20}$$

for every $x \in H_1$ and $y \in H_2$, where $\langle .,. \rangle_i$ are the inner products on H_i, i=1,2. It follows (see [5] for details) that the adjoint of H is its inverse; i.e.,

$$H^* = H^{-1}. \tag{5.21}$$

Consequently,

$$f\in L^2_\alpha \;\&\; g\in L^2_\gamma \Rightarrow \langle f,Hg\rangle_\alpha = \langle H^{-1}f,g\rangle_\gamma, \tag{5.22}$$

which is useful in reverse flow formulations.

Certain specific Fourier expansions in terms of airfoil polynomials will be useful in the sequel. Let

$$\log_x \xi = \log|x-\xi|. \tag{5.23}$$

Then it has been shown [8] that

$$\langle \log_x, \alpha_n\rangle_\alpha = -\frac{\gamma_{n+1}(x)}{2n} - (\log 2-\tfrac{1}{2})\gamma_n(x),\ n=1, \tag{5.24$_1$}$$

$$\langle \log_x, \alpha_n\rangle_\alpha = -\frac{\gamma_{n+1}(x)}{2n} - \frac{\gamma_n(x)}{2n(n-1)} + \frac{\gamma_{n-1}(x)}{2(n-1)},\ n\geq 2, \tag{5.24$_2$}$$

$$\langle \log_x, \gamma_n\rangle_\gamma = \frac{\alpha_{n+1}(x)}{2n} + (\log 2-\tfrac{1}{2})\alpha_n(x),\ n=1, \tag{5.24$_3$}$$

$$\langle \log_x, \gamma_n\rangle_\gamma = \frac{\alpha_{n+1}(x)}{2n} - \frac{\alpha_n(x)}{2n(n-1)} - \frac{\alpha_{n-1}(x)}{2(n-1)},\ n\geq 2. \tag{5.24$_4$}$$

These results are used in the solution of Bland's integral equation. For problems involving flaps, jump functions and their powers given by

$$\langle x\rangle^k = (\max(0,x))^k \tag{5.25}$$

are employed. We briefly indicate the method of computing their airfoil polynomial Fourier coefficients. To evaluate

$$\langle\langle x-a\rangle^k, \gamma_n\rangle_\gamma = \frac{1}{\pi}\int_a^1 \sqrt{\frac{1-x}{1+x}}\,(x-a)^k\,\gamma_n(x)\,dx, \tag{5.26}$$

use the changes of variables represented by

$$x = \cos\theta,\ a = \cos\theta_a.$$

Since

$$\sqrt{\frac{1-x}{1+x}} = \frac{2\sin^2\frac{\theta}{2}}{\sin\theta}$$

and

$$\gamma_n(x) = \frac{1}{\sqrt{\pi}} \frac{\sin(n-\frac{1}{2})\theta}{\sin \frac{1}{2}\theta},$$

it follows from the elementary identity

$$2 \sin \alpha \sin \beta = \cos(\alpha-\beta) - \cos(\alpha+\beta),$$

that

$$\langle\langle x-a\rangle^k, \gamma_n \rangle_\gamma = \frac{1}{\sqrt{\pi}} \int_0^{\theta_a} (\cos \theta - \cos \theta_a)^k (\cos(n-1)\theta - \cos n\theta) d\theta. \tag{5.27}$$

The advantage of (5.27) over (5.26) is that the integrand

$$F_{nk}(\theta) = (\cos \theta - \cos \theta_a)^k (\cos(n-1)\theta - \cos n\theta)$$

is an analytic function everywhere on $[0,\theta_a]$ and therefore (5.29) can be computed accurately and conveniently using ordinary Legendre-Gaussian quadrature. Thus,

$$\langle\langle x-a\rangle^k, \gamma_n \rangle_\gamma = \frac{\theta_a}{\sqrt{\pi}} \sum_{i=1}^{N} W_i^N F_{nk}(x_i^N \theta_a) + E_N,$$

where W_i^N and x_i^N are weights and nodes of the N point Legendre-Gaussian quadrature rule, and where

$$E_N = \theta_a \frac{2^{2N+1}}{(2N+1)} \frac{(N!)^4}{(2N!)^3} F_{nk}^{(2N)}(\bar{\theta}), \quad 0<\bar{\theta}<\theta_a$$

is the error [37,§8.5]. The integrals (5.26) can be determined in closed form, although they are increasingly cumbersome for larger values of k. The following closed form integrations are noted.

$$\langle\langle x-a\rangle^0, \gamma_1 \rangle_\gamma = \frac{1}{\sqrt{\pi}} (\theta_a - \sin\theta_a), \tag{5.28$_1$}$$

$$\langle\langle x-a\rangle^0, \gamma_n \rangle_\gamma = \frac{1}{\sqrt{\pi}} \left(\frac{\sin(n-1)\theta_a}{n-1} - \frac{\sin n\theta_a}{n}\right), \quad n \geq 2, \tag{5.28$_2$}$$

$$\langle\langle x-a\rangle, \gamma_1 \rangle_\gamma = \frac{1}{\sqrt{\pi}} \left(\sin \theta_a - \frac{\theta_a}{2} - \frac{\sin 2\theta_a}{4}\right)$$

$$- \frac{1}{\sqrt{\pi}} \cos \theta_a (\theta_a - \sin\theta_a), \tag{5.29$_1$}$$

$$\langle\langle x-a\rangle,\gamma_2\rangle_\gamma = \frac{1}{\sqrt{\pi}}\left(\frac{\theta_a}{2} - \frac{\sin\theta_a}{2} + \frac{\sin 2\theta_a}{4} - \frac{\sin 3\theta_a}{6}\right)$$

$$- \frac{1}{\sqrt{\pi}}\cos\theta_a\left(\sin\theta_a - \frac{\sin 2\theta_a}{2}\right), \tag{5.29$_2$}$$

$$\langle\langle x-a\rangle,\gamma_n\rangle_\gamma = \frac{1}{\sqrt{\pi}}\left(\frac{\sin(n-2)\theta_a}{2(n-2)} - \frac{\sin(n-1)\theta_a}{2(n-1)} + \frac{\sin n\theta_a}{2n} - \frac{\sin(n+1)\theta_a}{2(n+1)}\right)$$

$$- \frac{1}{\sqrt{\pi}}\cos\theta_a\left(\frac{\sin(n-1)\theta_a}{n-1} - \frac{\sin n\theta_a}{n}\right),\ n\geq 3. \tag{5.29$_3$}$$

We also note for future reference the Jacobi-Gaussian quadrature formulas [37]

$$\frac{1}{\pi}\int_{-1}^{1}\sqrt{\frac{1+x}{1-x}}\,f(x)dx = \sum_{n=1}^{N}\frac{1+x_i^{N+1}}{N+\frac{1}{2}}\,f(x_n^{N+1}) + E_N, \tag{5.30$_1$}$$

$$\frac{1}{\pi}\int_{-1}^{1}\sqrt{\frac{1-x}{1+x}}\,f(x)dx = \sum_{n=1}^{N}\frac{1-\xi_i^{N+1}}{N+\frac{1}{2}}\,f(\xi_n^{N+1}) + E_N, \tag{5.30$_2$}$$

where the nodes ξ_i^{N+1} and x_i^{N+1} are the zeros of the airfoil polynomials α_{N+1} and γ_{N+1} as given by (5-6), and where the error E_N for continuous functions is proportional to the 2Nth derivative of the integrand at some point in the interval (-1,1).

Sometimes it is desirable to convert from one airfoil polynomial basis to the other. Referring to (5.5), it is easy to show that

$$\alpha_1 = \gamma_1, \tag{5.31$_1$}$$

$$\alpha_2 = 2\gamma_1 + \gamma_2, \tag{5.31$_2$}$$

$$\alpha_3 = 2\gamma_1 - 2\gamma_2 + \gamma_3, \tag{5.31$_3$}$$

$$\alpha_4 = 2\gamma_1 + 2\gamma_2 - 2\gamma_3 + \gamma_4, \tag{5.31$_4$}$$

$$\alpha_5 = 2\gamma_1 - 2\gamma_2 + 2\gamma_3 - 2\gamma_4 + \gamma_5,\ldots \tag{5.31$_5$}$$

and

$$\gamma_1 = \alpha_1, \tag{5.32$_1$}$$

$$\gamma_2 = 2\alpha_1 + \alpha_2, \tag{5.32$_2$}$$

$$\gamma_3 = 2\alpha_1 + 2\alpha_2 + \alpha_3, \tag{5.32$_3$}$$

$$\gamma_4 = 2\alpha_1 + 2\alpha_2 + 2\alpha_3 + \alpha_4, \tag{5.32$_4$}$$

$$\gamma_5 = 2\alpha_1 + 2\alpha_2 + 2\alpha_3 + 2\alpha_4 + \alpha_5,\ldots \tag{5.32$_5$}$$

From (5.29 and (5.30), it appears that

$$\alpha_{n+1} = \gamma_{n+1} + 2\sum_{m=1}^{n}(-1)^{m+1}\gamma_m;\ n=1,2,\ldots \tag{5.33$_1$}$$

$$\gamma_{n+1} = \alpha_{n+1} + 2\sum_{m=1}^{n}\alpha_m;\ n = 1,2,\ldots \tag{5.33$_2$}$$

and in matrix notation that

$$\begin{bmatrix} \alpha_1 \\ \alpha_2 \\ \alpha_3 \\ \alpha_4 \\ \alpha_5 \\ \cdot \\ \cdot \\ \cdot \end{bmatrix} = \begin{bmatrix} 1 & 0 & 0 & 0 & 0 & \cdots \\ -2 & 1 & 0 & 0 & 0 & \cdots \\ 2 & -2 & 1 & 0 & 0 & \cdots \\ -2 & 2 & -2 & 1 & 0 & \\ 2 & -2 & 2 & -2 & 1 & \\ \cdot & \cdot & \cdot & & & \\ \cdot & \cdot & \cdot & & & \\ \cdot & \cdot & \cdot & & & \end{bmatrix} \begin{bmatrix} \gamma_1 \\ \gamma_2 \\ \gamma_3 \\ \gamma_4 \\ \gamma_5 \\ \cdot \\ \cdot \\ \cdot \end{bmatrix}, \qquad (5.34_1)$$

$$\begin{bmatrix} \gamma_1 \\ \gamma_2 \\ \gamma_3 \\ \gamma_4 \\ \gamma_5 \\ \cdot \\ \cdot \\ \cdot \end{bmatrix} = \begin{bmatrix} 1 & 0 & 0 & 0 & 0 & \cdots \\ 2 & 1 & 0 & 0 & 0 & \cdots \\ 2 & 2 & 1 & 0 & 0 & \cdots \\ 2 & 2 & 2 & 1 & 0 & \\ 2 & 2 & 2 & 2 & 1 & \\ \cdot & \cdot & \cdot & & & \\ \cdot & \cdot & \cdot & & & \\ \cdot & \cdot & \cdot & & & \end{bmatrix} \begin{bmatrix} \alpha_1 \\ \alpha_2 \\ \alpha_3 \\ \alpha_4 \\ \alpha_5 \\ \cdot \\ \cdot \\ \cdot \end{bmatrix}, \qquad (5.34_2)$$

or, more briefly

$$\{\alpha_n\} = [G^{\alpha}_{mn}]\{\alpha_n\}, \qquad (5.35_1)$$

$$\{\gamma_n\} = [G^{\gamma}_{mn}]\{\alpha_n\}. \qquad (5.35_2)$$

The problem of computing downwash from discrete displacement data will entail interpolation procedures and, differentiation as well. In any ascending polynomial basis, transformation matrices such as (5.34) will be lower triangular and when differentiation is performed they will be lower subtriangular. By differentiating the polynomial expressions (5.5) and recombining, one easily obtains

$$\alpha_1' = 0, \tag{5.36$_1$}$$

$$\alpha_2' = 2\alpha_1, \tag{5.36$_2$}$$

$$\alpha_3' = 2\alpha_1 + 4\alpha_2, \tag{5.36$_3$}$$

$$\alpha_4' = 4\alpha_1 + 2\alpha_2 + 6\alpha_3, \tag{5.36$_4$}$$

$$\alpha_5' = 4\alpha_1 + 6\alpha_2 + 2\alpha_3 + 8\alpha_4, \ldots \tag{5.36$_5$}$$

$$\gamma_1' = 0, \tag{5.37$_1$}$$

$$\gamma_2' = 2\gamma_1, \tag{5.37$_2$}$$

$$\gamma_3' = -2\gamma_1 + 4\gamma_2, \tag{5.37$_3$}$$

$$\gamma_4' = 4\gamma_1 - 2\gamma_2 + 6\gamma_3, \tag{5.37$_4$}$$

$$\gamma_5' = -4\gamma_1 + 6\gamma_2 - 2\gamma_3 + 8\gamma_4, \ldots \tag{5.37$_5$}$$

From this, it appears that in general

$$\alpha_{n+1}' = -\alpha_n' + 2n \sum_{m=1}^{n} \alpha_m ; \; n = 1,2,\ldots \tag{5.38$_1$}$$

$$\gamma_{n+1}' = \gamma_n' + 2n \sum_{m=1}^{n} (-1)^{n+m} \gamma_m ; n = 1,2,\ldots \tag{5.38$_2$}$$

and

$$\begin{bmatrix} \alpha_1 \\ \alpha_2 \\ \alpha_3 \\ \alpha_4 \\ \alpha_5 \\ \cdot \\ \cdot \\ \cdot \end{bmatrix}' = 2 \begin{bmatrix} 0 & 0 & 0 & 0 & 0 & \ldots \\ 1 & 0 & 0 & 0 & 0 & \ldots \\ 1 & 2 & 0 & 0 & 0 & \ldots \\ 2 & 1 & 3 & 0 & 0 & \\ 2 & 3 & 1 & 4 & 0 & \\ \cdot & \cdot & \cdot & & & \\ \cdot & \cdot & \cdot & & & \\ \cdot & \cdot & \cdot & & & \end{bmatrix} \begin{bmatrix} \alpha_1 \\ \alpha_2 \\ \alpha_3 \\ \alpha_4 \\ \alpha_5 \\ \cdot \\ \cdot \\ \cdot \end{bmatrix}. \tag{5.39$_1$}$$

$$\begin{bmatrix} \gamma_1 \\ \gamma_2 \\ \gamma_3 \\ \gamma_4 \\ \gamma_5 \\ \cdot \\ \cdot \\ \cdot \end{bmatrix}' = 2 \begin{bmatrix} 0 & 0 & 0 & 0 & 0 & \ldots \\ 1 & 0 & 0 & 0 & 0 & \ldots \\ -1 & 2 & 0 & 0 & 0 & \ldots \\ 2 & -1 & 3 & 0 & 0 & \\ -2 & 3 & -1 & 4 & 0 & \\ \cdot & \cdot & \cdot & & & \\ \cdot & \cdot & \cdot & & & \\ \cdot & \cdot & \cdot & & & \end{bmatrix} \begin{bmatrix} \gamma_1 \\ \gamma_2 \\ \gamma_3 \\ \gamma_4 \\ \gamma_5 \\ \cdot \\ \cdot \\ \cdot \end{bmatrix}. \tag{5.39$_2$}$$

Thus we may write the infinite matrix equations

$$\{\alpha_n\}' = [D^{\alpha}_{mn}]\{\alpha_n\}, \tag{5.40$_1$}$$

$$\{\gamma_n\}' = [D^{\gamma}_{mn}]\{\gamma_n\}, \tag{5.40$_2$}$$

where the differentiating matrices $[D^{\alpha}_{mn}]$ and $[D^{\gamma}_{mn}]$ are as shown in (5.39). For higher derivatives, we have

$$\{\alpha_n\}^{(k)} = [D^{\alpha}_{mn}]^{(k)}\{\alpha_n\}, \tag{5.41$_1$}$$

$$\{\gamma_n\}^{(k)} = [D^{\gamma}_{mn}]^{(k)}\{\gamma_n\}, \tag{5.41$_2$}$$

where (k) refers to the order of the derivative on the left hand side and to the power of the differentiating matrix on the right hand side.

Formulas expressing derivatives of the airfoil polynomials in terms the airfoil polynomials can also be derived in general by making use of their Fourier series properties.[1] Since the derivative of a polynomial is a polynomial of one degree less, we have

$$\alpha_n'(x) = \sum_{m=1}^{n-1} <\alpha_n', \alpha_m>_{\alpha} \alpha_m(x),$$

where the Fourier coefficients are given by

$$<\alpha_n', \alpha_m>_{\alpha} = \int_{-1}^{1} \sqrt{\frac{1+x}{1-x}}\, \alpha_n'(x)\alpha_m(x)\,dx.$$

Referring to equation (5.4), the substitution

$$x = \cos\theta,$$

together with the use of elementary trigonometric identities leads to

$$<\alpha_n', \alpha_m>_{\alpha} = \frac{1}{\pi}\int_0^{\pi} \left((n-\frac{1}{2})\,\frac{\sin(n+m-1)\theta+\sin(n-m)\theta}{\sin\theta}\right.$$

$$\left. - \frac{1}{2}\,\frac{\cos(m+n-1)\theta+\cos(n-m)\theta}{1+\cos\theta}\right)d\theta, \quad 1\le m\le n-1. \tag{5.42}$$

---

[1] S.R. Bland, private communication, dated 3 August 1977.

The tabulated integrals [39,p.366]

$$\frac{1}{\pi}\int_0^{\pi} \frac{\sin n\theta}{\sin \theta}\, d\theta = 0 \text{ if } n \text{ is even},$$

$$\frac{1}{\pi}\int_0^{\pi} \frac{\sin n\theta}{\sin \theta}\, d\theta = 1 \text{ if } n \text{ is odd},$$

$$\frac{1}{\pi}\int_0^{\pi} \frac{\cos n\theta}{1+a\cos \theta}\, d\theta = \frac{1}{\sqrt{1-a^2}}\left(\frac{\sqrt{1-a^2}-1}{a}\right)^n, \quad |a|<1$$

permit (5.42) to be calculated in general. Since for every pair (n,m) of integers, precisely one of n+m-1, n-m is odd, it follows that

$$\frac{1}{\pi}\int_0^{\pi} \frac{\sin(n+m-1)\theta+\sin(n-m)\theta}{\sin \theta}\, d\theta = 1.$$

By evaluating the limits

$$\lim_{a\to 1^-} \frac{1}{\pi}\int_0^{\pi} \frac{\cos(m+n-1)\theta+\cos(n-m)\theta}{1+a\cos \theta}\, d\theta$$

$$= \lim_{a\to 1^-} \left(\frac{(\sqrt{1-a^2}-1)^{m+n-1}}{\sqrt{1-a^2}\, a^{m+n-1}} + \frac{(\sqrt{1-a^2}-1)^{n-m}}{\sqrt{1-a^2}\, a^{n-m}}\right),$$

one obtains

$$\frac{1}{\pi}\int_0^{\pi} \frac{\cos(m+n-1) +\cos(n-m)\theta}{1+\cos \theta}\, d\theta = (-1)^{n-m}(2m-1).$$

In this manner, the following general formulas result,

$$\langle \alpha_n', \alpha_m \rangle_\alpha = 0 \quad \text{if } m \geq n, \tag{5.43$_1$}$$

$$\langle \alpha_n', \alpha_m \rangle_\alpha = n+m-1 \text{ if } m<n \text{ \& } n-m \text{ is odd}, \tag{5.43$_2$}$$

$$\langle \alpha_n', \alpha_m \rangle_\alpha = n-m-2 \text{ if } m<n \text{ \& } n-m \text{ is even}, \tag{5.43$_3$}$$

$$\langle \gamma_n', \gamma_m \rangle_\gamma = 0 \quad \text{if } m \geq n, \tag{5.43$_4$}$$

$$\langle \gamma_n', \gamma_m \rangle_\gamma = n+m-1 \text{ if } m<n \text{ \& } n-m \text{ is odd}, \tag{5.43$_5$}$$

$$\langle \gamma_n', \gamma_m \rangle_\gamma = n+m+2 \text{ if } m<n \text{ \& } n-m \text{ is even}, \tag{5.43$_6$}$$

which verify (5.39).

Although it appears that Bland was the first to make extensive application of the properties of the airfoil polynomials in unsteady flow problems, their use for solving singular integral equations goes back at least 40 years. In this regard we make the following historical observations.

First it can be shown that they are suitably renormalized Jacobi polynomials. Multhopp [40] (see also [41]) utilized Jacobi polynomials as early as 1938 to perform chordwise numerical integration on the problem of steady three dimensional flow over wings. This is the origin of the successful technique of interdigitated collocation and quadrature points used later by Hsu [42] and others for unsteady flow, and in the special case of one collocation point it reduces to collocating the downwash at the three-quarter chord.

The fact that H is unitary was apparently first shown by Akheizer in 1945. We became aware of this fact through the recent publication of Ivanov's book [7, p.133]. This result was obtained using the fact that $H\alpha_n = \gamma_n$. This important property occurs as a particular case of a result given by Tricomi in 1951 [31](see also [43]) who in turn refers to Szëgo's book, first published in 1939 [44].

In the western aerodynamics literature the specific form of the pressure polynomials first appeared in a 1967 paper on unsteady narrow channel flow by Bland, Rhyne and Pierce [10] and their properties were further developed in [8]. (See also [9].)

In view of the above observations it seems appropriate to name the transforms

$$H$$

and

$$H^{-1} = H^*$$

as the Akheizer-Bland transforms.

§6. Solution by collocation of the integral equation

Assume $w \in L^2_\alpha$ and $\psi \in L^2_\gamma$. Let Bland's integral equation (3.16) be written in operator notation as

$$T\psi = w. \tag{6.1}$$

Since the pressure polynomials $\{\gamma_n\}$ are a complete orthonormal basis for the pressure space L^2_γ, we have

$$\psi = \sum_{n=1}^{\infty} \langle \psi, \gamma_n \rangle_\gamma \gamma_n. \tag{6.2}$$

Because of this, we seek an approximate solution ψ_N to (6.1) of the form

$$\psi_N = \sum_{n=1}^{N} a_{nN} \gamma_n, \tag{6.3}$$

where $\{a_{nN}\}_{n=1}^{N}$ are to be determined. Substituting (6.3) into (6.1) gives

$$\sum_{n=1}^{N} a_{nN}\, T\gamma_n + r_N = w, \tag{6.4}$$

where

$$r_N = w - T\psi_N = T(\psi - \psi_N) \tag{6.5}$$

is the resulting downwash residual error. The general collocation equations are that

$$r_N(x_m) = 0; \quad m = 1, \ldots, N \tag{6.6}$$

where $\{x_m\}_1^N$ are the collocation points. Equation (6.6) may be written in matrix form as

$$[C^N_{mn}]\{a_{nN}\} = \{w(x_m)\}, \tag{6.7}$$

where $[C^N_{mn}]$ is the NxN collocation matrix given by

$$C^N_{mn} = (T\gamma_n)(x_m). \tag{6.8}$$

To compute the collocation matrix, it is convenient to split the operator T into

three parts. Referring to (3.10), we may write

$$T = H + K_L + K_c, \tag{6.9}$$

where H is the Akheizer-Bland transform, where K_L is given by

$$(K_L f)(x) = \frac{ik}{\pi\beta^2} \int_{-1}^{1} \sqrt{\frac{1-\xi}{1+\xi}} \log |x-\xi| f(\xi) d\xi, \tag{6.10}$$

and where K_c is the remaining part of the transformation with continuous kernel,

$$(K_c f)(x) = -\frac{1}{\pi} \int_{-1}^{1} \sqrt{\frac{1-\xi}{1+\xi}} K_c(x-\xi) f(\xi) d\xi. \tag{6.11}$$

In Bland's collocation method, the collocation points x_m are selected as the zeros x_m^{N+1} of the downwash polynomial α_{N+1}. The unitary and logarithmic parts are then computed exactly by (5.3) and (5.24), and the continuous part is computed approximately by (5.30) using N point Jacobi-Gaussian quadrature. Thus,

$$C_{mn}^N = \alpha_n(x_m^{N+1}) - \frac{ik}{\beta^2} \langle \log_{x_m} {}_{N+1}, \gamma_n \rangle_\gamma + \sum_{i=1}^{N} \frac{1-\xi_i^{N+1}}{N+\frac{1}{2}} K_c(x_m^{N+1} - \xi_i^{N+1}) \gamma_n(\xi_i^{N+1}) + E_{mn}^N. \tag{6.12}$$

The collocation solution is then completed upon solving (6.7) using (6.12) and the known downwash.

For closed wall wind tunnels, Bland [9] observed that (6.12) produced rapid convergence with N for smooth downwashes but offered no proof of convergence. In [5], we observed similar convergence characteristics for ventilated tunnels and established a rigorous proof of convergence of the method based on a three-way equivalence between collocation, complex least squares and Galerkin's method. Specifically, we showed that solving (6.7) using (6.12) gives

$$\lim_{N\to\infty} a_{nN} = \langle \psi, \gamma_n \rangle_\gamma \tag{6.13}$$

under very general conditions. In section 10 below we present a direct proof of convergence with sharper error estimates and discuss the computational problem of weak convergence in the presence of flaps. In section 11, we discuss various methods of accelerating convergence and show that a 500 fold reduction in error can be achieved for flaps with approximately a 20% increase in computing time. In section 12 we demonstrate an improved method of computing C_{mn}^N for unsteady flow which reduces quadrature errors in (6.12) by approximately 1000.

§7. Computation of airloads

7.1 Basic equations

Once the Fourier coefficients $\langle \psi, \gamma_n \rangle_\gamma$ are known, it is an easy matter to compute pressures from the expression

$$\Delta p(x) = \frac{4}{\beta} \sqrt{\frac{1-x}{1+x}} \sum_{n=1}^{\infty} \langle \psi, \gamma \rangle_\gamma \, \gamma_n(x). \tag{7.1}$$

Let the lift and moment coefficients be defined as in Ashley [45,p.53] according to

$$L = \frac{1}{2} \rho_\infty v_\infty^2 \, S \, C_L, \quad M = \frac{1}{2} \rho_\infty v_\infty^2 \, S \, \bar{c} \, C_M, \tag{7.2}$$

where L denotes lift, M denotes pitching moment about the quarter chord, positive in the direction of increasing angle of attack, S denotes planform surface area, and where $\bar{c}$ denotes mean aerodynamic chord. Then for an airfoil the lift and moment coefficients and center of pressure reduce to

$$C_L = \frac{1}{2} \int_{-1}^{1} \Delta p(x) dx = \frac{2\sqrt{\pi}}{\beta} \langle \psi, \gamma_1 \rangle_\gamma, \tag{7.3}$$

$$C_M = -\frac{1}{4} \int_{-1}^{1} (x+\tfrac{1}{2}) \Delta p(x) dx = -\frac{\sqrt{\pi}}{2\beta} \langle \psi, \gamma_2 \rangle_\gamma, \tag{7.4}$$

$$x_{CP} = \frac{1}{4} - \frac{C_M}{C_L}. \tag{7.5}$$

These particularly simple formulas involve only the first two pressure Fourier coefficients because of the orthogonality properties of the airfoil polynomials, and are among the most accurately computed quantities in the TWODI program.

The aerodynamic work matrix is useful in the solution of aeroelastic problems. Let the displacement function be expressed formally as

$$h(x,\omega) = \sum_{m=1}^{\infty} q_m(\omega) h_m(x) \tag{7.6}$$

where h_m are displacement basis functions and q_m are generalized coordinates in the sense of Lagrange's equations. Then the components of the aerodynamic work matrix

are given by

$$A_{mn} = \frac{\beta}{8} \int_{-1}^{1} \frac{\partial h}{\partial q_m} \frac{\partial \Delta p}{\partial q_n} d\xi, \tag{7.7}$$

or equivalently by

$$A_{mn} = \frac{1}{2} \int_{-1}^{1} \sqrt{\frac{1-x}{1+x}}\, h_m(x) \psi_n(x) dx, \tag{7.8}$$

where ψ_n represents the pressure factor corresponding to the displacement function h_n. The components of this matrix depend upon the particular deflection basis used (which in practice is often selected as the in vacuo vibrational eigenfunctions). We will assume that all displacement functions and their derivatives belong to L^2_α; that is, each h_n has a downwash function in L^2_α. Expanding both ψ_n and h_n in the pressure Fourier series, and integrating, (7.8) becomes

$$[A_{mn}] = \frac{1}{2} [\langle h_m, \gamma_n \rangle] [\langle \psi_m, \gamma_n \rangle_\gamma]^*, \tag{7.10}$$

where * denotes the complex conjugate transpose.

7.2 Energy properties of the airfoil polynomials

In our earlier report [5], we compared the results from the TWODI program against the exact Söhngen and Kussner-Schwarz solutions, and made a precise determination of the accuracy of TWODI. Originally, we used the downwash polynomials as a basis for the deflections and calculated the integrals for the aerodynamic work matrix using numerical integration. We have since observed that if one selects the pressure polynomials as the displacement basis, then the aerodynamic work matrix in steady free atmosphere flow is upper triangular with zero diagonal elements. To see this, choose the displacement basis functions as the pressure polynomials

$$h_n = \gamma_n;\ n = 1,2,... \tag{7.11}$$

Then the downwash functions

$$w_n = \gamma_n', \tag{7.12}$$

are readily found to be

$$w_1 = 0, \tag{7.13$_1$}$$

$$w_2 = 2a_1, \tag{7.13$_2$}$$

$$w_3 = 6a_1 + 4a_2, \tag{7.13$_3$}$$

$$w_4 = 12a_1 + 10a_2 + 6a_3, \tag{7.13$_4$}$$

$$w_5 = 20a_1 + 18a_2 + 14a_3 + 8a_4,..., \tag{7.13$_5$}$$

using (5.33) and (5.34). Using (5.12), the pressures Δp_n corresponding to each of the above w_n are given by

$$\Delta p_1 = \frac{8}{\beta}\sqrt{\frac{1-x}{1+x}}\,(0), \tag{7.14$_1$}$$

$$\Delta p_2 = \frac{8}{\beta}\sqrt{\frac{1-x}{1+x}}\,(\gamma_1), \tag{7.14$_2$}$$

$$\Delta p_3 = \frac{8}{\beta}\sqrt{\frac{1-x}{1+x}}\,(3\gamma_1+2\gamma_2), \tag{7.14$_3$}$$

$$\Delta p_4 = \frac{8}{\beta}\sqrt{\frac{1-x}{1+x}}\,(6\gamma_1+5\gamma_2+3\gamma_3), \tag{7.14$_4$}$$

$$\Delta p_5 = \frac{8}{\beta}\sqrt{\frac{1-x}{1+x}}\,(10\gamma_1+9\gamma_2+7\gamma_3+8\gamma_4),... \tag{7.14$_5$}$$

Therefore, by inspection, the lift and pitching moment coefficients and center of pressure are given by

$$C_{L_1} = 0 \quad , C_{M_1} = 0, \tag{7.15$_1$}$$

$$C_{L_2} = \frac{4\sqrt{\pi}}{\beta} , C_{M_2} = 0, \quad , \bar{x}_2 = .2500, \tag{7.15$_2$}$$

$$C_{L_3} = \frac{12\sqrt{\pi}}{\beta}, C_{M_3} = -\frac{4\sqrt{\pi}}{\beta} , \bar{x}_3 = .5833, \tag{7.15$_3$}$$

$$C_{L_4} = \frac{24\sqrt{\pi}}{\beta}, C_{M_4} = -\frac{10\sqrt{\pi}}{\beta}, \bar{x}_4 = .6667, \tag{7.15$_4$}$$

$$C_{L_5} = \frac{40\sqrt{\pi}}{\beta}, C_{M_5} = -\frac{18\sqrt{\pi}}{\beta}, \bar{x}_5 = .7000,... \tag{7.15$_5$}$$

and the aerodynamic work matrix is

$$[A_{mn}] = \begin{bmatrix} 0 & 1 & 3 & 6 & 10... \\ 0 & 0 & 2 & 5 & 9... \\ 0 & 0 & 0 & 3 & 7... \\ 0 & 0 & 0 & 0 & 4 \\ 0 & 0 & 0 & 0 & 0 \\ \vdots & \vdots & \vdots & & \end{bmatrix} \tag{7.16}$$

Because the components A_{mn} represent the work done on the structure as it deforms in mode m against the pressure due to mode n, it follows that <u>for steady free atmosphere flow, zero aerodynamic work is done on the structure as it deforms into the pure shape of any of the pressure basis functions</u>. The first column A_{m1} is trivially zero because the pressure is zero in steady vertical translation. The second column A_{m2} represents the work done as the structure deforms in its various modes against the pressure due to the second mode. In the second pressure mode, only the first deflection mode produces work on the structure, and since the second displacement mode represents a flat plate at uniform angle of attack, the element A_{12} corresponds to the lift coefficient derivative C_{L_α}. The diagonal element A_{22} represents the work done in pitching the airfoil about the node of mode 2; since this node and the center of pressure are both at the quarter chord, no aerodynamic work is done. Similar interpretations involving the flexible modes may be made for columns 3,4,...

7.3 Transformation properties of unsteady airloads

If the unsteady airloads are known with respect to one set of structural (displacement) basis functions, then they can be computed with respect to any other set of basis functions, provided the transformation from one basis to the other is known. This is a direct consequence of the invariance of airloads under change of basis.

To see this, let $\{h_m\}$ and $\{\hat{h}_m\}$ be two bases for the Hilbert space L^2_h of airfoil displacements and let $\{q_m\}$ and $\{\hat{q}_m\}$ be their corresponding generalized coordinates. Then

$$h(x,\omega) = \sum_{m=1}^{\infty} q_m(\omega) h_m(x) = \sum_{m=1}^{\infty} \hat{q}_m(\omega) \hat{h}_m(x) \tag{7.17}$$

(Throughout this subsection, we will regard all infinite series expressions in a formal sense.) Due to the assumed linearity of the problem, the pressure factor depends linearly upon the displacement and may be expressed as

$$\psi = \sum_{m=1}^{\infty} q_m \psi_m = \sum_{m=1}^{\infty} \hat{q}_m \hat{\psi}_m \tag{7.18}$$

where ψ_m and $\hat{\psi}_m$ represent the pressure factors due to h_m and $\hat{h}_m$, respectively. Similarly, the lift and pitching moment coefficients are given by

$$C_L = \sum_{m=1}^{\infty} q_m C_{L_m} = \sum_{m=1}^{\infty} \hat{q}_m \hat{C}_{L_m}, \tag{7.19}$$

$$C_M = \sum_{m=1}^{\infty} q_m C_{M_m} = \sum_{m=1}^{\infty} \hat{q}_m \hat{C}_{M_m}, \tag{7.20}$$

where C_{L_m} and C_{M_m}, and $\hat{C}_{L_m}$ and $\hat{C}_{M_m}$ represent the lift and pitching moment coefficients due to h_m and $\hat{h}_m$, respectively. The components of the aerodynamic work matrix are given by

$$A_{mn} = \frac{1}{2} \int_{-1}^{1} h_m \psi_n d\xi, \quad \hat{A}_{mn} = \frac{1}{2} \int_{-1}^{1} \hat{h}_m \hat{\psi}_n d\xi. \tag{7.21}$$

To establish the transformations between airloads in the $\{h_m\}$ basis and the $\{\hat{h}_m\}$ basis, we utilize the transformations (assumed known)

$$h_m = \sum_{n=1}^{\infty} \hat{H}_{mn} \hat{h}_n, \quad \hat{h}_m = \sum_{n=1}^{\infty} H_{mn} h_n \tag{7.22}$$

between these bases. Clearly these transformation matrices are the inverses of one another

$$\sum_{m=1}^{\infty} H_{\ell m} \hat{H}_{mn} = \delta_{\ell n}, \quad \sum_{m=1}^{\infty} \hat{H}_{\ell m} H_{mn} = \delta_{\ell n}. \tag{7.23}$$

Substituting (7.22) into (7.18)-(7.20) and equating coefficients of generalized coordinates gives the transformations between pressures and section coefficients,

$$\psi_m = \sum_{n=1}^{\infty} \hat{H}_{mn}\, \hat{\psi}_n, \quad \hat{\psi}_m = \sum_{n=1}^{\infty} H_{mn} \psi_n, \tag{7.24}$$

$$C_{L_m} = \sum_{n=1}^{\infty} \hat{H}_{mn}\, \hat{C}_{L_n}, \quad \hat{C}_{L_m} = \sum_{n=1}^{\infty} H_{mn}\, C_{L_n}, \tag{7.25}$$

$$C_{M_m} = \sum_{n=1}^{\infty} \hat{H}_{mn}\, \hat{C}_{M_n}, \quad \hat{C}_{M_m} = \sum_{n=1}^{\infty} H_{mn}\, C_{M_n}. \tag{7.26}$$

Combining (7.27) and (7.21), we immediately obtain

$$\int_{-1}^{1} \sqrt{\frac{1-\xi}{1+\xi}}\, h_m\, \psi_n\, d\xi = \sum_{k=1}^{\infty} \sum_{\ell=1}^{\infty} \hat{H}_{mk} \int_{-1}^{1} \sqrt{\frac{1-\xi}{1+\xi}}\, \hat{h}_k\, \hat{\psi}_\ell\, d\xi\, \hat{H}_{n\ell}, \tag{7.27$_1$}$$

$$\int_{-1}^{1} \sqrt{\frac{1-\xi}{1+\xi}}\, \hat{h}_m\, \hat{\psi}_n\, d\xi = \sum_{k=1}^{\infty} \sum_{\ell=1}^{\infty} H_{mk} \int_{-1}^{1} \sqrt{\frac{1-\xi}{1+\xi}}\, h_k\, \psi_\ell\, d\xi\, H_{n\ell}. \tag{7.27$_2$}$$

Thus, the components of the aerodynamic work matrix transform according to a *congruence transformation*: i.e.,

$$A_{mn} = \sum_{k=1}^{\infty} \sum_{\ell=1}^{\infty} \hat{H}_{mk}\, \hat{A}_{k\ell}\, \hat{H}_{n\ell}, \quad \hat{A}_{mn} = \sum_{k=1}^{\infty} \sum_{\ell=1}^{\infty} H_{mk}\, A_{k\ell}\, H_{n\ell}. \tag{7.28}$$

These transformations may be stated in matrix notation as

$$\{\psi_m\} = [\hat{H}_{mn}]\{\hat{\psi}_n\}, \quad \{\hat{\psi}_n\} = [H_{mn}]\{\psi_n\}, \tag{7.29}$$

$$\{C_{L_M}\} = [\hat{H}_{mn}]\{\hat{C}_{L_n}\}, \quad \{\hat{C}_{L_M}\} = [H_{M_n}]\{C_{L_n}\}, \tag{7.30}$$

$$\{C_{M_m}\} = [\hat{H}_{mn}]\{\hat{C}_{M_n}\}, \quad \{\hat{C}_{M_m}\} = [H_{mn}]\{C_{M_n}\}. \tag{7.31}$$

$$[A_{mn}] = [\hat{H}_{mn}][\hat{A}_{mn}][\hat{H}_{mn}]^T, \quad [\hat{A}_{mn}] = [H_{mn}][A_{mn}][H_{mn}]^T. \tag{7.32}$$

The above results are valid for an arbitrary pair $\{h_m\}$, $\{\hat{h}_m\}$ of bases for H_h. The special case $\{\hat{h}_m\} = \{\gamma_m\}$ is of particular interest. Since in this case

$$\hat{H}_{mn} = \langle h_m, \gamma_n \rangle_\gamma, \tag{7.33}$$

it follows that

$$\{\phi_m\} = [\langle h_m, \gamma_n \rangle_\gamma]\{\hat{\phi}_n\}, \tag{7.34}$$

$$\{C_{L_m}\} = [\langle h_m, \gamma_n \rangle_\gamma]\{\hat{C}_{L_n}\}, \tag{7.35}$$

$$\{C_{M_m}\} = [\langle h_m, \gamma_n \rangle_\gamma]\{\hat{C}_{M_n}\}, \tag{7.36}$$

$$[A_{mn}] = \frac{1}{2}\,[\langle h_m, \gamma_n \rangle_\gamma][\langle \phi_m, \gamma_n \rangle_\gamma]^*[\langle h_m, \gamma_n \rangle_\gamma]^T. \tag{7.37}$$

The formulations (7.34)-(7.37) have the advantage that the particular deflection basis $\{h_m\}$ can be factored from the solution process. In addition, the corresponding vector of downwashes may be computed by transforming the deflection basis to the downwash polynomials using (5.35)

$$(\frac{d}{dx}+ik)\{\gamma_m\} = (\frac{d}{dx} + ik)[G^\gamma_{mn}]\{a_n\} = [G^\gamma_{mn}](\frac{d}{dx} + ik)\{a_n\}$$

and then differentiating using (5.40_1) to obtain

$$(\frac{d}{dx}+ik)\{\gamma_m\} = [G^\gamma_{mn}][D^a_{mn}+ik\delta_{mn}]\{a_n\}, \tag{7.38}$$

or equivalently, by differentiating first using (5.40_2)

$$(\frac{d}{dx}+ik)\{\gamma_m\} = [D_{mn}+ik\delta_{mn}]\{\gamma_n\}$$

and then transforming to the downwash basis functions to obtain

$$(\frac{d}{dx}+ik)\{\hat{\gamma}_m\} = [D^\gamma_{mn} + ik\delta_{mn}][G^\gamma_{mn}]\{a_n\}. \tag{7.39}$$

Since all matrices in (7.38) and (7.39) are lower triangular, the resulting matrix product

$$[\hat{w}_{mn}] = [G^\gamma_{mn}][D^a_{mn} + ik\delta_{mn}] = [D^\gamma_{mn} + ik\delta_{mn}][G^\gamma_{mn}] \tag{7.40}$$

must be lower triangular also. Following (7.38),

$$[\hat{W}_{mn}] = 2 \begin{bmatrix} 1 & 0 & 0 & 0 & 0 & 0 & 0 & \cdots \\ 2 & 1 & 0 & 0 & 0 & 0 & 0 & \cdots \\ 2 & 2 & 1 & 0 & 0 & 0 & 0 & \cdots \\ 2 & 2 & 2 & 1 & 0 & 0 & 0 & \\ 2 & 2 & 2 & 2 & 1 & 0 & 0 & \\ 2 & 2 & 2 & 2 & 2 & 1 & 0 & \\ 2 & 2 & 2 & 2 & 2 & 2 & 1 & \\ \vdots & \vdots & \vdots & & & & & \end{bmatrix} \begin{bmatrix} ik & 0 & 0 & 0 & 0 & 0 & 0 & \cdots \\ 1 & ik & 0 & 0 & 0 & 0 & 0 & \cdots \\ 1 & 2 & ik & 0 & 0 & 0 & 0 & \cdots \\ 2 & 1 & 3 & ik & 0 & 0 & 0 & \\ 2 & 3 & 1 & 4 & ik & 0 & 0 & \\ 3 & 2 & 4 & 1 & 5 & ik & 0 & \\ 3 & 4 & 2 & 5 & 1 & 6 & ik & \\ \vdots & \vdots & \vdots & & & & & \end{bmatrix} .$$

Following (7.40),

$$[\hat{W}_{mn}] = 2 \begin{bmatrix} ik & 0 & 0 & 0 & 0 & 0 & 0 & \cdots \\ 1 & ik & 0 & 0 & 0 & 0 & 0 & \cdots \\ -1 & 2 & ik & 0 & 0 & 0 & 0 & \cdots \\ 2 & -1 & 3 & ik & 0 & 0 & 0 & \\ -2 & 3 & -1 & 4 & ik & 0 & 0 & \\ 3 & -2 & 4 & -1 & 5 & ik & 0 & \\ -3 & 4 & -2 & 5 & -1 & 6 & ik & \\ \vdots & \vdots & \vdots & & & & & \end{bmatrix} \begin{bmatrix} 1 & 0 & 0 & 0 & 0 & 0 & 0 & \cdots \\ 2 & 1 & 0 & 0 & 0 & 0 & 0 & \cdots \\ 2 & 2 & 1 & 0 & 0 & 0 & 0 & \cdots \\ 2 & 2 & 2 & 1 & 0 & 0 & 0 & \\ 2 & 2 & 2 & 2 & 1 & 0 & 0 & \\ 2 & 2 & 2 & 2 & 2 & 1 & 0 & \\ 2 & 2 & 2 & 2 & 2 & 2 & 1 & \\ \vdots & \vdots & \vdots & & & & & \end{bmatrix} .$$

One obtains the same result both ways.

$$[\hat{W}_{mn}] = 2 \begin{bmatrix} ik & 0 & 0 & 0 & 0 & \cdots \\ 1+2ik & ik & 0 & 0 & 0 & \cdots \\ 3+2ik & 2+2ik & ik & 0 & 0 & \cdots \\ 6+2ik & 5+2ik & 3+2ik & ik & 0 & \\ 10+2ik & 9+2ik & 7+2ik & 4+2ik & ik & \\ \vdots & \vdots & \vdots & & & \end{bmatrix} . \tag{7.41}$$

The matrix $[\hat{W}_{mn}]$ represents the linear transformation of downwash from the deflection basis $\{\gamma_m\}$ to downwash basis $\{\alpha_n\}$.

$$(\frac{d}{dx} + ik)\{\gamma_m\} = [\hat{W}_{mn}]\{\alpha_n\} \tag{7.42}$$

It is nonsingular if and only if the frequency is nonzero.

Referring back to equation (7.21), we see that the aerodynamic work matrix corresponding to this basis is given by

$$[\hat{A}_{mn}] = \frac{1}{2}\,[<\hat{\psi}_m, \gamma_n>_\gamma]^* \tag{7.43}$$

where $\hat{\psi}_m$ satisfies Bland's integral equation for the basis function $\hat{h}_m = \gamma_m$,

$$(\frac{d}{dx} + ik)\gamma_m = T\,\hat{\psi}_m. \tag{7.44}$$

In the special case of steady flow in an infinite atmosphere, (5.13) states that the Fourier coefficients of pressure in the basis $\{\gamma_n\}$ must equal the Fourier coefficients of downwash in the basis $\{\alpha_n\}$; i.e.,

$$<\hat{\psi}_m, \gamma_n>_\gamma = <(\frac{d}{dx} + ik)\gamma_m, \alpha_n>_\alpha = \hat{W}_{mn}.$$

This gives

$$(k=0 \;\&\; \eta=\infty) \qquad [\hat{A}_{mn}] = \frac{1}{2}\,[\hat{W}_{mn}]^T, \tag{7.45}$$

which reduces by inspection to equation (7.16) that previously was derived without benefit of the above matrix developments.

In general the aerodynamic work matrix is nonsymmetric. Physically this is because the interaction between the air and the airplane structure is nonconservative. Mathematically it cannot be guaranteed that an arbitrary nonsymmetric matrix is congruent to a triangular matrix. In other words on purely mathematical grounds there need not exist a deflection basis in which the aerodynamic work matrix is triangular. However it has been shown above in (7.16) and (7.45) that if the pressure polynomials are used as a deflection basis then the aerodynamic work matrix is in fact upper triangular for steady flow in an infinite atmosphere. At the present time, the meaning of this result is not fully clear, but it does cast the airfoil polynomials in a special role.

A somewhat more abstract algebraic interpretation may be given to the transformation properties (7.29)-(7.32) of the unsteady airloads. In the case of linear aerodynamics, the pressure factor depends linearly upon the airfoil displacements. Therefore, by the Riesz representation theorem, the vector space L^2_γ of pressure factors is contained in the dual space L^{2*}_h of airfoil displacements

$$L^2_\gamma \subset L^{2*}_h.$$

In this regard the section coefficients are functions which map elements of the dual space L_h^{2*} linearly into the complex numbers

$$C_L : L_h^{2*} \to \mathbb{C}$$

$$C_M : L_h^{2*} \to \mathbb{C}$$

and are therefore pure contravariant tensors of order 1 relative to L_h^2 [46,p.12]. In the same regard, the aerodynamic work matrix is a function which maps pairs of elements from the vector space of displacements L_h^2 and its dual space L_h^{2*} bilinearly into the complex numbers, i.e.,

$$[A_{mn}] : L_h^2 \times L_h^{2*} \to C.$$

and is therefore a mixed tensor of contravariant order 1 and covariant order 1 relative to L_h^2 [op cit].

§8. Representation of airfoils with multiple controls

In section 7 we discussed how unsteady airloads can be calculated for a general airfoil displacement in terms of the airloads corresponding to an arbitrary displacement basis and that certain advantages accrue if the airfoil pressure polynomials $\{\gamma_m\}$ are used as the canonical basis for displacements. This section describes how displacement functions $\{h_m\}$ possessing discontinuities of the type found with multiple leading and trailing edge controls can be specified by discrete input data, and how the matrix of Fourier coefficients

$$[\hat{H}_{mn}] = [\langle h_m, \gamma_n \rangle_\gamma]$$

can be calculated for such functions.

8.1 Input data specification of displacements

Consider an airfoil displacement function of the type illustrated in Figure 1. Such a function may represent an upper, lower or mean profile. There may be multiple leading and trailing edge controls with sealed gaps. Discontinuities in the first derivative of the displacement function usually correspond to control deflections. Discontinuities in higher derivatives correspond to changes in curvature due to design and/or aeroelastic effects such as changes in stiffness properties, etc.

Values of displacement will be specified at N_x distinct points

$$x_1, \ldots, x_{N_x}$$

which are called nodes. We shall assume without loss of generality that nodes are labeled from left to right along the chord.

$$x_1 < \ldots < x_{N_x} \tag{8.1}$$

The number of nodes may range from a minimum of one to some finite number $N_{x_{max}}$,

$$1 \leq N_x \leq N_{x_{max}}. \tag{8.2}$$

In addition, nodal values of N_h different displacement functions

$$h_{11}, \ldots, h_{1N_x}, \ldots, h_{N_h N_x}$$

are to be given as input data. Some of the nodes may also be hinges at which discontinuities in derivatives of displacement can occur. Hinge points must lie strictly between the leading and trailing edges.

$$-1<x_{m_1}<\ldots<x_{m_{N_\delta}}<1 \tag{8.3}$$

The total number of hinges may range from zero if there are none to at most $N_{\delta_{max}}$.

$$0\leq N_\delta \leq N_{\delta_{max}} \tag{8.4}$$

8.2 Subdivision of the chord into line elements

This subsection describes the procedure for computing interpolation functions of airfoil displacements with hinge type discontinuities. The scheme employed subdivides the chord into line elements and is illustrated in Figure 4 for two hinges.

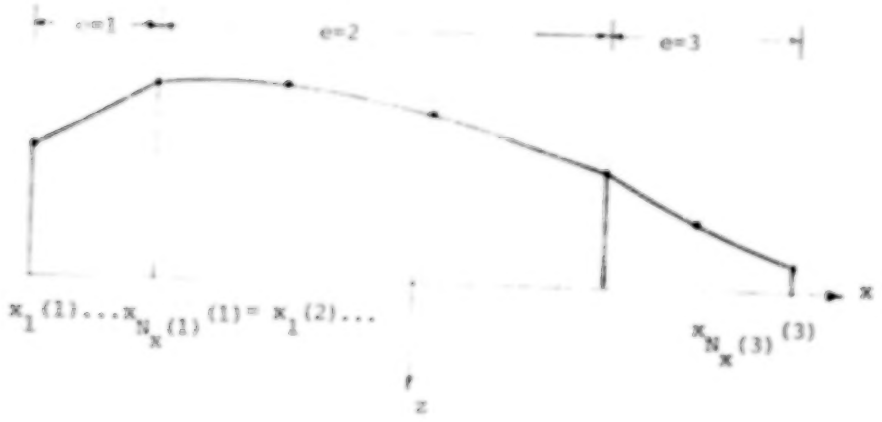

Figure 4. Subdivision into line elements

The number of line elements along the chord equals one more than the number of hinges.

$$N_e = 1 + N_\delta \tag{8.5}$$

If there is only one element, the element domain lies between the leading and trailing edges.

$$\Omega_e = \{x : -1<x<1\} \quad \text{if } e = 1 \;\&\; N_e = 1 \tag{8.6}$$

If there are more than one element, the first and last domains lie respectively between the leading edge and the first hinge, and between the last hinge and the trailing edge.

$$\Omega_e = \{x : -1<x<x_{n_1}\} \quad \text{if } e = 1 \;\&\; N_e>1 \tag{8.7}$$

$$\Omega_e = \{x : x_{n_{N_\delta}}<x<1\} \quad \text{if } e = N_e \;\&\; N_e>1 \tag{8.8}$$

All remaining domains are bounded by hinges.

$$\Omega_e = \{x : x_{n_{e-1}} < x < x_{n_e}\} \text{ if } 1 < e < N_e. \tag{8.9}$$

For theoretical purposes, these domains are disjoint, i.e.,

$$\Omega_{e_1} \cap \Omega_{e_2} = \phi \text{ if } e_1 \neq e_2,$$

their closures intersect only at hinges,

$$\bar{\Omega}_{e_1} \cap \bar{\Omega}_{e+1} = \{x_{n_e}\}, \ 1 \leq e \leq N_e - 1,$$

and the interior of the union of their closures equals the entire chord between the leading and trailing edges.

$$\Omega = \text{int}\left(\bigcup_{e=1}^{N_e} \bar{\Omega}_e\right) = \{x : -1 < x < 1\}.$$

These properties are those required of finite element models [47,Ch.6]. Thus, the interpolation procedures for the present method of solution in TWODI are consistent with the finite element method. The advantage of the element by element formulation above is that the interpolating functions for each element may be determined separately and by a uniform procedure.

The numbers $N_x(e)$ of nodes contained in the closure $\bar{\Omega}_e$ of the various line elements are given by

$$N_x(e) = N_x \text{ if } e = 1 \ \& \ N_e = 1, \tag{8.10}$$

$$N_x(e) = n_1 \text{ if } e = 1 \ \& \ N_e > 1, \tag{8.11}$$

$$N_x(e) = 1 + n_e - n_{e-1} \text{ if } 1 < e < N_e \ \& \ N_e > 1, \tag{8.12}$$

$$N_x(e) = 1 + N_x - n_{e-1} \text{ if } e = N_e \ \& \ N_e > 1. \tag{8.13}$$

The particular nodes $x_n(e)$ which are contained in $\bar{\Omega}_e$ are given by

$$x_n(e) = x_n \text{ if } 1 \leq n \leq N_x(e) \ \& \ e = 1, \tag{8.14}$$

$$x_n(e) = x_{n-1+m_{e-1}} \text{ if } 1 \leq n \leq N_x(e) \ \& \ 2 \leq e \leq N_e. \tag{8.15}$$

In this manner, the last node of one element is the same as the first node of the next element, as is indicated in Figure 4.

The nodal values of deflections within each element are given in similar fashion.

$$h_{mn}(e) = h_{mn} \text{ if } 1 \leq m \leq N_h \ \& \ 1 \leq n \leq N_x(e) \ \& \ e = 1, \tag{8.16}$$

$$h_{mn}(e) = h_{m,n-1+n_{e-1}} \text{ if } 1 \leq m \leq N_h \ \& \ 1 \leq n \leq N_x(e) \ \& \ 2 \leq e \leq N_e. \tag{8.17}$$

The interpolation functions which will be employed to represent displacements are <u>airfoil polynomial splines</u>

$$h_m^e(x) = \sum_{\ell=1}^{N_x(e)} \hat{H}_{m\ell}(e)\ \gamma_\ell(x),\ 1\le m\le N_h,\ 1\le e\le N_e. \tag{8.18}$$

At each element nodal point $x_n(e)\in\bar{\Omega}_e$, we require that the value of each interpolation function equal the value of displacement prescribed by input data. Thus,

$$h_{mn}(e) = \sum_{\ell=1}^{N_x(e)} \gamma_\ell(x_n(e))\hat{H}_{m\ell}(e),\ 1\le n\le N_x(e),\ 1\le m\le N_h,\ 1\le e\le N_e. \tag{8.19}$$

Since the airfoil polynomials are unisolvent [5,p.42] each coefficient matrix

$$[\gamma_\ell(x_n(e))],\ 1\le \ell,n\le N_x(e),\ 1\le e\le N_e$$

possesses an inverse, and since the nodal values,

$$h_{mn}(e),\ 1\le m\le N_h,\ 1\le n\le N_x(e),\ 1\le e\le N_e,$$

are given by (8.16) and (8.17), the coefficients

$$\hat{H}_{m\ell}(e),\ 1\le m\le N_h,\ 1\le \ell\le N_x(e),\ 1\le e\le N_e$$

are computable quantities.

8.3 Use of jump functions

Consider the displacement interpolation functions for two adjacent elements:

$$h_m^e(x) = \sum_{\ell=1}^{N_x(e)} H_{m\ell}(e)\,\gamma_\ell(x) \quad \text{if } x \in \Omega_e,$$

$$h_m^{e+1}(x) = \sum_{\ell=1}^{N_x(e+1)} \tilde{H}_{m\ell}(e+1)\gamma_\ell(x) \quad \text{if } x \in \Omega_{e+1}.$$

The expressions above are not yet in a form suitable for the solution process of TWODI because they are not uniform over the entire chord. This can be accomplished by utilizing jump functions and leads to infinite Fourier series whenever a discontinuity exists in a derivative.

A representation for h_m which is uniformly valid over both line elements

$$x \in \text{int}(\bar{\Omega} \cup \bar{\Omega}_{e+1})$$

is given by

$$\sum_{n=1}^{N_x(e)} H_{mn}(e)\gamma_n(x) + \sum_{k=1}^{N_x(e,e+1)} \sum_{\ell=k+1}^{N_x(e)} \frac{\tilde{H}_{m\ell}(e+1)-\tilde{H}_{m\ell}(e)}{k!}\gamma_\ell^{(k)}(x_{n_e})\langle x-x_{n_e}\rangle^k,$$

where

$$N_x(e,e+1) = \max\{N_x(e),\ N_x(e+1)\}-1. \tag{8.20}$$

The function above equals $h_m^e(x)$ and all its derivatives whenever $x \in \Omega_e$ and equals $h_m^{e+1}(x)$ and all its derivatives whenever $x \in \Omega_{e+1}$. At the hinge $x = x_{n_e}$, the function is continuous in accordance with the sealed gap condition, and will possess jumps in derivatives exactly equal to jumps in the derivatives from h_m^e to h_m^{e+1}.

Fourier series expansions have been computed for the jump functions

$$\langle x-a\rangle^k = \sum_{n=1}^{\infty} \langle\langle x-a\rangle^k, \gamma_n\rangle_\gamma\ \gamma_n(x) \tag{8.21}$$

as discussed above in section 5. In order to utilize these expansions, we extend the uniformization above to all chord elements by starting with the leading edge

element and adding jump contributions from all hinges downstream. It is easy to see that the result is

$$h_m(x) = \sum_{n=1}^{N_x(1)} \hat{H}_{mn}(1)\, \gamma_n(x)$$

$$+ \sum_{e=1}^{N_\delta} \sum_{k=1}^{N_x(e,e+1)} \sum_{i=k+1}^{N_x(e)} \frac{\hat{H}_{mi}(e+1)-\hat{H}_{mi}(e)}{k!}\, \gamma_i^{(k)}(x_{m_e}) \langle x-x_{m_e}\rangle^k. \tag{8.22}$$

Equation (8.22) is uniformly valid for all points $x \in \Omega$ between the leading and trailing edges.

The derivatives $\gamma_i^{(k)}(x_{n_e})$ at the hinges may be computed with the aid of equation (5.40) according to

$$\gamma_i' = \sum_{n_1=1}^{i-1} D^\gamma_{in_1}\, \gamma_{n_1}, \tag{8.23$_1$}$$

$$\gamma_i'' = \sum_{n_1=1}^{i-1} \sum_{n_2=1}^{i-2} D^\gamma_{in_1} D^\gamma_{n_1 n_2}\, \gamma_{n_2}, \tag{8.23$_2$}$$

$$\gamma_i^{(k)} = \sum_{n_1=1}^{i-1} \sum_{n_2=1}^{i-2} \cdots \sum_{n_k=1}^{i-k} D^\gamma_{in_1} D^\gamma_{n_1 n_2} \cdots D^\gamma_{n_{k-1}n_k}\, \gamma_{n_k},\ k \geq 3. \tag{8.23$_3$}$$

Upon combining (8.21)-(8.23), there results

$$h_n(x) = \sum_{n=1}^{\infty} \hat{H}_{mn}\, \gamma_n(x) \tag{8.24}$$

where $\hat{H}_{mn}$ is as introduced in (7.33) and is given by

$$\hat{H}_{mn} = \hat{H}_{mn}(1) + \sum_{e=1}^{N_\delta} \sum_{k=1}^{N_x(e,e+1)} \sum_{i=k+1}^{N_x(e)} \frac{\hat{H}_{mi}(e+1)-\hat{H}_{mi}(e)}{k!}\, \gamma_i^{(k)}(x_{n_e}) \langle\langle x_{n_e}\rangle^k, \gamma_n\rangle_\gamma \tag{8.25}$$

§9. Instructions for the use of TWODI

This section describes the preparation of input data for use of the current TWODI program (TWODI-III). It is assumed that the user knows the physical meaning of all terms used in this report and the procedures for accessing TWODI at his computer facility. Also, we reiterate that the solution is based upon the mathematical assumptions of inviscid subsonic linearized potential flow about a thin airfoil located midway between two parallel wind tunnel walls.

9.1 Summary of capabilities

TWODI will operate in either TIMESHARE (remote interactive terminals) or BATCH (noninteractive card jobs). Input and output are fully compatible between TIMESHARE and BATCH. In addition TWODI is coded in ANSI FORTRAN to achieve maximum machine independence.

TWODI will predict unsteady airloads consisting of any combination of the following output quantities:

(1) Fourier coefficients of pressure,

(2) Values of pressure,

(3) Section coefficients and center of pressure, and

(4) Aerodynamic work matrix.

The primary parameters determining the standard solution output are:

(1) Mach number,

(2) Reduced frequency,

(3) Height to chord ratio,

(4) Wall ventilation coefficient, and

(5) Airfoil profiles (i.e., displacement mode shapes).

The solution process in TWODI handles one case at a time, defined by a single combination of Mach number, reduced frequency, height to chord ratio and ventilation coefficient. Since the downwash corresponding to any given mode shape can be factored out of the solution equations, multiple downwashes are handled simultaneously within a given case.

Multiple cases may be handled under a single problem which consists of all combinations of various numbers of Mach number, reduced frequency, height to

chord ratio and ventilation coefficient. Within a given problem, selection of output quantities remains fixed.

Provision is also made to enter several different problems. This may be done by altering a previously defined problem or by entering a completely new problem. All data, including the selection of output quantities, may be changed from one problem to another, with the exception that all problems in a given run must be done in TIMESHARE only, or in BATCH only.

It is possible to solve the same problem using more than one method. This provision is preparatory to allowing TWODI to select automatically the optimum method of solution and thus to handle its own accuracy control at some time in the future. In addition certain special purpose and checkout calculations are available.

All input data are automatically checked for correctness. If the run is a BATCH job, unacceptable data are selectively deleted with an explanatory comment and execution continues to the extent that it can. If the run is an interactive TIMESHARE job the user will be prompted to correct unacceptable data.

9.2 Interactive input format for TIMESHARE

Queries and messages by TWODI are denoted with Q, responses by the user are denoted with A. Consecutive data entries must be separated by a comma or by one or more blanks. All data are assigned initial values by TWODI using subroutine INITLZ. These initial values are indicated within brackets [ ] below and are precisely defined in the glossary in section 9.4. After one or more problems have been entered, the most recently defined values are those of the most recently entered problem. In general, for default to the most recently defined values, type D followed by an immediate carriage return.

Data module 0. Introduction

Q: This is TWODI-III
FOR DEFAULT TO INITIAL OR MOST RECENTLY DEFINED VALUES
TYPE D FOLLOWED BY CARRIAGE RETURN IF IN TIMESHARE AND ENTER
AN OTHERWISE BLANK CARD WITH A D IN COLUMN 1 IF IN BATCH.
IF IN TIMESHARE TYPE HALT TO STOP.

Data module I. Run parameters

Q: ARE YOU IN TIMESHARE OR BATCH?

A: TIMESHARE [TIMESHARE]

Q: ENTER NUMBER OF LINES PER PAGE

A: Type integer number of lines per page or D followed by carriage return for default. [66]

Data module II. Output parameters

Q: ENTER TITLE

A: Type descriptive alphanumeric title of 1 to 72 characters or D followed by carriage return for default. [SAMPLE PROBLEM]

Q: ENTER DESIRED OUTPUT COMBINATION OF FOURIER, SECTION AND WORK

A: Type desired combination or D followed by carriage return for default. [FOURIER, SECTION]

Q: ENTER LIST OF PRESSURE POINTS

A. Use standard list format (refer to glossary in section 9.4). Type 0 if none or D followed by carriage return for default. [10/-.8,1]

Data module III. Flow parameters

Q: ENTER LIST OF MACH NUMBERS

A: Use standard list format or type D followed by carriage return for default. [1,0]

Q: ENTER LIST OF FREQUENCIES

A: Use standard list format or type D followed by carriage return for default. [2,0,1]

Q: ENTER LIST OF HEIGHT TO CHORD RATIOS

A: Use standard list format or type D followed by carriage return for default. [1, INFINITY]

Q: ENTER LIST OF MASS EFFECT VENTILATION COEFFICIENTS

A: Use standard list format or type D followed by carriage return for default. [1, INFINITY]

Q: ENTER LIST OF VISCOUS EFFECT VENTILATION COEFFICIENTS

A: Use standard list format or type D followed by carriage return for default. [1,0]

Data module IV. Modal parameters

Q: ENTER LIST OF NODES

A: Use standard list format or type D followed by carriage return for default. [3/-1,1]

Q: ENTER NUMBER OF MODE SHAPES

A: Type integer number of mode shapes or D followed by carriage return for default. [3]

A: ENTER MODE SHAPE 1

A: Type values of mode shape 1 at modal collcoation points or D followed by carriage return for default. $[1/\sqrt{\pi},\ 1/\sqrt{\pi}\ ,\ 1/\sqrt{\pi}]$

Repeat the last Q&A for the remaining mode shapes. $[-1/\sqrt{\pi},\ 1/\sqrt{\pi},\ 3/\sqrt{\pi}]$, $[1/\sqrt{\pi},\ -1/\sqrt{\pi},\ 5/\sqrt{\pi}]$

Q: ENTER LIST OF NODE NUMBERS OF HINGES

A: Use standard list format if downwash discontinuities are present. Type 0 if there are none or D followed by carriage return for default. [0]

Data module V. Method parameters

Q: ENTER NUMBER OF METHODS OF SOLUTION

A: Type integer number of methods of solution or type D followed by carriage return for default. [1]

Q: ENTER SOLUTION PARAMETERS FOR METHOD 1

A: Type the parameters for the first method of solution or type D followed by carriage return for default. Refer to the glossary for precise definitions. [3,5,0,0,0]

Repeat the last Q&A for the remaining methods of solution.

Data module IV. Data editing

Q: DO YOU WANT THE INPUT DATA LISTED?

A: Type YES or NO.

Q: DO YOU WANT TO MAKE CHANGES?

A: Type YES or NO.

Note: An answer of YES will result in the following sequence:

Q: DO YOU WANT TO LINE EDIT?

A: Type YES or NO.

Note: An answer of NO will result in data modules II-VI being repeated. For each data item which does not need to be corrected, simply type D followed by carriage return. An answer of YES will result in the following sequence:

Q: NOW OPEN FOR LINE EDITING. WHEN DONE TYPE END.

A: Enter keyword for data item you wish to change and you will be prompted for the relevant input. The keywords are as follows:

TITLE
OUTPUT
PRESSURE
MACH
FREQUENCY
HEIGHT
MASS
VISCOUS
NODE
MODE
HINGE
METHOD
END

The first three letters of any keyword are sufficient. This process may be repeated as often as desired. To terminate editing enter the keyword END.

Data module VII. Multiple problems

Q: DO YOU WANT TO ENTER ANOTHER PROBLEM?

A: Type YES or NO.

Note: An answer of NO will result in the current list of problems being run. An answer of YES will result in the query

Q: IF YOU WANT TO MODIFY AN OLD PROBLEM, ENTER ITS NUMBER
OTHERWISE TYPE D FOLLOWED BY CARRIAGE RETURN

A: Type N to alter problem N. Type D followed by carriage return to begin a completely new problem.

Once the last Q is answered with NO the list of problems will be run. Upon completion, prompting will continue as follows.

Q: DO YOU WANT TO ENTER ANOTHER PROBLEM?

A: Type YES or NO

Note: An answer of NO will stop the program. An answer of YES will result in the query

Q: IF YOU WANT TO RETAIN OR MODIFY PROBLEMS FROM THE OLD PROBLEM LIST
ENTER PROBLEM N OF THE OLD LIST AS PROBLEM M OF THE NEW LIST WHERE
M IS LESS THAN OR EQUAL TO N. OTHERWISE PROBLEM N WILL BE DESTROYED.
TO MODIFY AN OLD PROBLEM, ENTER ITS NUMBER
OTHERWISE TYPE D FOLLOWED BY CARRIAGE RETURN

A: Type N to alter or retain problem N as problem 1 of the new problem list. Type D followed by carriage return to begin a completely new problem list. Up to three problems may be defined.

The APPENDIX presents a sample interactive input/output.

9.3 Card input format for BATCH

Data are read in free format. Entries on a given card may be arbitrarily spaced so long as correct order is maintained. Consecutive entries on a card must be separated by a comma or one or more blanks. Otherwise blank cards with D in column 1 imply default to the most recently assigned values.

Data module I. Run parameters

Card 1: BATCH

Card 2: Number of lines per page or otherwise blank card with D in column 1 for default value of 66.

Data module II. Output parameters

Card 1: Descriptive alphanumeric title in columns 1-72.

Card 2: Desired combination of the words FOURIER, SECTION and WORK separated by commas or blanks. Use an otherwise blank card with D in column 1 for default.

Card(s) 3: Pressure points in standard list format (see glossary in section 9.4). Enter 0 if no pressure values are desired. Use an otherwise blank card with D in column 1 for default.

Data module III. Flow parameters

Card(s) 1: Mach numbers in standard list format. Use otherwise blank card with D in column 1 for default.

Card(s) 2: Reduced frequencies in standard list format. Use otherwise blank card with D in column 1 for default.

Card(s) 3: Height to chord ratios in standard list format. Use otherwise blank card with D in column 1 for default.

Card(s) 4: Mass effect ventilation coefficients in standard list format. Use otherwise blank card with D in column 1 for default.

Card(s) 5: Viscous effect ventilation coefficients in standard list format. Use otherwise blank card with D in column 1 for default.

Data module IV. Modal parameters

Card(s) 1: Nodes in standard list format. Use otherwise blank card with D in column 1 for default.

Card(s) 2: Number of modes, or otherwise blank card with D in column 1 for default.

Card(s) 3: Values of mode shape 1 at nodes, or otherwise blank card with D in column 1 for default.

Repeat this card(s) for the remaining mode shapes.

Card(s) 4: Node numbers of hinges if such discontinuities are present. Enter 0 if none are present, or use an otherwise blank card with D in column 1 for default.

Data module V. Method parameters

Card 1: Number of different methods of solution, or otherwise blank card with D in column 1 for default.

Card 2: Solution parameters for first method of solution, or otherwise blank card with D in column 1 for default. See glossary for precise definitions of names and parameters.

Repeat Card 2 for the remaining methods of solution.

Data module VI. Data editing

Data editing is not currently permitted with BATCH input.

Data module VII. Multiple problems

Card 1: YES or NO beginning in column 1. If YES then repeat data modules II-VII. If NO processing will terminate.

9.4 Glossary of input terminology

This subsection provides in alphabetical order definitions of input parameters needed to run TWODI. All data are automatically tested upon input and unacceptable values are deleted with an explanatory message.

BATCH. Indicates noninteractive jobs with punched card input.

FOURIER. Entering the word FOURIER causes the pressure Fourier coefficients to be printed upon output. Initial default condition is affirmative.

LIST FORMAT. There are two standard formats for entering lists of numbers, one for arbitrarily spaced data and another for equally spaced real data. To enter N arbitrarily spaced real or integer data with values V1,...,VN, type

N, V1,...,VN

Such an arbitrarily spaced list may contain one (and at most one) infinite value by entering INFINITY. To enter N equally spaced real numbers from A to B, type

N / A, B

To enter an empty list, type 0.

LIST OF FREQUENCIES. From 1 to 10 finite real numbers representing reduced frequency based on semichord. May not be an empty list. Initial default condition is two frequencies with values 0 and 1.

LIST OF HEIGHT TO CHORD RATIOS. From 1 to 5 positive numbers representing height to chord ratio. May not be an empty list. To specify free air conditions, type INFINITY. Initial default condition is one value of INFINITY.

LIST OF MACH NUMBERS. From 1 to 10 values of subsonic Mach number, each of which must be non-negative and less than one. May not be an empty list. Initial default condition is one Mach number with value 0.

LIST OF NODES. From 1 to 20 distinct points at which mode shapes are to be collocated. May not be an empty list. Initial default condition is 3 nodes with values -1, 0 and 1.

LIST OF NODE NUMBERS OF HINGES. From 0 to 3 integers locating possible flap hinges at the corresponding nodes. May be an empty list. Initial default condition is that there are no hinges.

LIST OF PRESSURE POINTS. From 0 to 100 points along the chord where pressures are to be printed upon output. Each value must be greater than -1 (i.e., aft of leading edge) and less than or equal to +1(i.e., not aft of trailing edge). Should not coincide with any hinge locations; if so, such pressure points will be deleted and the number of pressure points reduced accordingly. May be an empty list. Initial default condition is 10 points equally spaced from -.8 to 1.

LIST OF MASS EFFECT VENTILATION COEFFICIENTS. From 1 to 5 values of mass effect (slotted wall) ventilation coefficients. Enter INFINITY for closed walls. For open jet enter 0 for both mass effect and viscous effect (see below) ventilation coefficients. Initial default condition is one value of INFINITY.

LIST OF VISCOUS EFFECT VENTILATION COEFFICIENTS. From 1 to 5 values of viscous effect (porous wall) ventilation coefficients. Enter INFINITY for closed walls. For open jet enter 0 for both mass effect (above) and viscous effect ventilation coefficients. Initial default condition is one value of 0.

NUMBER OF LINES PER PAGE. Indicates number of lines per page of printed output. Not presently utilized. Initial default value is 66 in both BATCH and TIMESHARE.

NUMBER OF METHODS OF SOLUTION. Integer from 1 to 10 which controls the number of different methods by which each case is solved. Presently used for convergence and extrapolation control. Initial default value is 1.

NUMBER OF MODE SHARES. Integer from 1 to 5 which controls the number of different mode shapes for which airloads are calculated. Initial default value is 3.

SECTION. Entering the word SECTION causes section coefficients C_L and C_M for lift and moment and chordwise center of pressure x_{CP} to be printed upon output. Initial default condition is affirmative.

SOLUTION PARAMETERS.* Three integers I1, I2 and I3 followed by two real numbers R1 and R2. Used to control the method of solution and to perform special purpose and check calculations. Will be phased out in the future and replaced by automatic accuracy control. The five-tuple (I1, I2, I3, R1, R2) produces the following (a dot • indicates parameters not presently used, so enter 0):

(1,2,1,•,•) Checks the Legendre-Gaussian quadrature tables.

(1,2,2,•,•) Checks the logarithmic-Gaussian quadrature tables.

(1,2,3,•,•) Checks the inverse square root Gaussian quadrature tables.

(1,2,4,•,•) Checks the Laguerre-Gaussian quadrature tables.

(1,3,•,•,•) Checks the eigensolution of (3.11_4).

(1,4,•,•,•) Checks the infinite series summation (3.11_1).

(1,5,•,•,•) Checks the calculation of K_C in (3.10).

(1,6,•,•,•) Checks the calculation of F_1 in (12.26).

(1,7,•,•,•) Checks the calculation of F_2 in (12.33).

---

*Note added in proof. Since the writing of this report, TWODI has been modified for automatic extrapolation as described in section 11 and the Possio free air kernel is computed as described in section 12. This Glossary, the Addendum immediately following the Conclusions in section 15 and the Appendix reflect these changes.

(1,9,•,•,•) Checks the calculation of airfoil polynomials in (5.5).

(1,10,•,•,•) Checks the calculation of the collocation matrix (6.8).

(2,1,•,R1,R2) Special purpose. Calculates the Küssner-Schwarz solution for flaps with hinge at R1 and reduced frequency R2. $-1 \le R1 \le 1$.

(2,2,•,•,•) Special purpose. Quadrature evaluation of Possio kernel.

(2,4,•,•,•) Special purpose. Quadrature of $x \log x$ using Legendre-Gaussian quadrature.

(3,I2,I3,R1,•) Standard solution. Richardson extrapolation of order I3 based on Bland's collocation method with a period of I2 basis elements using internal error tolerances of R1. If R1=0, R1 is set to 10^{-6}. Final solution error is approximately 10R1. Reduces to Bland's collocation method with I2 basis elements when I3=0. $1 \le I1 \le 24$. This is the only combination of solution parameters needed to compute airloads.

Use of solution parameters with $I1 \neq 3$ requires expert interpretation and is not recommended for production usage. Initial default value of solution parameters is (3,5,0,0,0).

TIMESHARE. Indicates remote terminal jobs in which TWODI and the user communicate interactively. Initial default value is affirmative.

WORK. Entering the word WORK causes the aerodynamic work matrix $[A_{mn}]$ to be printed upon output. Not presently implemented. Initial default condition is negative.

§10. Convergence characteristics of TWODI

In our previous report [5] an extensive examination of the convergence of Bland's collocation method was made; both analytically and computationally. Our principal theoretical result was that collocation and Galerkin's method were numerically equivalent, so that convergence was analyzed in terms of Galerkin's method. On the assumption that the quadrature errors in the evaluation of the Galerkin matrix could be neglected, it was concluded that Bland's method was convergent. This theoretical result was validated by exhibiting the rapid numerical convergence of TWODI-I for a variety of steady and unsteady flow problems with smooth downwashes.

In the present section these results are extended in several directions. First our convergence result is strengthened by showing that one need not make the assumption of negligibility of quadrature errors in the Galerkin matrix and we present a direct proof of the convergence of collocation. This enables us to obtain improved error estimates along with strenthening the theoretical basis of collocation methods in aerodynamic calculations. Second, the numerical convergence of TWODI is demonstrated for problems with flaps. An important result in this case is the verification of the predicted slow rate of convergence, in contrast to the rapid rate achieved for smooth downwashes. This observation required us to make a detailed study of a number of convergence accelerating techniques; a topic which is taken up in detail in the following section.

10.1 L^2 convergence of collocation.

Since we wish our analysis to cover other equations than those with Bland's kernel we begin by making several assumptions concerning the kernel $\bar{K}(x)=K(x)-1/x$. These are:

(A-1) $\bar{K}(x-\xi)$ is Lebesgue-Stieltjes square integrable with respect to the product measure $\sqrt{\frac{1-\xi}{1+\xi}}\,\sqrt{\frac{1+x}{1-x}}$;i.e.,

$$\int_{-1}^{1}\int_{-1}^{1}\left(\sqrt{\frac{1-\xi}{1+\xi}}\,\sqrt{\frac{1+x}{1-x}}\right)|\bar{K}(x-\xi)|^2\,d\xi\,dx<\infty. \tag{10.1}$$

(A-2) $\bar{K}(x-\xi)$ is mean square continuous; i.e.,

$$\lim_{h\to 0}\int_{-1}^{1}\sqrt{\frac{1-\xi}{1+\xi}}\,|\bar{K}(x-\xi+h)-\bar{K}(x-\xi)|^2\,d\xi = 0. \tag{10.2}$$

For the next assumption we need the following definition.

Definition. Let $f \in L_\gamma^2$ and let $Q_N(f)$ denote the sum given by the quadrature rule (5.30_1). We say that f is quadrature convergent for $\{Q_N\}$ if $Q_N(f)$ is defined, $N \geq 1$, and if

$$\lim_{N\to\infty} Q_N(f) = \int_{-1}^{1} \sqrt{\frac{1+x}{1-x}}\, f(x)dx.$$

(A-3) For each fixed ξ, $\left|\tilde{K}_\xi(x)\right|^2 = \left|\tilde{K}(x-\xi)\right|^2$ is quadrature convergent.

Since for Bland's kernel $\tilde{K}(x) = K_L(x) + K_C(x)$ where $K_C(x)$ is continuous it follows by standard theorems [44],[48] that $K_C(x)$ satisfies (A-1)-(A-3). For $K_L(x)$[1] similar properties may be shown by direct, though lengthy computation [49]. The proof, particularly of (A-3), relies on the fact that $Q_N(f)$ may be viewed as a Riemann sum [49],[50] and that appropriately chosen Riemann sums converge to the integral of $(\log|x|)^2$.

Our next step is to recast the collocation method in a suitable abstract form.

Definition. Let $f \in L_\gamma^2$ and let $\{x_k\}_1^N$ be the zeros of ω_{N+1}. Then

$$L_N(f) = \sum_{k=1}^{N} \ell_k(x) f(x_k), \tag{10.3}$$

is the unique polynomial which interpolates to $f(x)$ at $\{x_k\}_1^N$. Here $\{\ell_k(x)\}_1^N$ are the fundamental polynomials of Lagrange interpolation.

Using (10.3) the sequence of operators $\{K_N\}$ is defined by

$$K_N(\phi) = L_N(K\phi), \quad \phi \in L_\gamma^2. \tag{10.4}$$

Let

$$\phi_N(\xi) = \sum_{k=1}^{N} a_k \gamma_k(\xi)$$

be the collocation approximation to ϕ using the N basis elements $\{\gamma_k\}_1^N$. Then a little algebra shows that ϕ_N satisfies the equation

$$H\phi_N + K_N\phi_N = L_N(w) = w_N. \tag{10.5}$$

---

[1] For technical reasons we shall consider $\log|x-\xi| = 0$ if $x = \xi$.

(Note that (10.5) is analogous to the equation satisfied by ϕ_N^G, where ϕ_N^G is the corresponding Galerkin approximation to ϕ.) The convergence of ϕ_N to ϕ is based on the following lemmas.

Lemma 10.1 Assume that $\{K_N\}$ are bounded and that

$$\lim_{N\to\infty} \| K-K_N \| = 0. \tag{10.6}$$

Then there exists an N_o such that for all $N>N_o$, $(H+K_N)^{-1}$ exists, is bounded and the norms $\tau_N = \|(H+K_N)^{-1}\|$ are uniformly bounded. From this it follows that for all $N>N_o$, ϕ_N exists and

$$\| \phi-\phi_N \|_\gamma \leq \tau_N \| H\phi-L_N(H\phi) \|_\alpha. \tag{10.7}$$

Proof. The existence and boundedness of $(H+K_N)^{-1}$ follow along standard lines [51]. To obtain (10.7) observe that

$$\begin{aligned} \phi - \phi_N &= \phi-(H+K_N)^{-1}w_N = (H+K_N)^{-1}[(H+K_N)\phi-w_N] \\ &= (H+K_N)^{-1}[H\phi+L_N(K\phi)-L_N(w)] \\ &= (H+K_N)^{-1}[H\phi-L_N(H\phi)]. \end{aligned} \tag{10.8}$$

Taking norms on both sides of (10.8) gives (10.7) □

Lemma 10.2. Let $f\in L^2_\alpha$ and assume that $|f|^2$ is quadrature convergent for $\{Q_N\}$. Then

$$\lim_{N\to\infty} \| f-L_N(f) \|_\alpha = 0. \tag{10.9}$$

Proof. In [44] it was shown that the lemma holds when f is assumed to Riemann Stieltjes square integrable, in particular when f is continuous. However, a careful examination of the proof presented there shows it is sufficient to require that $|f|^2$ be quadrature convergent□

Using Lemmas 10.1 and 10.2 it follows that $\phi_N\to\phi$ provided that $\|K-K_N\| \to 0$, K satisfies (A-1) - (A-3) and $|w|^2$ is quadrature convergent for $\{Q_N\}$. To see this, observe that it follows from the above discussion that $|H\phi|^2$ is quadrature convergent since $H\phi = K\phi - w$ and $|K\phi|^2$ is quadrature convergent (in fact continuous from (A-2)) and $|w|^2$ is quadrature convergent by assumption. Thus by Lemma 10.2

$$\lim_{N\to\infty} \| H\phi-L_N(H\phi) \|_\alpha^2 = 0, \tag{10.10}$$

and so (10.7) shows that $\varphi_N \to \psi$ in the norm of L^2_γ. Using this we arrive at our main convergence theorem.

Theorem 10.1. Let $\tilde{K}(x-\xi)$ satisfy (A-1)-(A-3). Assume that w is quadrature convergent, then

$$\lim_{N\to\infty} \| \psi - \psi_N \|_\gamma = 0.$$

Proof. From the preceeding discussion it suffices to show that $\{K_N\}$ are bounded and that

$$\lim_{N\to\infty} \| K - K_N \| = 0.$$

The boundedness of K_N is established first.

From (10.3) it is seen that

$$(K_N\psi)(x) = \sum_{k=1}^{N} \ell_k(x)(K\psi)(x_k).$$

From Eq. 14.2.4 in [44] we get that[2]

$$\int_{-1}^{1} |I_N(f)|^2 \, d\beta(x) = \sum_{k=1}^{N} \lambda_k |f(x_k)|^2,$$

where $\{\lambda_k = \frac{\pi(1+x_k)}{k+\frac{1}{2}}\}$ are the weights in the quadrature rule Q_N. Thus

$$\|K_N\psi\|^2_\gamma = \int_{-1}^{1} |I_N(K\psi)|^2 \, d\beta(x) = \sum_{k=1}^{N} \lambda_k |K\psi(x_k)|^2.$$

But

$$|K\psi(x_k)|^2 = \left| \int_{-1}^{1} \tilde{K}(x_k - \xi)\psi(\xi)\, d\alpha(\xi) \right|^2$$

$$\le \left(\int_{-1}^{1} |\tilde{K}(x_k - \xi)|^2 \, d\alpha(\xi) \right) \left(\int_{-1}^{1} |\psi(\xi)|^2 \, d\alpha(\xi) \right),$$

so that

$$\|K_N\psi\|^2_\gamma \le \left(\sum_{k=1}^{N} \lambda_k \tilde{c}_k \right) \|\psi\|^2_\gamma .$$

---

[2] In what follows we use $d\alpha(\xi) = \sqrt{\frac{1-\xi}{1+\xi}}\, d\xi$ and $d\beta(x) = \sqrt{\frac{1+x}{1-x}}\, dx$.

where

$$\delta_k = \int_{-1}^{1} |\tilde{K}(x_k-\xi)|^2 d\alpha(\xi).$$

This gives

$$\|K_N\varphi\|_\alpha \le C\|\varphi\|_\gamma .$$

since $\delta_k < \infty$, and so K_N is bounded.

To prove the uniform convergence of K_N to K observe that

$$(K\varphi-K_N\varphi) = \int_{-1}^{1} H_N(x,\xi)\varphi(\xi)d\alpha(\xi),$$

where

$$H_N(x,\xi) = \tilde{K}(x-\xi) - \sum_{k=1}^{N} \ell_k(x)\tilde{K}(x_k-\xi).$$

Thus

$$\|K-K_N\|^2 \le \int_{-1}^{1}\int_{-1}^{1} |H_N(x,\xi)|^2 d\beta(x)d\alpha(\xi).$$

Let $w_\xi(x) = \tilde{K}(x-\xi)$. Then

$$H_N(x,\xi) = w_\xi(x) - L_N(w_\xi)(x).$$

From Lemma 10.2 it follows that

$$\lim_{N\to\infty} \int_{-1}^{1} |H_N(x,\xi)|^2 d\beta(x) = \lim_{N\to\infty} \int_{-1}^{1} |w_\xi-L_N(w_\xi)|^2 d\beta(x) = 0$$

for each fixed ξ.

From the proof of Lemma 10.2 found in [44] we get

$$\lim_{N\to\infty} \sup\left(\int_{-1}^{1} |w_\xi-L_N(w_\xi)|^2 d\beta(x)\right) \le 4\int_{-1}^{1} |\tilde{K}(x-\xi)|^2 d\beta(x). \tag{10.11}$$

Since

$$\int_{-1}^{1}\int_{-1}^{1} |\tilde{K}(x-\xi)|^2 d\beta(x)d\alpha(\xi) < \infty$$

it follows from (10.11) that there exists a function $\rho(\xi)$ such that

$$\int_{-1}^{1} |H_N(x,\xi)|^2 d\beta(x) \leq \rho(\xi),$$

and

$$\int_{-1}^{1} |\rho(\xi)|^2 d\alpha(\xi) < \infty,$$

so that by the dominated convergence theorem

$$\lim_{N\to\infty} \int_{-1}^{1} \int_{-1}^{1} |H_N(x,\xi)|^2 d\beta(x) d\alpha(\xi)$$

$$= \int_{-1}^{1} [\lim_{N\to\infty} (\int_{-1}^{1} |H_N(x,\xi)|^2 d\beta(x))] d\alpha(\xi) = 0.$$

Thus

$$\lim_{N\to\infty} \|K - K_N\|^2 \leq \lim_{N\to\infty} \int_{-1}^{1}\int_{-1}^{1} |H_N(x,\xi)|^2 d\beta(x) d\alpha(\xi) = 0$$

and the theorem is proved□

We now make several observations concerning the convergence theorem. First we note that it has been shown that ϕ_N converges to ϕ in mean square and not pointwise, although numerically pointwise convergence is indicated [5]. However it is easily shown that the generalized Fourier coefficients $\{a_n\}$ converge to the true Fourier coefficients of ϕ. In addition integrated aerodynamic forces such as lift and pitching moment also converge to their true values. This was established in [5] and follows easily using the fact that such quantities are represented in terms of inner products of the pressure factor ψ and an appropriate function in L_2.

Second we observe that the rate of convergence is proportional to $\| H\phi - L_N(H\phi) \|_a$. If the downwash is smooth, then in general $H\phi$ will be smooth and we expect $L_N(H\phi)$ to converge rapidly to $H\phi$. This was observed in [5]. However if w is not smooth then $H\phi$ will be poorly behaved and thus slow convergence of $L_N(H\phi)$ to $H\phi$ is anticipated. In fact for the particular case of steady flow in free air, k=0 so that

$$\| \phi - \phi_N \|_\gamma \leq \| w - L_N(w) \|_a. \tag{10.12}$$

Although we have not obtained exact estimates of $\| w - L_N(w) \|_a$ we expect that asymptotically it should behave no worse than $O(1/\sqrt{N})$. The slowest convergence rate should occur for a downwash w(x) corresponding to a simple leading or trailing edge flap. Numerical results presented in Tables 3-4 indicate a somewhat better rate of O(1/N). For k≠0 the same rate is expected since

$$\| \phi - \phi_N \|_\gamma \leq \tau_N \| H\phi - L_N(H\phi) \|_a \leq \tau_N (\| w - L_N(w) \|_a + \| K\phi - L_N(K\phi) \|_a)$$

and by (A-1) $K\phi$ is continuous. Thus the dominant error term is $\tau_N \| w - L_N(w) \|$. Again the results exhibited in Tables 5-6 indicate an O(1/N) rate of convergence. In general for 24 basis elements, 1%-2% error might be anticipated using TWODI for flaps. This would be an unacceptably large error for high precision engineering work. Substantial increase in accuracy thus appears to require one of two strategies: an increase in the number of basis elements and/or the utilization of alternate solution methods.

Since present engineering technology allows pressure measurements to be made within an error of $O(10^{-3})$ this is the maximum error that we would like to have. From Table 3 we see that an error of $O(10^{-3})$ for a midchord flap would require several hundred basis elements. Such an increase in the number of basis elements is out of the question. The second option is pursued in the following section where it is shown that an error of $O(10^{-4})$ can be achieved for a midchord flap using 16 basis elements, and an error of $O(10^{-3})$ is obtained for a three-quarter chord flap using 12 basis elements.

Table 3. Principal error term in norm for a midchord flap (M=0,k=0,$\eta=\infty$)

NP	$\|\phi_{NP}\|_\gamma$	% error	|% error|xNP
1	1.77245	-10.545	10.5
2	1.50774	+5.964	11.2
3	1.67441	-4.430	13.3
4	1.54963	+3.352	13.4
5	1.64833	-2.843	14.2
6	1.56602	+2.330	14.0
7	1.63626	-2.051	14.4
8	1.57475	+1.785	14.3
9	1.62929	-1.617	14.5
10	1.58017	+1.447	14.5
11	1.62477	-1.335	14.7
12	1.58386	+1.217	14.6
13	1.62159	-1.136	14.8
14	1.58654	+1.049	14.7
15	1.61923	-0.989	14.8
16	1.58857	+0.923	14.8
17	1.61471	-0.876	14.9
18	1.59817	+0.823	14.8
19	1.61597	-0.786	14.9
20	1.59145	+0.743	14.9

$$\|\phi\|_{\gamma\ \text{exact}} = \sqrt{\frac{\pi}{2} + 1} = 1.60337$$

Table 4. Principal error term in lift for a midchord flap (M=0,k=0,$\eta=\infty$)

NP	C_L	% error	|% error|xNP
1	6.28319	+22.203	22.2
2	4.54656	-11.573	23.1
3	5.60728	+9.057	27.2
4	4.80272	-6.591	26.4
5	5.43401	+5.687	28.4
6	4.90481	-4.605	27.6
7	5.35469	+4.145	29.2
8	4.95964	-3.539	28.3
9	5.30922	+3.260	29.3
10	4.99386	-2.873	28.7
11	5.27974	+2.687	29.6
12	5.01725	-2.418	29.0
13	5.25908	+2.285	29.1
14	5.03424	-2.088	29.8
15	5.24379	+1.988	29.4
16	5.04715	-1.837	29.4
17	5.23202	+1.759	29.9
18	5.05729	-1.640	29.5
19	5.22269	+1.577	30.0
20	5.06546	-1.481	29.6

$$C_{L_{\text{exact}}} = 2\pi$$

Table 5. C_{L_δ} for an oscillating flap hinged at the 50% chord (M=0, k=.1, $\eta=\infty$)

source	real	imag	magn	phase	% error(magn)
NP=1	5.24189	-0.50914	5.26656	-5.55	+20.9665
NP=2	3.83875	-0.39049	3.85856	-5.81	-11.3735
NP=3	4.71938	-0.46530	4.74226	-5.63	+ 8.9240
NP=4	4.05062	-0.40762	4.07108	-5.75	- 6.4922
NP=5	4.57548	-0.45292	4.59785	-5.65	+ 5.6071
NP=6	4.13538	-0.41479	4.15613	-5.73	- 4.5387
NP=7	4.50954	-0.44719	4.53166	-5.66	+ 4.0868
NP=8	4.18095	-0.41868	4.20186	-5.72	- 3.4883
NP=9	4.47172	-0.44390	4.49370	-5.67	+ 3.2149
NP=10	4.20940	-0.42113	4.23041	-5.71	- 2.8326
NP=11	4.44720	-0.44177	4.46909	-5.67	+ 2.6496
NP=12	4.22884	-0.42281	4.24993	-5.71	- 2.3842
NP=13	4.43001	-0.44027	4.45184	-5.68	+ 2.2534
NP=14	4.24298	-0.42403	4.26411	-5.71	- 2.0585
NP=15	4.41730	-0.43916	4.43907	-5.68	+ 1.9601
NP=16	4.25371	-0.42495	4.27489	-5.71	- 1.8109
NP=17	4.40751	-0.43831	4.42925	-5.68	+ 1.7345
NP=18	4.26214	-0.42568	4.28335	-5.70	- 1.6166
NP=19	4.39974	-0.43764	4.42145	-5.68	+ 1.5554
NP=20	4.26894	-0.42627	4.29017	-5.70	- 1.4600

Table 6. C_{L_δ} for an oscillating flap hinged at the 75% chord (M=0, k=.1, $\eta=\infty$)

source	real	imag	magn	phase	% error(magn)
NP=1	5.20343	-0.76937	5.25999	-8.41	+62.2622
NP=2	3.80393	-0.57961	3.84783	-8.66	+18.6994
NP=3	2.86126	-0.44037	2.89495	-8.75	-10.6954
NP=4	4.01530	-0.60740	4.06098	-8.60	+25.2747
NP=5	3.45638	-0.52720	3.49635	-8.67	+ 7.8568
NP=6	3.01247	-0.46186	3.04767	-8.72	- 5.9843
NP=7	3.70555	-0.56291	3.74806	-8.64	+15.6216
NP=8	3.36432	-0.51342	3.40298	-8.68	+ 4.9765
NP=9	3.07119	-0.47035	3.10700	-8.71	- 4.1540
NP=10	3.56680	-0.54280	3.60786	-8.65	+11.2967
NP=11	3.32122	-0.50707	3.35971	-8.68	+ 3.6417
NP=12	3.10241	-0.47489	3.13854	-8.70	- 3.1811
NP=13	3.48818	-0.53135	3.52842	-8.66	+ 8.8461
NP=14	3.29653	-0.50341	3.33475	-8.68	+ 2.8717
NP=15	3.12177	-0.47771	3.15811	-8.70	- 2.5774
NP=16	3.43758	-0.52397	3.47729	-8.67	+ 7.2688
NP=17	3.28046	-0.50103	3.31850	-8.68	+ 2.3704
NP=18	3.13496	-0.47963	3.17144	-8.70	- 2.1662
NP=19	3.40229	-0.51882	3.44162	-8.67	+ 6.1684
NP=20	3.26916	-0.49936	3.30708	-8.68	+ 2.0181

10.2 Stability and integration error.

The error estimate given by (10.7) is a theoretical one based on the assumption that all arithmetic is performed exactly. In general there will be other sources of error, particularly roundoff and errors in the evaluation of the collocation matrix. To see the effect of these assume that $\hat{\psi}_N$ is the computed value of ψ_N. Then letting $\delta\psi_N=\psi_N-\hat{\psi}_N$ it is seen that

$$\psi-\hat{\psi}_N=(\psi-\psi_N)+\delta\psi_N. \tag{10.13}$$

Taking norms on both sides of (10.13) shows that

$$\|\psi-\hat{\psi}_N\|_\gamma \leq \|\psi-\psi_N\|_\gamma+\|\delta\psi_N\|_\gamma \tag{10.14}$$

Since $\|\psi-\psi_N\|_\gamma$ is estimated in (10.7) we concentrate on evaluating $\|\delta\psi_N\|_\gamma$ Now ψ_N is given by

$$\psi_N = \sum_{n=1}^{N} a_n\gamma_n \tag{10.15}$$

where $\{a_n\}_{m=1}^N$ solve the collocation equations (6.7). Let $\{\hat{a}_n\}_{n=1}^N$ be the numerically computed values of $\{a_n\}_{n=1}^N$. Then

$$\hat{\psi}_N = \sum_{n=1}^{N} \hat{a}_n\gamma_n.$$

This gives

$$\delta\psi_n = \sum_{n=1}^{N} (a_n-\hat{a}_n)\gamma_n = \sum_{n=1}^{N} \delta a_n\gamma_n.$$

Using the orthonormality of $\{\gamma_n\}_{n=1}^N$ we get that

$$\|\delta\psi_N\|_\gamma = \left(\sum_{n=1}^{N} |\delta a_n|^2\right)^{\frac{1}{2}} \tag{10.16}$$

Letting $\delta a = \{\delta a_n\}_{n=1}^N$, $\|\delta\psi_N\|_\gamma = \|\delta a\|_2$, where $\|\delta a\|_2$ is the usual Euclidean length of a complex N-vector.

If C_N denotes the collocation matrix, then

$$C_N\underline{a} = \underline{w} \tag{10.17}$$

and

$$(C_N+\Delta C_N)\hat{\underline{a}} = \underline{w}, \tag{10.18}$$

where $\underline{a} = \{a_n\}_{n=1}^N$, $\hat{\underline{a}} = \{\hat{a}_n\}_{n=1}^N$, $\underline{w} = \{w(x_K)\}_{K=1}^N$ and ΔC_N is the error in the evaluation of C_N. Standard error estimates show that

$$\|\delta a\|_2 \leq \sigma \|\Delta C_N\| \, \|C_N^{-1}\| \tag{10.19}$$

where σ is independent of N [51]. Consequently the progagation of error is determined by $\|C_N^{-1}\|$. We now turn to the problem of estimating this quantity.

Rather than analyze $\|C_N^{-1}\|$ directly we introduce a suitable vector norm on $\mathbb{C}^N$ ($\mathbb{C}^N = \{(z_1,z_2,\ldots,z_N) \mid z_i$ complex, i = 1,2,...,N$\}$) and use the induced matrix norm instead.

Definition. Let $\{\lambda_k\}_{k=1}^N$ be the weights of the quadrature rule Q_N. Let $z \in \mathbb{C}^N$ and define

$$\|z\|_2^Q = \left(\sum_{k=1}^N \lambda_k |z_k|^2\right)^{1/2}. \tag{10.20}$$

Since $\lambda_k > 0$ it is straightforward to verify that $\|z\|_2^Q$ is a norm on $\mathbb{C}^N$. Let $T:\mathbb{C}^N \to \mathbb{C}^N$ be an NxN complex matrix, and let $\|T\|^Q$ be the matrix norm of T induced by $\|\ \|_2^Q$. Using these definitions we arrive at the following theorem.

Theorem 10.2. Let C_N be the collocation matrix and let $\tau = \sup_N \|(H+K_N)^{-1}\|$. Let $a=[\alpha_n(x_K)]$, where $\{x_k\}_{k=1}^N$ are the collocation points. Then

$$\|C_N^{-1}\|^Q \leq \tau \, \|a^{-1}\|^Q.$$

Proof. Let $\underline{a} = \{a_n\}_{n=1}^N$ and $\underline{w} = \{w(x_K)\}_{k=1}^N$. Then

$$C_N \underline{a} = \underline{w}.$$

Now

$$\psi_N(x) = \sum_{n=1}^N a_n \gamma_n(x)$$

so that

$$H\psi_N(x) = \sum_{n=1}^N a_n \alpha_n(x)$$

and

$$(H\psi_N)(x_K) = \sum_{n=1}^N a_n \alpha_n(x_K). \tag{10.21}$$

From (10.5) it follows that

$$\psi_N = (H+K_N)^{-1} w_N \tag{10.22}$$

so that

$$\| \psi_N \|_\gamma \leq \| (H+K_N)^{-1} \| \| w_N \|_\alpha \leq \tau \| w_N \|_\alpha = \tau \Big(\sum_{n=1}^{N} \lambda_K |w(x_K)|^2 \Big)^{1/2} = \tau \| \underline{w} \|_2^Q .$$

Since H is unitary [5], $\| \psi_N \|_\gamma = \| H\psi_N \|_\alpha$, giving

$$\| H\psi_N \|_\alpha \leq \tau \| \underline{w} \|_2^Q$$

Letting $\underline{H} = \{\psi_N(x_K)\}_{k=1}^N$, (10.21) gives

$$\underline{a} = \underline{\alpha}^{-1} \underline{H}.$$

Taking norms we get

$$\| \underline{a} \|_2^Q \leq \| \alpha^{-1} \|^Q \| \underline{H} \|_2^Q .$$

But $\| \underline{H} \|_2^Q = \| H\psi_N \|_\alpha$ giving

$$\| \underline{a} \|_2^Q \leq \tau \| \alpha^{-1} \|^Q \| w \|_2^Q \tag{10.24}$$

From (10.24) it follows that

$$\| C_N^{-1} \|^Q \leq \tau \| \alpha^{-1} \|^Q \square$$

Using the theorem it is easily shown that

$$\| \delta\psi_N \|_2 \leq \frac{1}{(\min_k \sqrt{\lambda_k})} (\tau \| \alpha^{-1} \|^Q).$$

Thus the propagation of numerical error in the collocation matrix depends essentially on $\| \alpha^{-1} \|^Q$. At present we have no theory to predict the growth of $\| \alpha^{-1} \|^Q$. However numerical experimentation has shown that $\| \alpha^{-1} \|^Q$ grows slowly

with N so that for $1 \leq N \leq 20$ the collocation matrix is well-conditioned. From this we conclude that reduction in numerical error for fixed N requires careful evaluation of the integrals in C_N.

In TWODI-I difficulties arose in unsteady problems where we found it difficult to obtain more than 3-4 decimal accuracy. Since the above analysis indicates that inverting the collocation matrix is numerically stable, we conjecture that the source of the difficulty is the improper integration of the log terms in the kernel. In section 12 we show that this is in fact the case. A thousand fold increase in accuracy is obtained by efficient integration of the singular terms.

§11. Convergence Acceleration

This section presents a theoretical error analysis of various methods which might be used for improving the rate of computational convergence when flaps are present.

As we have shown in section 10 Bland's collocation method converges rapidly when the downwash is smooth. However, if the airfoil contains flaps, the results presented in Table 3-6 indicate that for physically important w's a convergence rate no better than o(1/N) can be expected. This is disappointing, since an engineering accuracy of $0(10^{-3})$ would appear to require something on the order of 300 basis elements. As TWODI can presently accommodate a maximum of 24 basis elements it might appear that the flap problem is essentially intractable with today's computing capability.

This circumstance naturally leads one to look for alternate methods of solving the genralized airfoil equation when flaps are present: the goal being to obtain a convergence rate sufficiently great so that the stated degree of accuracy can be achieved within the limitations of our existing code.

A great many possibilities present themselves. Among the choices are:

(a) Modification of the collocation method by either changing the basis elements, the collocation points, or both.

(b) Changing the basic method of solution to something like Galerkin's method [5] or least squares [8].

(c) Singularity subtraction. This is commonly referred to as Landahl's method [52] in three dimensional problems and has been developed by Rowe et al [53], [54].

(d) Iterative improvement.

(e) The use of reverse flow theorems [55], [56].

(f) The use of extrapolation methods.

Since Bland's collocation method is understood theoretically, and is efficient for smooth downwashes, it is presently felt that improvements should be sought utilizing as much of the output of TWODI as possible. For this reason we have ruled out category (a). In addition, our examination of results achieved by Milne in [56] indicates that the 0(1/N) rate of convergence of flaps may be inherent in any collocation method using a continuous representation of ψ_N, regard-

less of the choice of colloation points or basis elements. However, some recent work by Nissim and Lottati [57] using a piecewise continuous representation of ϕ_N for Possio's equation seems to indicate that considerable improvement may be achieved over standard methods. Since we have had little time to evaluate this work, such representations are not considered in this report.

Because of the three way equivalence of Galerkin's method, collocation and least squares established in [5], use of methods in category (b) is also ruled out. We are thus left with techniques in (c)-(f).

Although such methods have been discussed in the literature for many years, we have been unable to find any discussion of their theoretical properties and little evidence of the controlled numerical experimentation necessary to distinguish among competing techniques. For this reason we have included a fairly detailed examination of these procedures which we hope will clarify our reasons for not finding them effective at the present time. Since the analysis that follows in sections 11.1 to 11.3 is fairly involved, we observe that the reader may, with little loss in continuity, skip these and proceed to section 11.4. The principal results reported in sections 11.1 - 11.3 indicate that the techniques (c)-(e) yield only a modest increase in the rate of convergence of Bland's collocation method at the expense of substantially increased arithmetic. These facts ultimately lead us to examine the use of Richardson extrapolation as a means of accelerating convergence.

While we have not yet completely automated this technique, it presently can be used in conjunction with some preliminary data analysis to obtain the stated goal of errors of order 10^{-3} or less for a wide variety of flow problems. The principal drawback to total automation is the oscillatory nature of the convergence when flaps are present. In addition, the period of oscillation appears to depend on the location of the hinge point, and cannot, at present, be predicted theoretically. As the analysis that follows shows, there is reason to believe that a combination of either singularity subtraction and/or iterative improvement in conjunction with extrapolation may yield the most efficient algorithms.

11.1 Landahl's method

Because of its widespread use in three dimensional calculations [53], [54] we begin with an examination of Landahl's method for the solution of (6.1). The aim is to find an equivalent integral equation with a smoother downwash than w. In principal there are a variety of implementations of the basic idea, and we discuss two of these. From a mathematical point of view the method may be seen as a generalization of the well known Kantorovich regularization method used for solving integral equations of the second kind [51] and our analysis follows closely that of Atkinson presented in [51].

11.1.1 Landahl I.

We consider solving the integral equation

$$(H+K)\psi = w. \tag{11.1}$$

Let ψ_o be an approximation to ψ. Using ψ_o we define the residual downwash w_R by

$$w_R = w-(H+K)\psi_o, \tag{11.2}$$

and the residual pressure ψ_R by

$$(H+K)\psi_R = w_R. \tag{11.3}$$

Theorem 11.1. $\psi = \psi_o+\psi_R.$

Proof. From (11.2) and (11.3) it is seen that

$$(H+K)(\psi_o+\psi_R) = (H+K)\psi_o+(H+K)\psi_R = w-w_R+w_R = w.$$

Thus $\psi_o+\psi_R$ solves (11.1). Using the fact that (11.1) has a unique solution it follows that $\psi = \psi_o+\psi_R$ □

From Theorem (11.1) it is seen that ψ can be determined by solving (11.3) instead of (11.1). Basically we are considering a generalization of iterative refinement used for solving linear algebraic equations [51]. For the method to be effective ψ_o must somehow be determined so that the residual downwash is smoother than w; thus solving for ψ_R would give a more rapid rate of convergence than obtaining ψ directly.

Viewing the technique as iterative refinement we might proceed as follows. Let ψ_o be obtained using Bland's collocation with the maximal number of basis elements N. (presently N=20). That is, ψ_o solves

$$(H+K_N)\psi_o = w_N. \tag{11.4}$$

In this case

$$w_R = (H+K)\phi_o - w$$

and letting ϕ_R^N be the approximation to ϕ_R using N basis elements gives

$$(H+K_N)\phi_R^N = L_N(w_R). \tag{11.5}$$

We take our approximation to ϕ as

$$\phi_N = \phi_R^N + \phi_o. \tag{11.6}$$

Hence, (11.6) gives

$$\begin{aligned}\phi_N &= (H+K_N)^{-1}w_N + (H+K_N)^{-1}L_N(w_R)\\ &= (H+K_N)^{-1}[w_N + L_N(w_R)]\\ &= (H+K_N)^{-1}[L_N(w) + L_N([(H+K)\phi_o] - w)]\\ &= (H+K_N)^{-1}[L_N(w)].\end{aligned}$$

Thus $\phi_N = \phi_o$ and no improvement can be expected. From the above result it is seen that ϕ_o must be chosen in some other way than by (11.4).

To do this let H+K be decomposed as

$$H+K = H+K_1+K_2 \tag{11.7}$$

where it is assumed that $(H+K_1)^{-1}$ exists. Let

$$\phi_o = (H+K_1)^{-1}w \tag{11.8}$$

and assume that ϕ_o can be determined accurately (essentially analytically). Then in this case

$$w_R = w - (H+K)\phi_o = w - (H+K_1)\phi_o - K_2\phi_o = -K_2\phi_o.$$

Thus the residual pressure ϕ_R satisfies the equation

$$(H+K)\phi_R = -K_2\phi_o. \tag{11.9}$$

If it is assumed that K_2 satisfies (A-2), then $w_R = -K_2\phi_o$ is continuous. If it is possible to effect the kernel splitting $K=K_1+K_2$ so that K_2 is highly differentiable and $(H+K_1)$ has a known inverse, then (11.9) should present a more tractable

problem to solve than (11.1). To obtain a numerical approximation to ψ (11.9) is solved by collocation giving a function ψ_R^N satisfying

$$(H+K_N)\psi_R^N = -I_N(K_2\psi_o) = w_R^N. \tag{11.10}$$

Let

$$\tilde{\psi}_N = \psi_o + \psi_R^N. \tag{11.11}$$

$\tilde{\psi}_N$ is then taken as our approximation to ψ. The following theorem justifies this procedure.

Theorem 11.2. Let $\tilde{\psi}_N$ be defined by (11.11). Assume that K_1 satisfies (A-1)-(A-3) so that $\| K_{1N}-K\| \to 0$. Then $\tilde{\psi}_N$ converges to ψ in L^2_γ and

$$\| \psi-\tilde{\psi}_N\|_\gamma \le \| (H+K_N)^{-1}\| \{ \| (K_{1N}-K)(H+K_1)^{-1}K_2\psi\|_\alpha + \|(K_{2N}-K)\psi\|_\alpha \}. \tag{11.12}$$

Proof. We first show that $\tilde{\psi}_N$ satisfies

$$(H+K_N)\tilde{\psi}_N = w+(K_{1N}\psi_o - K_1\psi_o). \tag{11.13}$$

To see this observe that

$$\begin{aligned} H\tilde{\psi}_N &= H\psi_R^N + H\psi_o \\ &= -K_{2N}\psi_o-(K_{1N}+K_{2N})\psi_R^N + H\psi_o \\ &= -K_{2N}\psi_o-(K_{1N}+K_{2N})\psi_R^N+w-K_1\psi_o \\ &= -K_{2N}\tilde{\psi}_N-K_{1N}\psi_R^N - K_1\psi_o+w \\ &= -K_{2N}\tilde{\psi}_N-K_{1N}\psi_R^N - K_{1N}\psi_o+K_{1N}\psi_o-K_1\psi_o+w \\ &= -K_N\tilde{\psi}_N +(K_{1N}-K_1)\psi_o+w. \end{aligned} \tag{11.14}$$

Thus (11.13) follows. To obtain (11.12) write

$$\psi = (H+K)^{-1}w$$

and

$$\tilde{\psi}_N = (H+K_N)^{-1}w+(H+K_N)^{-1}[(K_{1N}-K)\psi_o].$$

Subtracting gives

$$\psi-\bar{\psi}_N = (H+K)^{-1}w-(H+K_N)^{-1}w-(H+K_N)^{-1}[(K_{1N}-K_1)\psi_o]$$

$$= (H+K_N)^{-1}\{(K_N-K)(H+K)^{-1}w-(K_{1N}-K_1)\psi_o\}$$

$$= (H+K_N)^{-1}\{(K_N-K)(H+K)^{-1}w-(K_{1N}-K_1)(H+K_1)^{-1}w\}$$

$$= (H+K_N)^{-1}\{(K_N-K)(H+K)^{-1}-(K_{1N}-K_1)(H+K_1)^{-1}\}w. \qquad (11.15)$$

Now

$$K_N-K = (K_{1N}-K_1)+(K_{2N}-K_2)$$

so that the inner term in (11.15) becomes

$$(K_{1N}-K_1)(H+K)^{-1}+(K_{2N}-K_2)(H+K)^{-1}-(K_{1N}-K_1)(H+K_1)^{-1}$$

$$= (K_{1N}-K_1)\{(H+K)^{-1}-(H+K_1)^{-1}\}+(K_{2N}-K_1)(H+K_1)^{-1}$$

$$= (K_{1N}-K_1)(H+K_1)^{-1}(K_1-K)(H+K)^{-1}+(K_{2N}-K_2)(H+K)^{-1}$$

$$= \{(K_{1N}-K)(H+K_1)^{-1}(K_1-K_2)+(K_{2N}-K_2)\}(H+K)^{-1}. \qquad (11.16)$$

Substituting (11.16) into (11.15), using $(H+K)^{-1}w = \psi$ and taking norms gives (11.12)□

Equation (11.12) shows explicitly how the convergence rate of $\bar{\psi}_N$ to ψ depends on the splitting of K. If K_2 can be chosen so that it is very smooth, then on the basis of (11.12) we would expect rapid convergence of $\bar{\psi}_N$ to ψ. (This probably justifies its success in three dimensional free air calculations.) At present the only feasible splitting when walls are present seems to be the trivial one, $K_1=0$, $K_2=K$. In this case ψ_o is determined by

$$H\psi_o = w \qquad (11.17)$$

which can generally be obtained analytically via the Söhngen inversion formula [30]. The residual pressure then satisfies

$$(H+K)\psi_R = -KH^{-1}w,$$

and $\bar{\psi}_N$ is obtained from

$$(H+K_N)\bar{\psi}_N = w.$$

The error estimate 11.12 now simplifies to

$$\| \phi-\tilde{\phi}_N \|_\gamma \leq \| (H+K_N)^{-1} \| \| K\phi-K_N\tilde{\phi} \|_\alpha . \tag{11.18}$$

Using (11.18) we can directly compare the rate of convergence of $\tilde{\phi}_N$ to that of ϕ_N. For ϕ_N the rate is proportional to $\| H\phi-L_N(H\phi) \|_\alpha$ while for $\tilde{\phi}_N$ it is proportional to $\| K\phi-L_N(K\phi) \|_\alpha$. Since $K\phi$ is continuous $\tilde{\phi}_N$ should converge faster than ϕ_N, but for discontinuous downwashes of the type associated with flaps we anticipate a rate no better than $O(1/N^2)$ since $K\phi$ will in general not be differentiable due to the logarithmic singularity in K_1.

Thus Landahl's method can be expected to give some improvement, but at the expense of having to determine the functions ϕ_o and $K\phi_o$. Generally $K\phi_o$ will have to be calculated to high accuracy numerically. This requires the evaluation of the kernel $\bar{K}(x-\xi)$ at the points $x_i-\xi_j$ where $\{x_i\}_1^N$ are the collocation points and $\{\xi_j\}_1^N$ are quadrature nodes. Using logarithmic Gaussian quadrature one should be able to evaluate these integrals fairly efficiently. Since for Bland's equation the bulk of the computing time goes into the calculation of the kernel, there should be an N where the amount of arithmetic needed to implement Landahl's method is less for a given accuracy than using collocation directly on (11.1). This tradeoff point will have to be determined experimentally and will be a topic of future investigation.

11.1.2 Landahl II

In order to achieve a possible analytic simplification in the evaluation of ϕ_o via (11.17) we consider the following modification of the previous procedure.

Assume that w can be decomposed as

$$w = w_s + w_c \tag{11.19}$$

where w_s is the singular part of w and w_c is the continuous part. In this case

$$\phi_o = H^{-1}w_s \tag{11.20}$$

and the residual downwash is given by

$$w_R = w_c - KH^{-1}w. \tag{11.21}$$

The residual pressure is obtained from

$$(H+K)\phi_R = w_c - K\phi_o . \tag{11.22}$$

Eq. (11.22) is solved by collocation to give an approximation ϕ_R^N to ϕ_R. The approximation to ϕ is taken to be

$$\tilde{\phi}_N = \phi_o + \phi_R^N. \tag{11.23}$$

Using arguments similar to those above we arrive at the following theorem.

Theorem 11.3. Let $\tilde{\phi}_N$ be given by (11.23). Then $\tilde{\phi}_N$ converges to ϕ and

$$\| \phi - \tilde{\phi}_N \|_\gamma \leq \| (H+K_N)^{-1} \| \left(\| K\phi - K_N\phi \|_\alpha + \| w_c - L_N(w_c) \|_\alpha \right) . \tag{11.24}$$

Proof. See Ref. [58] for details. Note that from (11.24) the convergence rate of Landahl II should be the same as that of Landahl I, but that ϕ_o should be easier to evaluate□

11.2 Iteration

A common procedure in numerical analysis for solving an equation is to use iteration. For linear equations Picard iteration is a well-known method. Application of this to (11.1) determines a sequence of approximations to ϕ by the following scheme. Let ϕ_0 be an initial approximation to ϕ and recursively define ϕ_n, $n \geq 1$ by

$$H\phi_n + K\phi_{n-1} = w. \tag{11.25}$$

Since $\|H\| = 1$ a sufficient condition for ϕ_n to converge to ϕ is that $\|K\| < 1$. The error is given by

$$\|\phi - \phi_n\|_\gamma \leq \|K^n\| \, \|\phi - \phi_0\|_\gamma . \tag{11.26}$$

From (11.26) one sees that the closer ϕ_0 is to ϕ the more rapidly ϕ_n converges to ϕ. If ϕ_0 is chosen as a collocation approximation to ϕ then on the basis of the above argument it seems reasonable that iterating on it would be a useful method for accelerating convergence. The basic difficulty that we encounter is the apparent problem of calculating more than one iterate, so that we restrict ourselves to considering the effect of a single iteration.

Before proceeding, we point out that our attention was drawn to this method by the work of Sloan, Burn and Datyner [59], and Sloan [60], on the use of iteration for Galerkin's method for integral equations of the second kind. It was apparently first demonstrated in[59] that iteration on a Galerkin approximation gave <u>super-linear</u> convergence. In addition to Sloan et al the method has also been used by Phillips in conjunction with collocation for equations of the second kind [61]. Since we will discuss both collocation and Galerkin's method in this section a slight change in notation is introduced. ϕ_N^C will denote the collocation approximation to ϕ and ϕ_N^G will denote the Galerkin approximation [5].

Let $\bar{\phi}_N$ be the first Picard iterate of ϕ_N^C defined by

$$H\bar{\phi}_N + K\phi_N^C = w. \tag{11.27}$$

<u>Theorem 11.4.</u> $\bar{\phi}_N$ converges uniformly to the solution ϕ of 11.1.

<u>Proof.</u> From (11.27) it is seen that

$$\bar{\phi}_N = w - H^{-1}K\phi_N^C. \tag{11.28}$$

It now follows from the Schongen inversion formula that $H^{-1}K$ is an integral operator with Hilbert-Schmidt kernel [5]. Let $\tilde{K}$ denote the kernal of $H^{-1}K$. Then

$$\tilde{\psi}_N(x) = w(x) - \int_{-1}^{1} \sqrt{\frac{1-\xi}{1+\xi}}\ \tilde{K}(x,\xi)\psi_N^C(\xi)d\xi.$$

Similarly

$$\psi(x) = w(x) - \int_{-1}^{1} \sqrt{\frac{1-\xi}{1+\xi}}\ \tilde{K}(x,\xi)\psi(\xi)d\xi.$$

This gives

$$\psi(x) - \tilde{\psi}_N(x) = \int_{-1}^{1} \sqrt{\frac{1-\xi}{1+\xi}}\ \tilde{K}(x,\xi)[\psi(\xi) - \psi_N^C(\xi)]d\xi.$$

By the Cauchy-Schwarz inequality

$$\max_{-1\le x\le 1} |\psi(x) - \tilde{\psi}_N(x)| \le C \| \psi - \psi_N^C \|_\gamma$$

But $\| \psi - \psi_N^C \|_\gamma \to 0$ so that $\tilde{\psi}_N(x)$ converges uniformly to $\psi(x)$ □

From the uniform convergence of $\tilde{\psi}_N$ to ψ we anticipate that the sequence $\{\tilde{\psi}_N\}$ should be better behaved than $\{\psi_N^C\}$, and possibly free of the Gibbs phenomena present in L^2 convergence. One also expects a more rapid rate of convergence than that for collocation alone. For equations of the second kind the results of Phillips appear to indicate this [61]. However we have not been able to prove this at present for Bland's equation.

Using Theorem (4.5) of [5] as a guide we expect that for even moderate N that the collocation and Galerkin solutions should be close, and it is for Galerkin's method that accelerated convergence can be established.

Let ψ_N^G be the Galerkin approximation to ψ [ ], and observe that ψ_N^G satisfies

$$H\psi_N^G + \tau_N K\psi_N^G = \tau_N w \tag{11.30}$$

where τ_N is the operator of orthogonal projection onto Span $\{\gamma_n\}_1^N$. Let ψ_N^S be the first Picard iterate of ψ_N^G. Then ψ_N^S solves

$$H\psi_N^S + K\psi_N^G = w. \tag{11.31}$$

Applying τ_N to both sides of (11.31) gives

$$\tau_N H\psi_N^S + \tau_N K_N \psi_N^G = \tau_N w. \tag{11.32}$$

TABLE OF CONTENTS

Since ψ_N^G satisfies (11.30) we get

$$\pi_N H\psi_N^S = H\psi_N^G. \tag{11.33}$$

Using (11.33) in (11.31) shows that ψ_N^S solves

$$H\psi_N^S + K(H^{-1}\pi_N H)\psi_N^S = w. \tag{11.34}$$

Let $Q_N = H^{-1}\pi_N H$ and observe that by the unitarity of H that Q_N is the operator of orthogonal projection onto Span $\{\alpha_n\}_1^N$. This gives ψ_N^S as the solution to

$$(H+KQ_N)\psi_N^S = w.$$

We now consider the convergence of ψ_N^S to ψ. First, note that by the same argument that was used in Theorem 11.4 that ψ_N^S converges uniformly to ψ. However, here we can establish a superlinear rate of convergence. Our result is a generalization of Sloan's [59],[60] for integral equations of the second kind.

Theorem 11.5 ψ_N^S converges in L_α^2 to ψ and

$$\|\psi-\psi_N^S\|_\gamma \leq \|(H+KQ_N)^{-1}\| \, \|K-KQ_N\| \, \|\psi-Q_N\psi\|_\gamma. \tag{11.35}$$

Proof. First observe that $\|K-KQ_N\| \to 0$ [5]. From this it follows that $(H+KQ_N)^{-1}$ exists for N sufficiently large. Thus

$$\psi_N^S = (H+KQ_N)^{-1}w.$$

This gives

$$\begin{aligned}\psi-\psi_N^S &= (H+K)^{-1}w-(H+KQ_N)^{-1}w \\ &= (H+KQ_N)^{-1}(KQ_N-K)\psi. \end{aligned}\tag{11.36}$$

Now

$$\psi = Q_N\psi+(I-Q_N)\psi,$$

so that

$$(KQ_N-K)\psi = (KQ_N-K)Q_N\psi+(KQ_N-K)(I-Q_N)\psi.$$

Since $Q_N^2 = Q_N$,

$$(KQ_N)Q_N\psi-KQ_N\psi = KQ_N\psi-KQ_N\psi = 0. \tag{11.37}$$

Using (11.37) in (11.36) gives

$$\psi-\psi_N^S = (H+KQ_N)^{-1}(KQ_N-K)(\psi-Q_N\psi) \tag{11.38}$$

Taking norms on both sides of (11.38) gives the result□

By a similar argument to that above it is easily shown that

$$\| \psi-\psi_N^G\|_\gamma \leq \| (H+\pi_N K)^{-1}\| \, \|\psi-Q_N\psi\|_\gamma . \tag{11.39}$$

Comparing (11.35) and (11.39) shows that the rate of convergence of ψ_N^S to ψ is enhanced by the factor $\|K-KQ_N\|$ over that of ψ_N^G. For steady problems the logarithmic terms in K will be absent so that $\| K-KQ_N\|$ should converge to 0 rapidly thus providing a more rapid rate of convergence than ψ_N^G. For unsteady problems it follows from Theorem (4.5) of [5] that

$$\| K-KQ_N\| = 0(1/\sqrt{N}), \tag{11.40}$$

so that for discontinuous downwashes it follows that

$$\| \psi-\psi_N^S\|_\gamma = 0(1/N), \tag{11.41}$$

a rate equal to that observed for collocation. As indicated in section 10, this may very well be pessimistic, however a rate no better than $0(1/N^{3/2})$ is anticipated. This at present appears to be too slow a rate to achieve the desired accuracy of $0(10^{-3})$ error with $N\leq 24$.

11.3 Reverse flow theorems

A method of long standing in the aerodynamics literature for solving flow problems has been the use of reverse flow theorems [55],[56]. Originally introduced as a technique for decreasing the computation time in calculating lift and pitching moment it also appears to have some promise for increasing the rate of convergence of integrated quantities for problems with flaps.

It was shown in [5] that such quantities as lift, pitching moment and generalized aerodynamic forces could be calculated in terms of inner products $\langle f, \psi \rangle_\gamma$ where f is the function representing the particular moment of interest. The basic idea of a reverse flow theorem consists of evaluating $\langle f,\psi \rangle_\gamma$ in terms of the solution to an appropriate adjoint problem.

To be more precise let H^* and K^* be the Hilbert space adjoints of H and K [5] and consider calculating the inner product $\langle f,\psi \rangle_\gamma$, where $f \in L^2_\gamma$. Let ψ^* be the unique solution to

$$(H^*+K^*)\psi^* = f. \tag{11.42}$$

(That ψ^* exists and is unique follows from the fact that H+K is one to one and the Fredholm alternative.)

Theorem 11.6. $$\langle f,\psi \rangle_\gamma = \langle \psi^*,w \rangle_\alpha \tag{11.43}$$

Proof. By the definition of adjoint we find that

$$\langle f,\psi \rangle = \langle (H^*+K^*)\psi^*, \psi \rangle_\gamma = \langle \psi^*,(H+K)\psi \rangle_\alpha$$
$$= \langle \psi^*,w \rangle_\alpha \square$$

From the theorem we observe that if f is "smoother" than w, then solving for ψ^* should present a better behaved problem than solving for ψ directly if one only wants to calculate $\langle f,\psi \rangle_\gamma$ rather than ψ itself.

Theorem (11.6) suggests the following scheme for approximating $\langle f,\psi \rangle_\gamma$. Let ψ^*_N be a collocation approximation to ψ^* and take $\langle w,\psi^*_N \rangle_\gamma$ as an approximation

to $\langle f,\psi\rangle_\gamma$. It is easily shown that ψ_N^* converges to ψ so that $\langle w,\psi_N^*\rangle_\alpha$ converges to $\langle w,\psi^*\rangle_\alpha = \langle f,\psi\rangle_\gamma$. Thus the method is well defined. Using the Cauchy-Schwarz inequality it follows [48] that

$$|\langle f,\psi\rangle_\gamma - \langle w,\psi_N^*\rangle_\alpha| \leq \|w\|_\alpha \{\|(K^*-K_N^*)\psi\|_\alpha + \|f-f_N\|_\alpha\}. \tag{11.44}$$

If f is a polynomial, then for N sufficiently large $f = f_N$ and (11.44) becomes

$$|\langle f,\psi\rangle_\gamma - \langle w,\psi_N^*\rangle_\alpha| \leq \|w\|_\alpha [\|(K^*-K_N^*)\psi^*\|_\alpha]. \tag{11.45}$$

The convergence given by (11.45) is then analogous to that achieved using a "degenerate" kernel rather than a projection method [51].

Although (11.45) indicates good convergence for a "polynomial" moment the method discussed above will generally be ineffective if f represents a discontinuous moment such as the hinge moment, because in this case the adjoint problem (11.42) is of the same type as $(H+K)\psi=w$. Since for some problems the reverse flow Theorem 11.6 appears to have improved convergence properties we feel that its use should be further investigated.

11.4 Other Methods

There are other procedures that have recently been proposed for the solution of problems with flaps. Among these are the semi-analytic methods of Williams [62] and [63], and several projection methods proposed by Milne [56]. These techniques have yet to be investigated and would require one to develop algorithms different from that employed in TWODI. Although we have ruled out none of the above as future candidates, our analysis indicates that none of these would provide sufficiently increased accuracy without making major alterations in our existing code.

11.5 Extrapolation

As the discussion above pointed out it is presently felt that incorporating any of the above methods of convergence acceleration would not provide an acceptable degree of accuracy without making substantial changes in TWODI. For this reason we have begun investigating methods which can make the maximum use of the output of our program. As we presently have the capability of solving many problems at once, and with considerable efficiency, a reasonable approach is to try to combine these solutions effectively for enhanced accuracy. A standard procedure for doing this in numerical analysis is the method of extrapolation [50]. Here various solutions computed for different numbers of basis elements are combined either linearly or non-linearly to produce solutions which have higher order accuracy than any of the original ones. Such methods are commonplace in codes for solving differential equations [37],[64] but seem not to have attracted much attention for the solution of integral equations [50],[65]. As we shall see, their effective use requires one to have available known asymptotic expansions for the error in the numerical approximation as a function of the number of basis elements. Such expansions seem to be lacking in general for collocation methods and in particular for the solution of Bland's integral equation. However, using the error estimate (10.7) as a guide, along with the examination of results for the free air case we show how to obtain the proper form of the error and thus to extrapolate correctly.

Although many forms of extrapolation are possible, we have chosen the analogue of Richardson extrapolation [50] because one can easily obtain the correct order of convergence. For other methods, such as Aitken extrapolation, this is not easily done [37]. We begin by presenting the basic theory of this method.

Let α be a complex number and let $\{\alpha_n\}$ be a sequence converging to α. Suppose

it is known that the error $\epsilon_n = \alpha - a_n$ has an expansion of the form

$$\epsilon_n = a_1/n^{\sigma_1} + a_2/n^{\sigma_2} + \ldots \tag{11.46}$$

where $\sigma_1 < \sigma_2 < \sigma_3 \ldots$ The sequence $\{a_n\}$ is not necessarily convergent but is assumed to have the property that

$$\lim_{n\to\infty} n^{\sigma_m}(\epsilon_n - \sum_{j=1}^{m} a_j/n^{\sigma_j}) = 0. \tag{11.47}$$

Such an expansion is called asymptotic.

For simplicity we restrict ourselves to the case where all the σ_j's are integers and in particular assume that $\sigma_j = j$. Thus ϵ_n has the form

$$\epsilon_n = a_1/n + a_2/n^2 + a_3/n^3 + \ldots \tag{11.48}$$

The basic idea of Richardson extrapolation is to compute subsequences $\{a_{k_n}\}_{k=1}^{\infty}$, and then to combine these in such a way to form new approximations which converge more rapidly to α than $\{a_n\}$. For example, consider $Z_n^1 = 2a_{2n} - a_n$. Then

$$\alpha - Z_n^1 = [2(\alpha - a_1/n - a_2/4n^2 \ldots) - (\alpha - a_1/n - a_2/n^2 \ldots)] = -a_2/2n^2 + \ldots \tag{11.49}$$

Thus $\{Z_n^1\}$ is accurate to order $1/n^2$. $\{Z_n^1\}$ is referred to as a sequence of first order extrapolations of $\{a_n\}$.

For each j it is possible to calculate a sequence $\{Z_n^j\}$ which has the property that

$$\alpha - Z_n^j = a_j^1/n^{j+1} + a_j^2/n^{j+2} \ldots \tag{11.50}$$

Such a sequence will be called a sequence of j^{th} order extrapolations of $\{a_n\}$. For example, one possibility for Z_n^2 is

$$Z_n^2 = a_n/3 - 2a_{2n} + 8a_{4n}/3, \tag{11.51}$$

and for Z_n^3

$$Z_n^3 = -a_n/21 + 2a_{2n} - 8a_{4n}/3 + 64a_{8n}/21. \tag{11.52}$$

Higher order extrapolation formulas can also be obtained. We illustrate these with a derivation of (11.52).

From (11.48) it follows that

$$\varepsilon_n = a_1/n+a_2/n^2+a_3/n^3+\ldots, \tag{11.53$_1$}$$

$$\varepsilon_{2n} = a_1/2n+a_2/4n^2+a_3/8n^3+\ldots, \tag{11.53$_2$}$$

$$\varepsilon_{4n} = a_1/4n+a_2/16n^2+a_3/8n^3+\ldots, \tag{11.53$_3$}$$

$$\varepsilon_{8n} = a_1/8n+a_2/64n^2+a_3/512n^3+\ldots \tag{11.53$_4$}$$

(α,β,γ) are now determined so that

$$\varepsilon_n + \alpha\varepsilon_{2n}+\beta\varepsilon_{4n}+\gamma\varepsilon_{8n} = a_4^1/n^4+\ldots \tag{11.54}$$

From (11.53) this requires that

$$\alpha/2+\beta/4+\gamma/8+1 = 0, \tag{11.55$_1$}$$

$$\alpha/4+\beta/16+\gamma/64+1 = 0, \tag{11.55$_2$}$$

$$\alpha/8+\beta/64+\gamma/512+1 = 0, \tag{11.55$_3$}$$

Solving (11.55) gives

$$\alpha = -14,\beta = 56, \gamma = -64. \tag{11.56}$$

Substituting into (11.54) gives

$$(\alpha-a_n)-14(\alpha-a_{2n})+56(\alpha-a_{4n})-64(\alpha-a_{8n})$$

$$= \alpha-(-a_n/21+2a_{2n}/3-8a_{4n}/3+64a_{8n}/21) = a_4^1/21n^4+\ldots$$

Letting

$$z_n^3 = -a_n/21+2a_{2n}/3-8a_{4n}/3+64a_{8n}/21$$

shows that (11.50) is satisfied for $j=3$.

In practice it is most common to use the subsequences $\{a_{2^k n}\}$, $1\le k\le j$, to obtain the sequence $\{z_n^j\}$. Solving the following set of linear equations allows one to

obtain the appropriate coefficients for jth order extrapolation.

$$\begin{bmatrix} 1/2 & 1/4 & \dots & 1/2^{j} \\ 1/4 & 1/16 & & 1/4^{j} \\ \vdots & \vdots & & \vdots \\ 1/2^{j} & 1/2^{2j} & \dots & 1/2^{j^2} \end{bmatrix} \begin{bmatrix} \beta_1 \\ \beta_2 \\ \vdots \\ \beta_j \end{bmatrix} = \begin{bmatrix} 1 \\ 1 \\ \vdots \\ 1 \end{bmatrix} \tag{11.57}$$

In this case we have

$$\varepsilon_n+\beta_1\varepsilon_{2n}+\beta_2\varepsilon_{4n}+\dots+\beta_j\varepsilon_{2^j n} = a_{j+1}/n^{j+1}+\dots \tag{11.58}$$

Since the coefficient matrix in (11.57) is a Vandermonde matrix [5], equation (11.57) is uniquely solvable and the sequence $\{z_n^j\}$ satisfying (11.58) is well defined.

To determine the applicability of these formulas to the solution of problems with flaps the results of Tables 3-6 were used. Here we observe the curious fact that for a midchord flap the subsequence $\{\alpha_{2n}\}_{n=1}^{10}$ (α_n = lift or norm) appears to satisfy (11.48) and for a three-quarter chord flap the subsequence $\{\alpha_{3n}\}_{n=1}^{6}$ appears to have the same property. Thus for a mid-chord flap it seems to be appropriate to extrapolate on $\{\alpha_2,\alpha_4,\alpha_8,\alpha_{16}\}$ and for the three-quarter chord flap we use $\{\alpha_3,\alpha_6,\alpha_{12}\}$. This oscillatory behavior, with the period of oscillation apparently depending on the location of the hinge point was unanticipated based on our experience with the rapid and monotone convergence of TWODI-I for smooth downwashes. At present it appears that the period of oscillation is independent of the kernel K so that a suitable subsequence for extrapolation can be obtained by solving a series of steady free air problems. This can be done rapidly with our existing program.

To see the effect of using successively higher order extrapolations z_8^1, z_4^2, and z_2^3 were calculated for the lift and norm for the mid-chord flap and z_6^1, z_3^2 were obtained for the three quarter chord flap. The results are listed in Tables 7-9 below.

Table 7. Extrapolation of C_{L_δ} and norm for a midchord flap (M=0,k=0,$\eta=\infty$)

	Norm	C_{L_δ}	% error (norm)	% error (C_{L_δ})
Exact	1.60337	5.14159		
z_8^1	1.60241	5.13466	-.0599	-.1348
z_4^2	1.60327	5.14069	-.0062	-.0175
z_2^3	1.60335	5.14139	-.0012	-.0039

Table 8. Extrapolation of C_{L_δ} for an oscillating flap hinged at the 50% chord (M=0, k=.1, n=∞)

	real	imag	magn	phase	% error(magn)
Exact	4.33227	-0.43177	4.35373	-5.69	
z_8^1	4.32647	-0.43122	4.34791	-5.69	-0.1337
z_4^2	4.33153	-0.43171	4.35299	-5.69	-0.0171
z_2^3	4.33210	-0.43176	4.35359	-5.69	-0.0033

Table 9. Extrapolation of C_{L_δ} for an oscillating flap hinged at the 75% chord (M=0, k=.1, n=∞)

	real	imag	magn	phase	% error(magn)
Exact	3.20444	-0.48982	3.24166	-8.69	
z_6^1	3.19235	-0.48792	3.22942	-8.69	-0.3776
z_3^2	3.20191	-0.48944	3.23910	-8.69	-0.0790

Table 10. Effect of using incorrect subsequences for extrapolation

	real	imag	magn	phase	% error(magn)
midchord flap					
z_6^1	4.32230	-0.43083	4.34372	-5.69	-0.2300
z_3^2	4.57927	-0.45301	4.60163	-5.65	+5.6939
three-quarter chord flap					
z_8^1	3.51114	-0.53452	3.55159	-8.66	9.5608
z_4^2	3.77727	-0.57288	3.82352	-8.92	17.9494
z_2^3	4.00144	-0.60507	4.04693	-8.60	24.8413

The results are quite interesting showing that 4-5 decimal accuracy is obtained using at most 16 basis elements. Thus it appears that an error of $0(10^{-3})$ can be obtained using the present code, followed by the minimal amount of manual arithmetic required to do the necessary extrapolations.

As an independent check on the validity of the above procedures we have extrapolated some results presented by Milne [56] in his development of finite element methods for solving (3.8). Table 11 taken from [56] gives values of lift, pitching moment and hinge moment for approximate solutions to (3.8) using basis elements which were piecewise linear.

Again it is easy to show that the errors ϵ_n satisfy $\epsilon_n = a_1/n+0(1/n^2)$ so that extrapolation is feasible. Second order extrapolations are given in Table 11. It is interesting to note that the "exact" values are obtained using 48 basis elements with extrapolation, whereas the raw value for lift and hinge moments are correct to only 2 significant figures using 60 basis elements.

Table 11. Convergence of section coefficients for 50% flap using finite elements (M=0, k=0, n=∞)

No. of basis elements	Lift	Pitching Moment	Hinge Moment
Exact	.3460	.1365	.0780
12	.3410	.1353	.0756
24	.3435	.1359	.0767
36	.3443	.1361	.0771
48	.3447	.1362	.0775
60	.3450	.1362	.0780
2^2_{12}	.3460	.1365	.0780

On the basis of these observations we feel confident that the use of extrapolation will result in accurate solutions for flow problems with flaps. The main obstacle remaining to complete automation seems to be the necessity of performing the preliminary analysis of a sequence of free air problems in order to determine the appropriate subsequence for extrapolation. In this regard it is interesting to note that while Bland's collocation method produces oscillatory convergence, Milne's finite element procedure does not. Monotone convergence is, as we have seen more desirable and further investigation of the methods studied in this section for this behavior should be done.

§12. Efficient integration of singularities in the kernel

The basic accuracy of the TWODI program for smooth downwashes is about 6 decimals in steady flow and 3 decimals in unsteady flow using 5-10 basis elements. We will now show how this can be improved to 6 decimals in both steady and unsteady flow with little increase in the amount of arithmetic.

12.1 General procedure for logarithmic singularities

An efficient solution of the airfoil equation (3.16) requires that the integral for the collocation matrix

$$C_{mn} = \frac{1}{\pi}\int_{-1}^{1} \sqrt{\frac{1-\xi}{1+\xi}}\, K(x_m-\xi,M,k,\eta,\ldots)\gamma_n(\xi)\, d\xi \qquad (12.1)$$

be computed efficiently for all values of the parameters M,k,η, etc. In general, the kernel contains a dominant Cauchy singularity, a weaker logarithmic singularity, and is otherwise analytic. It can be shown that

$$K(x,k,M,\eta,\ldots) = \frac{1}{x} - \frac{ik}{\beta^2}\, e^{-ikx} F_1\,(x,k,M)\,\log|x| - e^{-ikx}\, F_2\,(x,k,M,\eta,\ldots), \qquad (12.2)$$

where F_1 and F_2 are analytic. We will identify these functions below.

The procedure originally used by Bland [8], [9] to compute C_{mn} is the one presently used in TWODI and is described in section 6. The Cauchy singularity is integrated in closed form using the Akheizer-Bland transform (5.3) and an additional closed form integration is obtained by using the logarithmic transform (5.24). The remaining continuous part of the kernel multiplied by the appropriate basis function is then integrated approximately by Jacobi-Gaussian quadrature (5.30). Thus the only source of error (other than roundoff) in computing C_{mn} presently is quadrature error from integrating the continuous part of the kernel.

It is well known [37], [38] that high precision Gaussian quadrature formulas work best with analytic integrands. Splitting the kernel into the Cauchy, logarithmic and continuous parts as described in section 6,

$$K(x,k,M,\eta,\ldots) = \frac{1}{x} - \frac{ik}{\beta^2}\,\log|x| + K_c\,(x,k,M,\eta,\ldots), \qquad (12.3)$$

we see by (12.2) that the continuous part of the kernel is given by

$$K_C(x,k,M,\eta,\ldots) = \frac{ik}{\beta^2}\,(1-e^{-ikx}F_1\,(x,k,M))\,\log|x| - e^{-ikx}F_2\,(x,k,M,\eta,\ldots) \qquad (12.4)$$

and is clearly not analytic because it contains nondifferentiable terms of the form

$$x\,\log|x|,\ x^2\,\log|x|,\ldots$$

To assess the errors resulting from integrating K_C without properly accounting for these logarithmic terms, we computed

$$\int_0^1 x^n \log x\,dx$$

using Legendre-Gaussian quadrature for various n and for various numbers NQ of quadrature points. The results, shown in Table 12, indicate that for n=1, 16 point quadrature is at best 5 decimal accurate.

Table 12. Error in $\int_0^1 x^n \log x dx$ using NQ point Legendre-Gaussian quadrature

% error	n = 0	n = 1	n = 2
NQ = 1	30.685	-38.629	-55.958
NQ = 2	10.412	-3.1413	2.3139
NQ = 4	3.1464	-.25967	.04269
NQ = 8	.87610	-.01956	.00083
NQ = 16	.23207	-.00136	.00001

Since the number of quadrature points used in TWODI equals the number of pressure basis functions, it is not reasonable to expect to obtain accurate calculations for unsteady flow using a small number of basis functions. For example, using 8 basis functions we might expect at most 3 or 4 decimal accuracy. This has been borne out in practice; using NP = 8, the TWODI-I program was 3 decimal accurate for unsteady flow [5, p.81].

In order to correctly integrate the logarithmic kernel singularity in the presence of leading and trailing edge pressure singularities, it is necessary to separate

the interval [-1,1] into four subintervals [-1,a], [a,x], [x,b] and [b,1] where

$$-1 < a < x < b < 1. \tag{12.5}$$

Making the necessary transformations gives six different kinds of integrals, all of which can be evaluated quite accurately (12 decimals) using tables stored in TWODI:

$$\frac{1}{\pi}\int_{-1}^{1}\sqrt{\frac{1-\xi}{1+\xi}}\,\log|x-\xi|\,f(x,\xi)\,d\xi$$

$$= \frac{\sqrt{1+a}}{\pi}\int_0^1 \frac{1}{\sqrt{u}}\left[\sqrt{1-\xi}\,\log(x-\xi)f(x,\xi)\right]du \qquad \xi = -1+(1+a)u$$

$$- \frac{x-a}{\pi}\int_0^1 \log\frac{1}{u}\left[\sqrt{\frac{1-\xi}{1+\xi}}\,f(x,\xi)\right]du \qquad \xi = x-(x-a)u$$

$$+ \frac{(x-a)\log(x-a)}{\pi}\int_0^1 \left[\sqrt{\frac{1-\xi}{1+\xi}}\,f(x,\xi)\right]du \qquad \xi = x-(x-a)u$$

$$+ \frac{(b-x)\log(b-x)}{\pi}\int_0^1 \left[\sqrt{\frac{1-\xi}{1+\xi}}\,f(x,\xi)\right]du \qquad \xi = x+(b-x)u$$

$$- \frac{b-x}{\pi}\int_0^1 \log\frac{1}{u}\left[\sqrt{\frac{1-\xi}{1+\xi}}\,f(x,\xi)\right]du \qquad \xi = x+(b-x)u$$

$$+ \frac{\sqrt{1-b}}{\pi}\int_0^1 \frac{1}{\sqrt{u}}\left[\frac{1-\xi}{\sqrt{1+\xi}}\log(\xi-x)f(x,\xi)\right]du \qquad \xi = 1-(1-b)u. \tag{12.6}$$

Each of the six integrals appearing in the right hand side of (12.6) possesses an integrand which is the product of an analytic function shown in square brackets, multiplied possibly by a function representing an inverse square root or logarithmic singularity. For obvious reasons, we call these six integrals the leading edge inverse square root, upstream logarithm, upstream continuous, downstream continuous, downstream logarithm, and trailing edge square root parts, respectively.

12.2 The free air incompressible case

This is the simplest case with which we can test the merits of integrating the logarithmic singularity in the kernel using high precision Gaussian quadrature. We will show that a thousand fold increase of accuracy results, with only five basis functions being required to produce six decimal accuracy. Previously, eight basis functions produced three place accuracy. Since accuracy can be traded for reduced computer time, the results of this subsection constitute an important step toward TWODI handling its own accuracy control in the future.

In this case the kernel may be written as [5,p.7]

$$K(x,k,0,\infty,\ldots) = \frac{1}{x} - ike^{-ikx}(Ci(k|x|) + i\,Si(kx) + \frac{i\pi}{2}) \tag{12.7}$$

where Ci and Si are the cosine and sine integrals. They are given [66,p.232] by

$$Ci(z) = \gamma + \log z + \sum_{n=1}^{\infty} \frac{(-1)^n z^{2n}}{(2n)(2n)!}, \tag{12.8}$$

$$Si(z) = \sum_{n=0}^{\infty} \frac{(-1)^n z^{2n+1}}{(2n+1)(2n+1)!}, \tag{12.9}$$

where γ =.57721566490153... is Euler's constant. Combining the above, we obtain

$$K(x,k,0,\infty,\ldots) = \frac{1}{x} - ike^{-ikx}\log|x| - ike^{-ikx}(\log k + \gamma + \frac{i\pi}{2} + \sum_{n=1}^{\infty} \frac{(ikx)^n}{(n)(n!)}). \tag{12.10}$$

Thus we can identify the analytic functions in this case as

$$F_1(x,k,0) = 1, \tag{12.11}$$

$$F_2(x,k,0,\infty,\ldots) = ik\,(\log k + \gamma + \frac{i\pi}{2} + \sum_{m=1}^{\infty} \frac{(ikx)^n}{(n)(n!)}). \tag{12.12}$$

The effect of using equations (12.6) and (12.10) to integrate the complete logarithmic singularity, leaving an analytic integrand to be done by Jacobi-Gaussian quadrature is shown in Table 13 for the case of a plunging airfoil. The exact solution was obtained from the Küssner-Schwarz comparison [5,p.83]. Using the earlier method based on the logarithmic transform with an $x\log|x|$ singularity in the continuous part of the kernel, 8 basis functions produced only 3 place accuracy. Table 13 shows that this is true both of TWODI-I using Bland's kernel with very large height

to chord ratios (and large computer times), and of TWODI-III which calculates the special kernel (12.10) which is more efficient; this verifies that using Bland's kernel with η = 300 is an accurate representation of (12.10). Thus the rather low 3 decimal accuracy obtained by the original method is due to the manner of integrating the remaining part, K_c, of the kernel. Finally, Table 13 shows that using the analytic form of the remaining part of the kernel produces six decimal accuracy with only 4 or 5 basis functions.

The evidence presented by these data strongly indicate that the most efficient computing strategy dictates a switchover to integrating the singularities in the kernel separately.

Table 13. Method of integrating singularities in the kernel

Method	K_c type	NP	C_{L_1} - plunge mode (k = 1)
Exact	-	-	-2.51156+3.38937i = (4.21850,126.54^0)
TWODI-I	x log|x|[1]	8	-2.50990+3.38758i = (4.21608,126.54^0)
TWODI-III	x log|x|[2]	8	-2.50990+3.38757i = (4.21607,126.54^0)
TWODI-III	analytic[2]	1	-1.59997+1.58414i = (2.25153,135.28^0)
TWODI-III	analytic[2]	2	-2.55260+3.42614i = (4.27249,126.69^0)
TWODI-III	analytic[2]	3	-2.51089+3.38900i = (4.21781,126.53^0)
TWODI-III	analytic[2]	4	-2.51156+3.38937i = (4.21851,126.54^0)
TWODI-III	analytic[2]	5	-2.51156+3.38937i = (4.21850,126.54^0)

[1]Using Bland's kernel with η = 300. Approx. 20 min CPU.

[2]Using eq. (12.10) for kernel. A few sec. CPU.

12.3 The free air compressible case

Identification of the singularities in the Possio kernel is certainly important to an efficient solution of the free air compressible case, and also may prove useful in efficiently computing more general kernels for unsteady flow in wind tunnels with slotted and porous walls.

The Possio kernel may be expressed [5,p.9] as

$$K(x,k,M,\infty,\ldots) = -\frac{\pi k}{2\beta^2} e^{-ikx}\left(\left(e^{\frac{ikx}{\beta^2}}\right)\left(iM\ \mathrm{sgn}(x)\ H_1^{(2)}\left(\frac{kM|x|}{\beta^2}\right) - H_0^{(2)}\left(\frac{kM|x|}{\beta^2}\right)\right)\right.$$

$$\left. + \frac{2i\beta}{\pi}\log\frac{1+\beta}{M} + ik\int_0^x e^{\frac{ik\lambda}{\beta^2}} H_0^{(2)}\left(\frac{kM|\lambda|}{\beta^2}\right)\right) d\lambda, \qquad (12.13)$$

where the Hankel functions of the second kind [66,p.360] are given by

$$H_\ell^{(2)} = J_\ell - i\,Y_\ell. \qquad (12.14)$$

Clearly (12.13) is not in a form suitable for numerical computation. Substituting (12.14) gives

$$K(x,k,M,\infty,\ldots) = e^{-ikx}\left\{e^{\frac{ikx}{2\beta^2}}\left[-\frac{\pi kMi}{2\beta^2}\ \mathrm{sgn}(x)\ \left(J_1\left(\frac{kM|x|}{\beta^2}\right) - i\,Y_1\left(\frac{kM|x|}{\beta^2}\right)\right)\right.\right.$$

$$\left. + \frac{\pi k}{2\beta^2}\left(J_0\left(\frac{kM|x|}{\beta^2}\right) - iY_0\left(\frac{kM|x|}{\beta^2}\right)\right)\right] - \frac{ik}{\beta}\log\frac{1+\beta}{M}$$

$$\left. - \frac{\pi k^2 xi}{2\beta^2}\int_0^1 e^{\frac{ikxu}{\beta^2}}\ J_0\left(\frac{kM|x|u}{\beta^2}\right) - iY_0\left(\frac{kM|x|u}{\beta^2}\right)\right)du\right\}. \qquad (12.15)$$

In order to identify the singularities in (12.15), we first identify the specific singularities, as well as analytic functions, which appear in the Bessel functions. Clearly

$$J_\ell(z) = \left(\frac{z}{2}\right)^\ell \sum_{m=0}^{\infty} \frac{\left(-\frac{z^2}{4}\right)^m}{m!\ (m+\ell)!} \qquad (12.16)$$

is analytic. Let

$$\psi(1) = -\gamma,\ \psi(n+1) = \psi(n) + \frac{1}{n} = -\gamma + \sum_{m=1}^{n}\frac{1}{m} \text{ if } n \geq 2 \qquad (12.17)$$

denote values of the psi or digamma function [66] for integer arguments. Then it follows that

$$Y_o(z) = \frac{2}{\pi}(\gamma+\log\frac{z}{2})\,J_o(z) + \frac{2}{\pi}\,G_o(z), \tag{12.18$_1$}$$

$$Y_1(z) = -\frac{2}{\pi z} + \frac{2}{\pi}\log\frac{z}{2}\,J_1(z) - \frac{2}{\pi}\,G_1(z), \tag{12.18$_2$}$$

where

$$G_o(z) = \frac{(\frac{z}{2})^2}{(1!)^2} - (1+\frac{1}{2})\frac{(\frac{z}{2})^4}{(2!)^2} + (1+\frac{1}{2}+\frac{1}{3})\frac{(\frac{z}{2})^6}{(3!)^2} - \ldots, \tag{12.19$_1$}$$

$$G_1(z) = \frac{z}{4}\sum_{n=0}^{\infty}(\psi(n+1)+\psi(n+2))\frac{(-\frac{z}{4}^2)^n}{n!(n+1)!}. \tag{12.19$_2$}$$

Obviously G_o and G_1 are analytic. We note that they may be computed using (12.19) or, using standard Bessel function subroutines according to

$$G_o(z) = \frac{\pi}{2}\,Y_o(z) - (\gamma+\log\frac{z}{2})\,J_o(z), \tag{12.20$_1$}$$

$$G_1(z) = \frac{\pi}{2}\,Y_1(z) - \frac{1}{z} + \log\frac{z}{2}\,J_1(z). \tag{12.20$_2$}$$

Combining the above and rearranging it can be shown that

$$\begin{aligned}
K(x,k,M,\infty,\ldots) = {} & \frac{1}{x} - \frac{ik}{\beta^2}\,e^{-ikx}\log|x| + [(J_o(\tfrac{kMx}{\beta^2}) - iMJ_1(\tfrac{kMx}{\beta^2}))e^{\frac{ikx}{\beta^2}} \\
& - ikx\int_0^1 e^{\frac{ikxu}{\beta^2}}\,J_o(\tfrac{kMxu}{\beta^2})\,du] \\
& - e^{-ikx}\{[\frac{e^{\frac{ikM^2x}{\beta^2}}-1}{x} - \frac{\pi k}{2\beta^2}\,J_o(\tfrac{kMx}{\beta^2}) + \frac{ik}{\beta^2}\,G_o(\tfrac{kMx}{\beta^2}) \\
& + \frac{ik}{\beta^2}(\gamma+\log\frac{kM}{\beta^2})\,J_o(\tfrac{kMx}{\beta^2}) + \frac{\pi kMi}{2\beta^2}\,J_1(\tfrac{kMx}{\beta^2}) \\
& + \frac{kM}{\beta^2}\log\frac{kM}{2\beta^2}\,J_1(\tfrac{kMx}{\beta^2}) - \frac{kM}{\beta^2}\,G_1(\tfrac{kMx}{\beta^2})]e^{\frac{ikx}{\beta^2}} \\
& + \frac{ik}{\beta}\log\frac{1+\beta}{M} + \frac{\pi k^2xi}{2\beta^2}\int_0^1 e^{\frac{ikxu}{\beta^2}}\,(J_o(\tfrac{kMxu}{\beta^2}) - \frac{2i}{\pi}\,G_o(\tfrac{kMxu}{\beta^2}))\,du \\
& + \frac{k^2x}{\beta^2}(\gamma+\log\frac{kM}{2\beta^2})\int_0^1 e^{\frac{ikxu}{\beta^2}}\,J_o(\tfrac{kMxu}{\beta^2})\,du \\
& - \frac{k^2x}{\beta^2}\int_0^1 \log\frac{1}{u}\,e^{\frac{ikxu}{\beta^2}}\,J_o(\tfrac{kMxu}{\beta^2})\,du\},
\end{aligned} \tag{12.21}$$

which in view of (12.2) gives

$$F_1(x,k,M) = [J_o(\frac{kMx}{\beta^2}) - iM\, J_1(\frac{kMx}{\beta^2})]e^{\frac{ikx}{\beta^2}} - ikx \int_0^1 e^{\frac{ikxu}{\beta^2}} J_o(\frac{kMxu}{\beta^2})\, du \tag{12.22}$$

and

$$\begin{aligned} F_2(x,k,M,\infty,\ldots) = {} & \frac{e^{\frac{-ikM^2x}{\beta^2}} - 1}{x} - \frac{\pi k}{2\beta^2} J_o(\frac{kMx}{\beta^2}) + \frac{ik}{\beta^2} G_o(\frac{kMx}{\beta^2}) \\ & + \frac{ik}{\beta^2}(\gamma + \log\frac{kM}{2\beta^2}) J_o(\frac{kMx}{\beta^2}) + \frac{\pi kMi}{2\beta^2} J_1(\frac{kMx}{\beta^2}) \\ & + \frac{kM}{\beta^2}\log\frac{kM}{2\beta^2} J_1(\frac{kMx}{\beta^2}) - \frac{kM}{\beta^2} G_1(\frac{kMx}{\beta^2})]e^{\frac{ikx}{\beta^2}} \\ & + \frac{ik}{\beta}\log\frac{1+\beta}{M} + \frac{\pi k^2 xi}{2\beta^2}\int_0^1 e^{\frac{ikxu}{\beta^2}}(J_o(\frac{kMxu}{\beta^2}) - \frac{2i}{\pi} G_o(\frac{kMxu}{\beta^2}))\, du \\ & - \frac{k^2x}{\beta^2}(\gamma + \log\frac{kM}{2\beta^2})\int_0^1 e^{\frac{ikxu}{\beta^2}} J_o(\frac{kMxu}{\beta^2})\, du \\ & - \frac{k^2x}{\beta^2}\int_0^1 \log\frac{1}{u}\, e^{\frac{ikxu}{\beta^2}} J_o(\frac{kMxu}{\beta^2})\, du. \end{aligned} \tag{12.23}$$

Equations (12.22) and (12.23) display the desired functions F_1 and F_2, but they are not yet in final form and (12.23) is still indeterminate for M=0. F_1 can be put into final form by first noting that

$$J_o' = - J_1 \tag{12.24}$$

and integrating by parts to yield

$$ikx\int_0^1 e^{\frac{ikxu}{\beta^2}} J_o(\frac{kMxu}{\beta^2})\, du = \beta^2(J_o(\frac{kMx}{\beta^2})e^{\frac{ikx}{\beta^2}} - 1) + kMx\int_0^1 e^{\frac{ikxu}{\beta^2}} J_1(\frac{kMxu}{\beta^2})\, du. \tag{12.25}$$

Substituting (12.25) into (12.22) and simplifying, we finally obtain

$$F_1(x,k,M) = 1 + M^2(J_o(\frac{kMx}{\beta^2})e^{\frac{ikx}{\beta^2}} - 1) - iMJ_1(\frac{kMx}{\beta^2})e^{\frac{ikx}{\beta^2}} - kMx\int_0^1 e^{\frac{ikxu}{\beta^2}} J_1(\frac{kMxu}{\beta^2})\, du. \tag{12.26}$$

In this form (12.26) reduces by inspection to (12.11), is easy to compute, and we see that

$$F_1(x,k,M) = 1 + M^2 O(kx) \tag{12.27}$$

is analytic as asserted earlier.

We now obtain a similar reduction for F_2. Integrating the last term in (12.21) by parts gives

$$- \frac{k^2x}{\beta^2} \int_0^1 \log \frac{1}{u} e^{\frac{ikxu}{\beta^2}} J_o(\frac{kMxu}{\beta^2}) \, du$$

$$= ik \int_0^1 \frac{e^{\frac{ikxu}{\beta^2}} - 1}{u} J_o(\frac{kMxu}{\beta^2}) \, du + \frac{ik^2Mx}{\beta^2} \int_0^1 \log \frac{1}{u} (e^{\frac{ikxu}{\beta^2}} - 1) J_1(\frac{kMxu}{\beta^2}) \, du. \qquad (12.28)$$

(We note that when M=0, (12.28) reduces to

$$ik \int_0^1 \frac{e^{ikxu} - 1}{u} du = ik \sum_{n=1}^{\infty} \frac{(ikx)^n}{(n)(n!)} , \qquad (12.29)$$

which is the last term in (12.12).) Substituting (12.28) into (12.23) gives

$$F_2(x,k,M,\infty,\ldots) = ik \int_0^1 \frac{e^{\frac{ikxu}{\beta^2}} - 1}{u} J_o(\frac{kMxu}{\beta^2}) \, du$$

$$+ \frac{ik^2Mx}{\beta^2} \int_0^1 \log \frac{1}{u} (e^{\frac{ikxu}{\beta^2}} - 1) J_1(\frac{kMxu}{\beta^2}) \, du$$

$$+ ik[\frac{e^{\frac{-ikM^2x}{\beta^2}} - 1}{ikx} + \frac{i\pi}{2\beta^2} J_o(\frac{kMx}{\beta^2}) + \frac{1}{\beta^2} G_o(\frac{kMx}{\beta^2})$$

$$+ \frac{1}{\beta^2} (\gamma + \log \frac{kM}{2\beta^2}) J_o(\frac{kMx}{\beta^2}) + \frac{\pi M}{2\beta^2} J_1(\frac{kMx}{\beta^2})$$

$$- \frac{iM}{\beta^2} \log \frac{kM}{2\beta^2} J_1(\frac{kMx}{\beta^2}) + \frac{iM}{\beta^2} G_1(\frac{kMx}{\beta^2})]e^{\frac{ikx}{\beta^2}}$$

$$+ \frac{ik}{\beta} \log \frac{1+\beta}{M} + \frac{\pi k^2 x i}{2\beta^2} \int_0^1 e^{\frac{ikxu}{\beta^2}} (J_o(\frac{kMxu}{\beta^2}) - \frac{2i}{\pi} G_o(\frac{kMxu}{\beta^2})) \, du$$

$$+ \frac{k^2x}{\beta^2} (\gamma + \log \frac{kM}{2\beta^2}) \int_0^1 e^{\frac{ikxu}{\beta^2}} J_o(\frac{kMxu}{\beta^2}) \, du. \qquad (12.30)$$

Integrating by parts again, it follows that

$$J_o(\tfrac{kMx}{\beta^2})e^{\frac{ikx}{\beta^2}} - ikx\int_0^1 e^{\frac{ikxu}{\beta^2}} J_o(\tfrac{kMxu}{\beta^2})du = \beta^2+M^2\ J_o(\tfrac{kMx}{\beta^2})e^{\frac{ikx}{\beta^2}} - kMx\int_0^1 e^{\frac{ikxu}{\beta^2}} J_1(\tfrac{kMxu}{\beta^2})du. \quad (12.31)$$

Substituting (12.31) and the identity

$$ik(\gamma+\log\tfrac{kM}{2\beta^2}) - \tfrac{\pi k}{2} + \tfrac{ik}{\beta}\log\tfrac{1+\beta}{M} = ik(\log k+\gamma+\tfrac{i\pi}{2}) + \tfrac{ik}{\beta}(\tfrac{M^2}{1+\beta}\log\tfrac{2\beta^2}{M} + \log\tfrac{1+\beta}{2\beta^2}) \quad (12.32)$$

into (12.30) gives

$$\begin{aligned} F_2(x,k,M,\infty,\ldots) = {} & ik[\log k+\gamma+\tfrac{i\pi}{2} + \int_0^1 \frac{e^{\frac{ikxu}{\beta^2}}-1}{u} J_o(\tfrac{kMxu}{\beta^2})\,du] \\ & + ik\,[\frac{e^{\frac{-ikM^2x}{\beta^2}}-1}{ikx} + \tfrac{M^2}{\beta^2}(\tfrac{i\pi}{2}+\gamma+\log\tfrac{kM}{2\beta^2})\ J_o(\tfrac{kMx}{\beta^2}) \\ & - \tfrac{iM}{\beta^2}(\tfrac{i\pi}{2}+\log\tfrac{kM}{2\beta^2})\ J_1(\tfrac{kMx}{\beta^2}) \\ & + \tfrac{1}{\beta^2}G_o(\tfrac{kMx}{\beta^2}) + \tfrac{iM}{\beta^2}G_1(\tfrac{kMx}{\beta^2})]e^{\frac{ikx}{\beta^2}} \\ & - \tfrac{ik^2x}{\beta^2}\int_0^1 [M(\gamma+\log\tfrac{kM}{2\beta^2} + \tfrac{i\pi}{2})\ J_1(\tfrac{kMxu}{\beta^2}) + iG_o(\tfrac{kMxu}{\beta^2})\ e^{\frac{ikxu}{\beta^2}}\,du \\ & + \tfrac{ik^2Mx}{\beta^2}\int_0^1 \log\tfrac{1}{u}\ J_1(\tfrac{kMxu}{\beta^2})(e^{\frac{ikxu}{\beta^2}}-1)\,du \\ & + \tfrac{ik}{\beta}(\tfrac{M^2}{1+\beta}\log\tfrac{2\beta^2}{M} + \log\tfrac{1+\beta}{2\beta^2}) \end{aligned} \quad (12.33)$$

which, in view of (12.29), reduces by inspection to (12.12) when M=0, and is clearly analytic with the property that

$$F_2(x,k,M,\infty,\ldots) = F_2(x,k,0,\ldots) + O(kM^2\log M). \quad (12.34)$$

One reason for the importance of (12.27) and (12.33) is the ease with which they can be computed numerically compared with the original expression (12.13). In TWODI, Bland's kernel (3.10)-(3.11) is presently used for all cases except the incompressible free air case given by (12.10) and the steady porous wall case given by (4.13). However, using Bland's kernel for free air conditions is inefficient because the series expressions in (3.11) are quite slowly convergent for large values of η. We have already seen in Table 13 the dramatic benefit of using the efficient expression (12.10) to compute the kernel for the special case of incompressible flow in free air. We would expect a comparable reduction in computer time if (12.2), (12.27) and (12.33) were used to compute the kernel for compressible flow in free air. Furthermore, (12.2) represents a computationally efficient splitting of the kernel into three parts

$$K(x,k,M,\eta,\ldots) = \frac{1}{x} + K_1(x,k,M) + K_2(x,k,M,\eta,\ldots), \tag{12.35}$$

where

$$K_1(x,k,M) = -\frac{ik}{\beta^2} e^{-ikx} \log|x| \; P_1(x,k,M), \tag{12.36}$$

and where

$$K_2(x,k,M,\eta,\ldots) = K_2(x,k,M,\infty,\ldots) + \Delta K_2(x,k,M,\eta,\ldots) \tag{12.37}$$

with

$$K_2(x,k,M,\infty,\ldots) = -e^{-ikx} \; F_2(x,k,M,\infty,\ldots) \tag{12.38}$$

and with ΔK_2 representing the interference kernel due to the wind tunnel walls. Since we now have computationally efficient expressions for all quantities except ΔK_2 and since the Fourier transforms of all kernels are easily obtained, it may be that the application of Laguerre-Gaussian quadrature to the expression

$$\Delta K_2(x,k,M,\eta,\ldots) = \frac{1}{\sqrt{2\pi}} \int_{-\infty}^{\infty} e^{isx} [\hat{K}(s,k,M,\eta,\ldots) - \hat{K}(s,k,M,\infty,\ldots)] ds \tag{12.39}$$

is an efficient way to compute numerically the interference kernels for porous as well as slotted wall tunnels. Since the determination of the unsteady porous wall kernel remains an open problem, the possibilities of this approach will have to await future research.

§13. Steady airloads for porous wall tunnels

In this section we present numerical computations for steady airloads in ideal porous wall wind tunnels; i.e., those governed by the viscous effect boundary condition (2.10). Agreement with previous results is demonstrated and new results are given in the form of compact three dimensional graphs showing airloads for all possible combinations of Mach number, height to chord ratio and viscous effect ventilation coefficient. These graphs are for a fixed downwash but otherwise include all possible flow conditions. They can be generalized to unsteady flow but we have not done so. This section is an extension of similar results by us [5,§§11-12] for fixed Mach numbers in ideal slotted wall tunnels; i.e., those governed by the mass effect boundary condition (2.9), and uses the parametric analysis presented above in section 4 to combine three independent variables (M,η,ν) into two $(\beta\eta,\beta\nu)$.

Table 14 and Figure 4 present values of lift coefficient and center of pressure vs. leakage angle ζ. The center of pressure is relatively insensitive to small amounts of ventilation and shifts more strongly forward as the open jet condition is approached. The trends in both lift and center of pressure using the ideal porous wall boundary condition differ appreciably from the trends obtained using the ideal slotted wall condition. This is evident upon comparing Figures 4 below with Figures 14 and 16 in [5]. Since the limiting case of open or closed walls are independent of the boundary condition selected, verification with previous results is obtained automatically. Only 5 pressure basis functions were required to obtain 6 decimal accuracy. Also, the computations proceeded quickly since the kernel (4.13) is in closed form.

Table 15 and Figures 5, 6 and 7 present lift coefficient, pitching moment coefficient and center of pressure for the full range of Mach number, height to chord ratio[1] and ventilation. The capability to do this so simply is a direct result of the parametric reductions

$$(x,M,\eta,\nu) \to (\frac{x}{\beta\eta}, \beta\eta,\beta\nu)$$

presented in section 4. The doubly infinite domain of the airload surfaces is made compact by the transformations

$$\zeta = \tan^{-1}(\frac{1}{\beta\nu}), \quad \theta_\eta = \tan^{-1}(\frac{1}{\beta\eta}).$$

---

[1] In the present context, we restrict our consideration to tunnels with acoustic height to chord ratios not less than 1; thus $1 \leq \beta\eta \leq \infty$. This restriction is entirely one of context since the numerics are well behaved for narrower tunnels.

The lines θ_η=0 correspond to the free air condition and show constant airloads for all ventilation conditions; this is in keeping with the physical condition that airloads not be affected by the tunnel walls when they are infinitely far away. The lines ζ=0° correspond to a completely closed wall and indicate that both C_{L_α} and C_{M_α} increase as the walls become closer together; at the same time the center of pressure moves aft. The lines ζ=90° correspond to an open jet tunnel; C_{L_α} and C_{M_α} decrease as the walls become closer while the center of pressure shifts forward. Between these bounding lines, the airloads are shown to be continuous. Finally, by comparing the lift and moment surfaces, it is clear that the ventilation coefficients corresponding to zero lift interference differ from those corresponding to zero moment interference.

Table 14. Lift and center of pressure vs. ventilation for a porous wall tunnel

M=.85 η=7.5 w(x)=1 NP≤5 (6 decimal accuracy)

ζ	C_{L_α}	x_{CP}
0°	12.235	.25624
15°	11.460	.25633
30°	10.739	.25529
45°	10.051	.25529
60°	9.4086	.24936
75°	8.8017	.24416
90°	8.2270	.23723

Table 15. Section coefficients vs. M, η and ν for unit downwash

βC_{L_α}	$\theta_\eta = \tan^{-1}(\frac{1}{\beta\eta})$			
ζ	0° (free)	15°	30°	45°
0°	6.28319	6.46436	7.06254	8.29957
30°	6.28319	5.62903	5.31359	5.28501
60°	6.28319	4.89657	3.97490	3.34116
90°	6.28319	4.24753	2.89934	1.91357
βC_{M_α}	$\theta_\eta = \tan^{-1}(\frac{1}{\beta\eta})$			
ζ	0° (free)	15°	30°	45°
0°	.000000	-.022470	-.094292	-.233113
30°	.000000	-.016798	-.076374	-.197892
60°	.000000	.001509	-.011706	-.060754
90°	.000000	.030282	.085436	.132578
x_{CP}	$\theta_\eta = \tan^{-1}(\frac{1}{\beta\eta})$			
ζ	0° (free)	15°	30°	45°
0°	.250000	.256952	.276702	.306175
30°	.250000	.255968	.278747	.324888
60°	.250000	.249384	.255890	.286367
90°	.250000	.235741	.191065	.111435

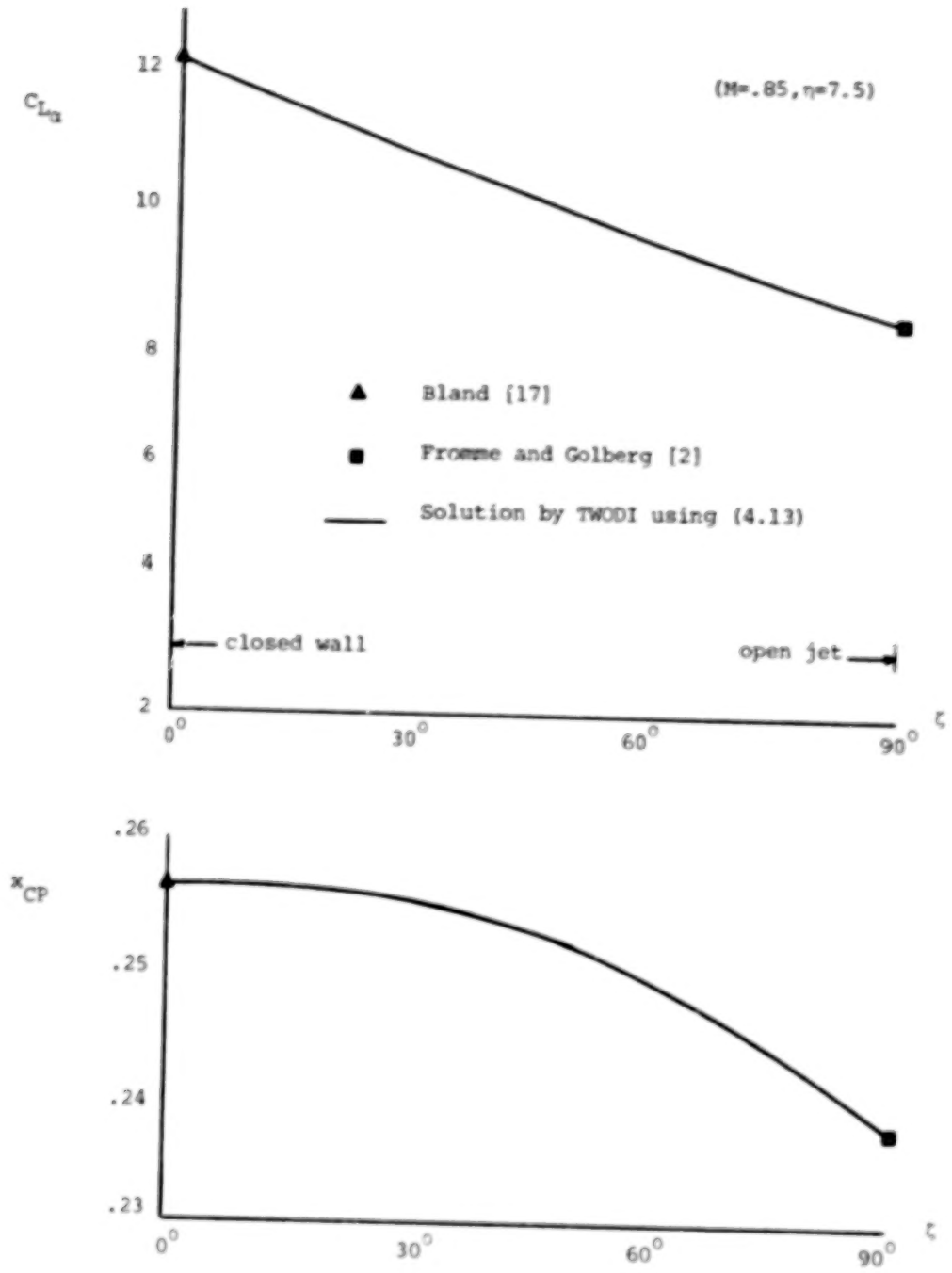

Figure 4. Steady lift and center of pressure vs. ventilation for a porous wall tunnel

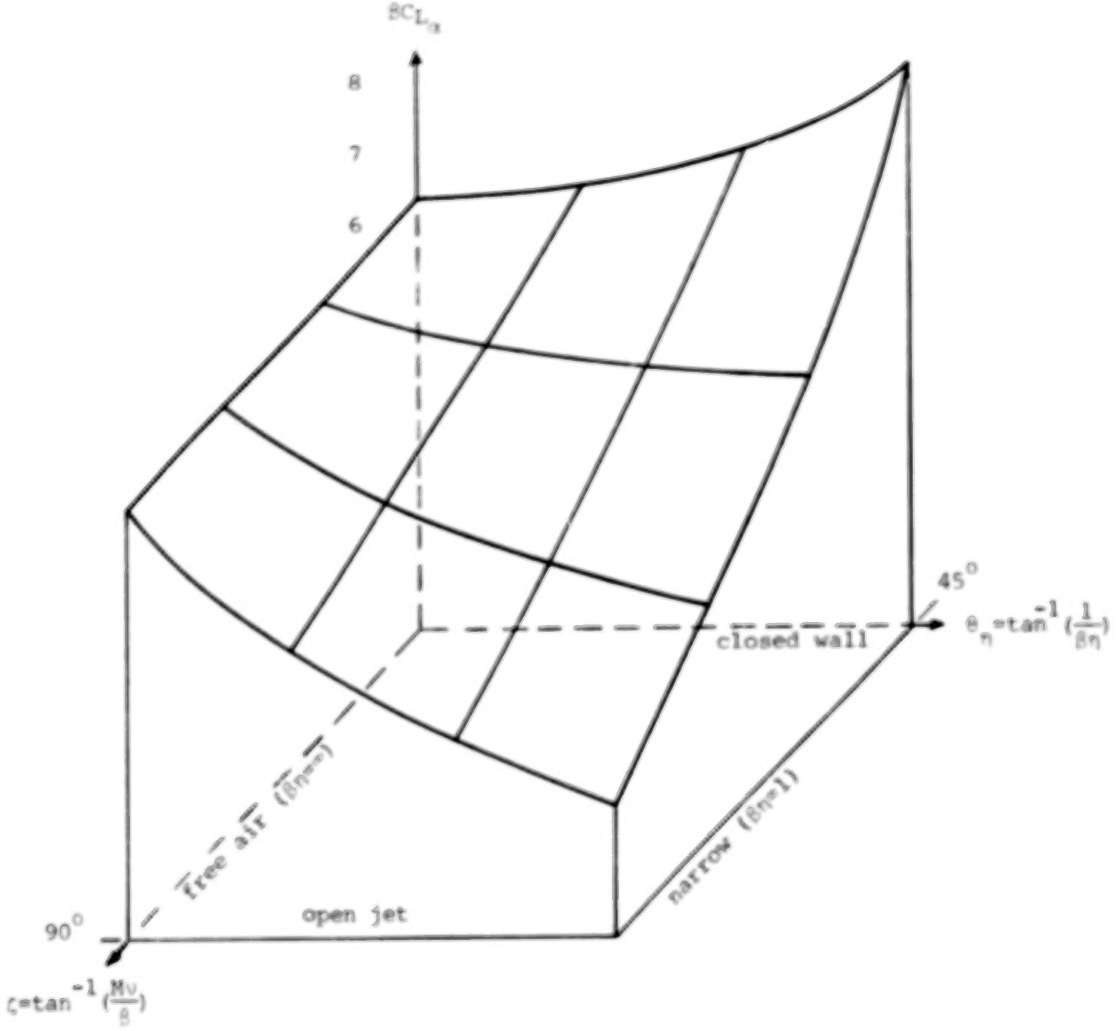

Figure 5. Steady lift vs. M, η and ν for unit downwash

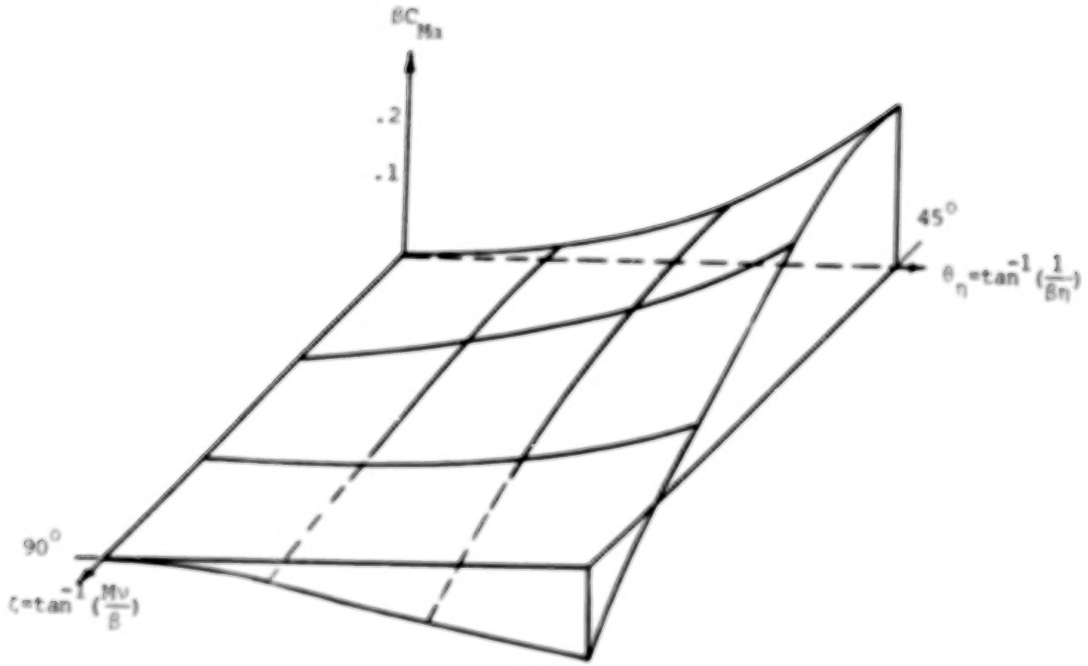

Figure 6. Steady moment vs. M, η and ν for unit downwash

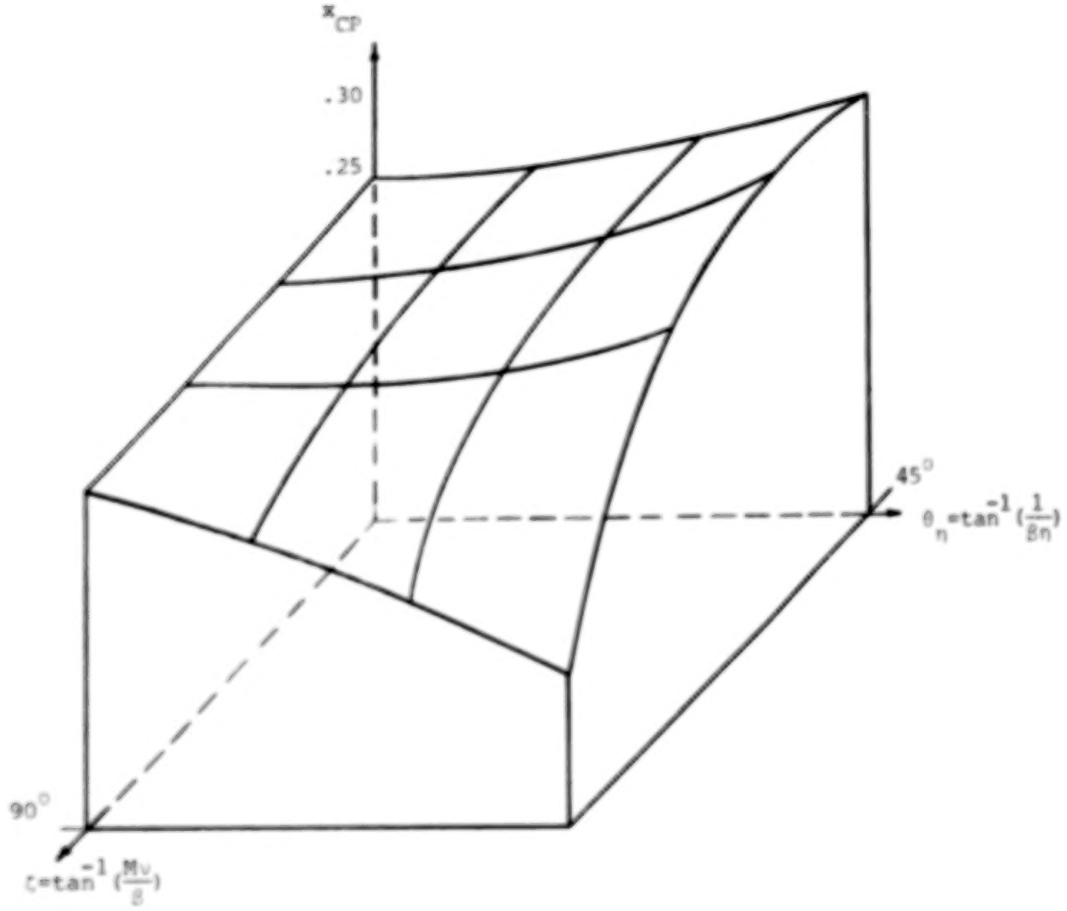

Figure 7. Steady center of pressure vs. M, η and ν for unit downwash

§14. Steady and unsteady interference calculations for airfoils with flaps

The nature of unsteady aerodynamic interference in wind tunnels is not well understood at the present time, especially when the walls are ventilated. This problem is made mathematically more difficult when flaps are present because of the attendant downwash discontinuity at the hinge and the resulting slow convergence of the numerical calculations. In this section, we present new results for steady and unsteady lift interference on airfoil with flaps at various combinations of Mach number, reduced frequency and wall ventilation condition. These results are based on the method of convergence acceleration by extrapolation to the limit as described in section 11 above.

We take as our configuration of interest an airfoil of chord 180mm with a 45mm trailing edge flap mounted in a wind tunnel of height 550 mm. All calculations below were performed using second order extrapolation with NP=3,6 and 12. Based on our analysis in section 11, we expect these results to have mathematical errors of less than .1%.

Table 16 and Figure 8(a) show the C_{L_δ} envelope vs. Mach number, along with the exact free air solution. The Mach numbers listed correspond to the Multhopp angles, $M=\sin\theta$, $\theta=0^\circ$, 18°,..., 72°. Figure 8(b) shows the interference ratio for C_{L_δ} vs. M using the same data. In all cases the effect of wall interference is to increase the lift for a closed wall and to decrease it for an open jet. At very low speeds, these effects are roughly +3% and -36% respectively, increasing in magnitude as the Mach number increases. The increase is less and is more delayed with the closed wall and it is greater and more gradual with the open jet. At high subsonic speeds, especially those above the critical Mach number, transonic nonlinearities will increasingly alter the interference effects from those predicted by the present linear theory.

Table 16. Steady lift interference vs. M for a flap at the three quarter chord

η=3.05556 $\qquad \beta C_{L_\delta}^{free} = \sqrt{3} + \frac{2\pi}{3}$ (exact)

	closed wall		open jet	
M	C_{L_δ}	$\frac{C_{L_\delta}-C_{L_\delta}^{free}}{C_{L_\delta}^{free}}$	C_{L_δ}	$\frac{C_{L_\delta}-C_{L_\delta}^{free}}{C_{L_\delta}^{free}}$
.000000	3.93081	+.027274	2.45693	-.357908
.309016	4.14457	+.030125	2.53450	-.370054
.587785	4.92542	+.014371	2.78953	-.410216
.809017	7.00387	+.075873	3.30696	-.492014
.951057	15.26128	+.232474	4.35129	-.648597

The phenomenon of acoustic resonance was orgininally discovered theoretically by Runyan and Watkins [67] in 1953 and subsequently verfied experimentally by Runyan, Woolston and Rainey [36]. Later, Bland [8], [9] showed that for ideal slotted wall tunnels described by the boundary condition (2.9), acoustic resonance will occur at reduced frequencies given by

$$k_n = \frac{M\lambda_n}{\beta\eta}, \quad n=1,2,... \tag{14.1}$$

where λ_n is the nth positive eigenvalue of (3.11_4). Theoretical calculations showing the effect of acoustic resonance on airloads over the full range of ventilation coefficients were recently given by Fromme and Golberg [5].

Table 17 and Figure 9 present values of C_{L_δ} vs. Mach number for open and closed tunnel walls at four values of reduced frequency, k=0,.1,.2 and .3. The calculations utilize Bland's kernel (3.10) for an ideal slotted wall based on the mass effect boundary condition (2.9). A condition of acoustic resonance between the airfoil and the wind tunnel walls is displayed at k=.249 for M=.9. A precursor of acoustic resonance may be detected at M=.8 in that the magnitude of the lift coefficient for the closed wall condition has dropped below the value for the open jet condition. This is because the fundamental resonant frequency for an open jet is twice as high as the fundamental frequency for a closed wall. The onset of resonance may also be detected by the dramatic shift in phase angle beginning around M=.6 to M=.8.

It should be emphasized that the effect of frequency on wind tunnel interference is a continuous one except of course at the actual resonant frequencies. For this reason, unsteady wind tunnel tests should carefully take into consideration such unsteady interference effects even though the reduced frequencies to be tested may lie below their resonance values.

Table 17. C_{L_δ} vs. M,k and μ for an oscillating flap in a wind tunnel

75% hinge η=3.05556

		C_{L_δ} ($\mu=\infty$ - closed wall)				C_{L_δ} (μ=0-open jet)			
M	k	real	imag	magn	phase	real	imag	magn	phase
.0	.0	3.93081	0.00000	3.93081	0.00	2.45693	0.00000	2.45693	0.00
.0	.1	3.63755	-0.52198	3.67481	-8.17	2.43951	0.03078	2.43970	0.72
.0	.2	3.15090	-0.60877	3.20917	-10.94	2.39288	0.07723	2.39413	1.85
.0	.3	2.80157	-0.45100	2.83764	-9.15	2.32977	0.14703	2.33441	3.61
.2	.0	4.01629	0.00000	4.01629	0.00	2.48840	0.00000	2.48840	0.00
.2	.1	3.70295	-0.56739	3.74617	-8.71	2.47107	0.02451	2.47119	0.57
.2	.2	3.19239	-0.66681	3.26128	-11.80	2.42506	0.06541	2.42594	1.55
.2	.3	2.83538	-0.51065	2.88100	-10.21	2.36358	0.13075	2.36720	3.17
.4	.0	4.31034	0.00000	4.31034	0.00	2.59221	0.00000	2.59221	0.00
.4	.1	3.91916	-0.73544	3.98757	-10.63	2.57547	0.00202	2.57547	0.05
.4	.2	3.31937	-0.87977	3.43398	-14.84	2.53205	0.02405	2.53216	0.54
.4	.3	2.93429	-0.73451	3.02483	-14.05	2.47706	0.07086	2.47808	1.64
.6	.0	4.98528	0.00000	4.98528	0.00	2.80743	0.00000	2.80743	0.00
.6	.1	4.35658	-1.18762	4.51556	-15.25	2.79291	-0.05360	2.79343	-1.10
.6	.2	3.50453	-1.44000	3.78884	-22.34	2.75829	-0.08640	2.75965	-1.79
.6	.3	3.02163	-1.36395	3.31521	-24.30	2.72364	-0.08998	2.72512	-1.89
.8	.0	6.84313	0.00000	6.84313	0.00	3.27336	0.00000	3.27336	0.00
.8	.1	5.00685	-2.81467	5.74377	-29.34	3.27198	-0.22175	3.27949	-3.88
.8	.2	2.88884	-3.24022	4.34102	-48.28	3.28232	-0.45312	3.31345	-7.86
.8	.3	0.65287	-2.84171	2.91574	-77.06	3.33763	-0.74720	3.42024	-12.62
.9	.0	9.92111	0.00000	9.92111	0.00	3.79549	0.00000	3.79549	0.00
.9	.1	3.69704	-5.68253	6.77941	-56.95	3.83945	-0.51021	3.87320	-7.57
.9	.2	-0.75925	-1.22187	1.43855	-121.86	3.99142	-1.33569	4.20898	-18.50
.9	.3	1.80588	-0.32653	1.83517	-10.25	3.28022	-4.17219	5.30726	-51.83

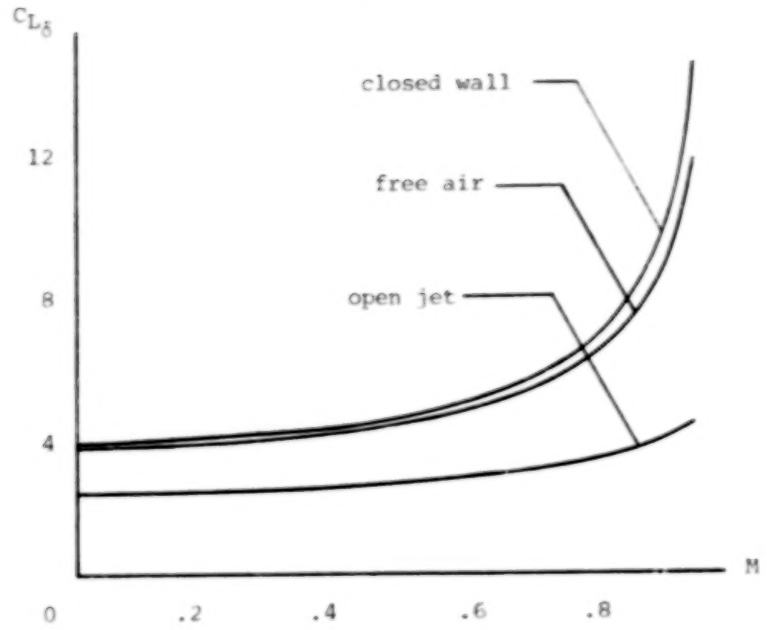

(a) Lift coefficient

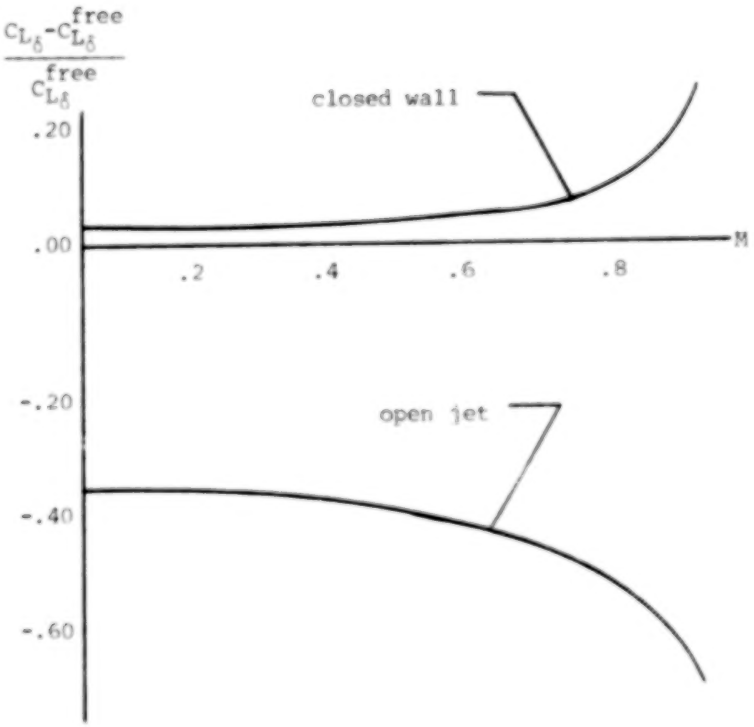

(b) Lift interference ratio

Figure 8. Steady lift interference vs. M for a flap at the three quarter chord

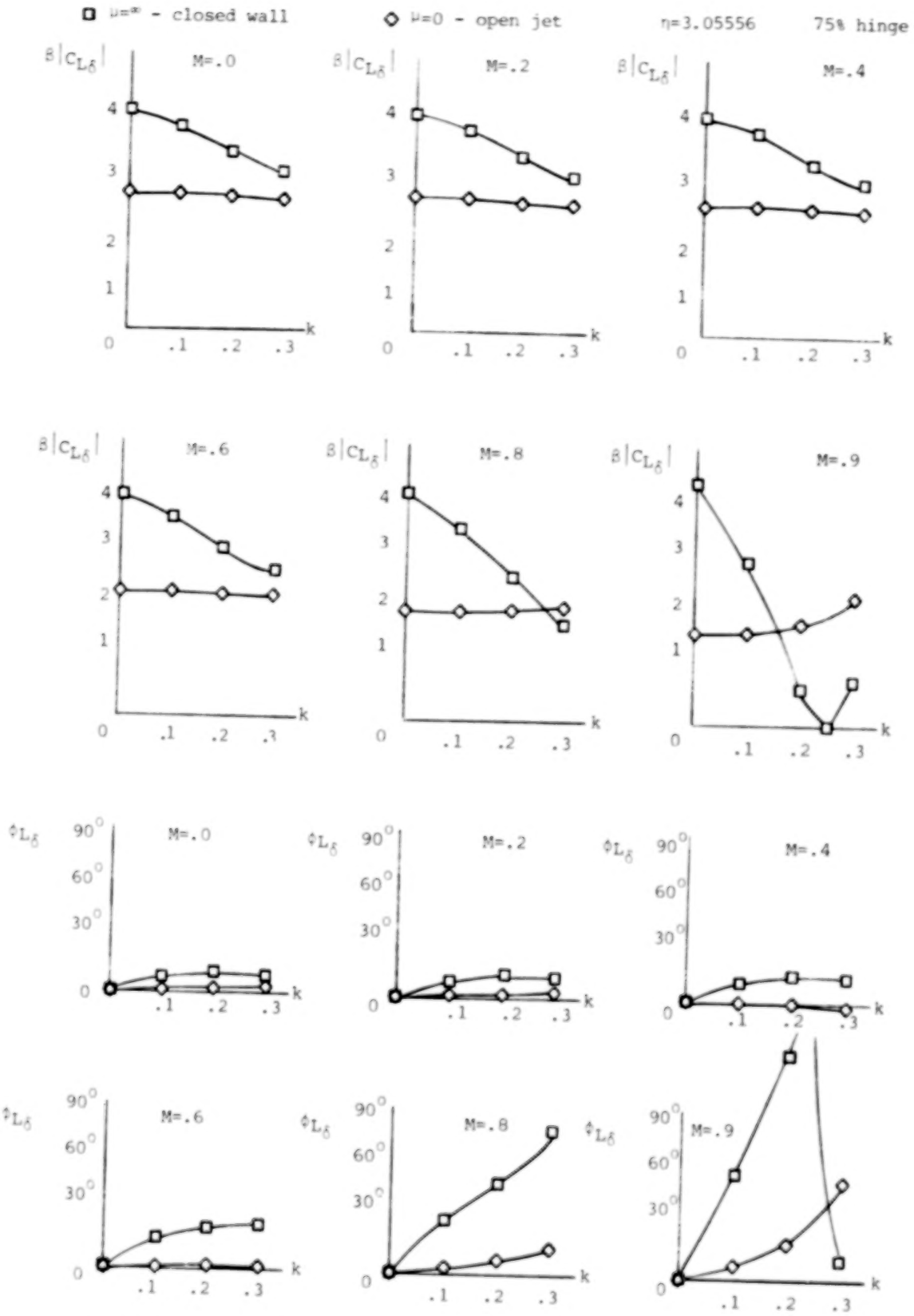

Figure 9. C_{L_δ} vs. M,k and μ for an oscillating flap in a wind tunnel

§15. Conclusions

The numerical calculation of unsteady airloads in ventilated wind tunnels has been extended from our previous work [5] to include airfoils with multiple leading and trailing edge flaps. This has been accomplished with further developments both in the mathematical theory and in the computer program TWODI.

The computational foundation has been strengthened by establishing a more powerful existence and convergence theory for arbitrary downwashes having finite norm. This has led to improved error estimates and to a better understanding of the behavior of collocation for solving integral equations with a leading Cauchy singularity. Using the method of collocation for discontinuous downwash, our theoretical estimates predict errors no better than $0(1/N)$ where N is the number of basis functions. In practice this works out to 1-2% error using collocation alone with the maximum number of basis functions (presently twenty-four). We have shown in this work that such errors can be reduced by several orders of magnitude using Richardson extrapolation; for essentially the same amount of arithmetic, error reduction by factors of 500 have been achieved. Furthermore, the method of extrapolation appears to work equally well for steady and unsteady flow. To demonstrate this technique, we have presented accurate numerical results for an airfoil in a ventilated tunnel with a three quarter chord flap oscillating at high frequencies up to and beyond resonance.

We have also shown that Bland's collocation method can be made much more efficient by identifying the singularities in the kernel and integrating them separately with suitable quadrature rules. In the case of incompressible flow in free air, we have demonstrated with TWODI using five basis functions for continuous downwashes, that six decimal accuracy can be obtained uniformly for steady and unsteady flow with little increase in computer time.

The applicability of TWODI has been extended by incorporating the kernel (4.13) for steady flow in porous wall tunnels. The complete computational solution to this problem is presented for unit downwash, and solutions for other downwashes can be obtained at will.

The practical utility of TWODI has been improved by the incorporation of a completely new input module. The entire program has been coded in ANSI FORTRAN and is available for general use. Complete user instructions and a set of sample problems are provided in this report.

Several areas of future research appear to be particularly promising at the present time. From a practical standpoint, the method of extrapolation should be incorporated into the solution process for airfoils with flaps and preliminary steps should be undertaken toward automatic accuracy control in the future. Additional progress remains to be made through more efficient integration of singularities in the kernel, and in the actual computation of the kernel as well. The entire problem of boundary conditions at ventilated wind tunnel walls remains open to research, and the possibility of using nonlinear integral equation methods for transonic flow is an intriguing one. Also, the study of solution methods other than collocation, both theoretically and computationally, can be expected to be useful in the future.

While a general and fully satisfactory theory of unsteady wind tunnel interference effects does not yet exist, the present work should increase our practical computational capability and we hope it will add to the reliability and precision of aerodynamic testing.

Addendum Added in Proof

Since the writing of this report, the TWODI program has been extended to provide automatic extrapolation and to utilize the improvements arising from the reformulation of the Possio kernel described in section 12. These changes are reflected only in the user instructions and sample input/output found in section 9 and the Appendix.

REFERENCES

[1] H. Garner, E. Rogers, W. Acum and E. Maskell, *Subsonic wind tunnel wall corrections*, NATO Advisory Group for Aeronautical Research and Development, AGARDograph 109, 1966.

[2] B. Goethert, *Transonic wind tunnel testing*, Pergamon Press, London, 1961.

[3] A. Pope and J. Harper: *Low speed wind tunnel testing*, John Wiley and Sons, New York, 1966.

[4] H. Glauert, *Wind tunnel interference on wings, bodies and airscrews*, British Aeronautical Research Council, Reports and Memoranda 1566, 1933.

[5] J. Fromme and M. Golberg, *Unsteady two dimensional airloads acting on oscillating thin airfoils in subsonic ventilated wind tunnels*, NASA CR-2967, 1978.

[6] J. Fromme and M. Golberg, *Numerical solution of a class of integral equations arising in two dimensional aerodynamics*, J. Opt. Theory and Analysis 24(1), 169-206, 1978.

[7] V.V. Ivanov, *The theory of approximate methods and their application to the numerical solution of singular integral equations*, translated from the Russian by A. Ideh, edited by R.S. Anderssen and D. Elliott, Noordhoff International Publishing Company, Amsterdam, 1976.

[8] S.R. Bland, *The two dimensional oscillating airfoil in a wind tunnel in subsonic compressible flow*, Doctoral Thesis, North Carolina State University, Raleigh, N.C., 1968.

[9] S.R. Bland, *The two dimensional oscillating airfoil in a wind tunnel in subsonic flow*, SIAM J. Appl. Math. 18 (4), 830-848, 1970.

[10] S.R. Bland, R.H. Rhyne and H.B. Pierce, *Study of flow-induced vibrations of a plate in narrow channels*, Trans. ASME, Ser. B, 89, 824-830, 1967.

[11] L. Prandtl, *Tragflügeltheorie, Teil 2, Nachrichten der K. Gesellschaft der Wissenschaften zu Göttingen*, 1919. Reprinted in *Vier Abhandlungen zur Hydrodynamik und Aerodynamik* by L. Prandtl and A. Betz, Göttingen, 1927.

[12] E. Kraft, *An integral equation method for boundary interference in perforated-wall wind tunnels at transonic speeds*, Ph.D. Dissertation, University of Tennessee, 1975.

[13] R. Barnwell, *Improvements in the slotted wall boundary condition*, AIAA Ninth Aerodynamic Testing Conference, Arlington, Texas, 1976.

[14] D. Davis and D. Moore, *Analytical study of blockage and lift interference corrections for slotted tunnels obtained by the substitution of an equivalent homogeneous boundary for the discrete slots*, NACA RM L53E07b, 1953.

[15] G. Guderley, *Simplification of the boundary conditions at a wind tunnel wall with longitudinal slots*, WADC TR 53-150, Wright-Patterson Air Force Base, Ohio, 1953.

[16] B. Baldwin, J. Turner and E. Knechtel, *Wall interference in wind tunnels with slotted and porous boundaries at subsonic speeds*, NACA TN 3176, 1954.

[17] C. Chen and J. Mears, *Experimental and theoretical study of mean boundary conditions at perforated and longitudinally slotted wind tunnel walls*, AEDC TR 57-20, Arnold Air Force Station, Tennessee, 1957.

[18] M. Pindzola and C. Lo, *Boundary interference at subsonic speeds in wind tunnels with ventilated walls*, AEDC TR-69-47, Arnold Air Force Station, Tennessee, 1969.

[19] R. Barnwell, *Design and performance evaluation of slotted walls for two-dimensional wind tunnels*, NASA TM 78648, 1978.

[20] H. Darcy, *Les fontaines publique de la ville de Dijon*, V. Dalmont, Paris, 1856.

[21] T. Goodman, *The porous wall wind tunnel. Part II. Interference effect on a cylindrical body in a two dimensional tunnel at subsonic speed*, Report No. AD-594-A-3, Cornell Aeronautic Laboratory, Buffalo, New York, 1950.

[22] L. Woods, *On the theory of two-dimensional wind tunnels with porous walls*, Proc. Roy. Soc. A, 233, 74-90, London, England, 1955.

[23] L. Woods, *On the lifting aerofoil in a wind tunnel with porous walls*, Proc. Roy. Soc. A, 242, 341-364, London, England, 1957.

[24] D. Drake, *The oscillating two dimensional airfoil between porous walls*, The Aeronautical Quarterly, 8, 226-239, London, England, 1957.

[25] D. Drake, *Quasi-steady derivatives for the subsonic flow past an oscillating aerofoil in a porous wind tunnel*, The Aeronautical Quarterly, 8, 211-229, London, England, 1959.

[26] G. Parkinson and A. Lim, *On the use of slotted walls in two dimensional testing of low speed airfoils*, CASI Transactions, 4(2), 81-87, 1971.

[27] M. Ebihara, *A study of subsonic two dimensional wall interference effects in a perforated wind tunnel*, National Aerospace Lab TR-252T, Tokyo, Japan, 1972.

[28] M. Mokry, *Integral equation method for subsonic flow past airfoils in ventilated wind tunnels*, AIAA J., 13(1), 47-53, 1975.

[29] E. Kraft and C. Lo, *Analytical determination of blockage effects in a perforated wall transonic wind tunnel*, AIAA Journal, 15(4), 511-517, 1977.

[30] H. Söhngen, *Die Lösungen der Integralgleichung*

$$g(x) = \frac{1}{2\pi} \int_{-a}^{a} \frac{f(t)}{x-t}\, dt$$

und deren Anwendung in der Tragflügeltheorie, Mathematische Zeitschrift 45, 245-264, 1939.

[31] F. Tricomi, *On the finite Hilbert transformation*, Quart. J. Math., 2(2), 199-211, 1951.

[32] H. Söhngen, *Zur Theorie der endlichen Hilbert-Transformation*, *Mathematische Zeitschrift* 60, 31-51, 1954.

[33] R. Courant and D. Hilbert, *Methods of mathematical physics*, Vol. II, Wiley-Interscience, 1962.

[34] L. Schwartz, *Mathematics for the physical sciences*, Addison-Wesley International series, 1966.

[35] L. Jolley, *Summation of series*, Dover, 1961.

[36] H. Runyan, D. Woolston and A. Rainey, *Theoretical and experimental investigation of the effect of tunnel walls on the forces on an oscillating airfoil in two dimensional subsonic flow*, NACA Report 1262, 1956.

[37] F. Hildebrand, *Introduction to numerical analysis*, McGraw-Hill, 2nd ed., 1974.

[38] A. Stroud and D. Secrest, *Gaussian quadrature formulas*, Prentice Hall, 1966.

[39] I. Gradshteyn and I. Ryzhik, *Table of integrals, series and products*, Academic Press, 1965.

[40] H. Multhopp, *Die Berechnung der Auftriebeverteilung von Tragflügeln*, Luftfahrtforschung 15, 153-169, 1938.

[41] H. Multhopp, *Methods for calculating the lift distribution of wings (subsonic lifting surface theory)*, Great Britain Aeronautical Research Council, Reports and Memoranda No. 2884, 1950.

[42] P. Hsu, *Some recent developments in the flutter analysis of low aspect ratio wings*, Proc. National Specialists Meeting on Dynamics and Aeroelasticity, pp. 7-26, Fort Worth, Texas, 1958.

[43] F. Tricomi, *Integral equations*, Vol. V of Pure and Applied Mathematics, Interscience Publishers, 1957.

[44] G. Szëgo, *Orthogonal polynomials*, Amer. Math Soc. Colloquium Publications, Vol. 23, 4th ed., Providence, R.I., 1975.

[45] H. Ashley, *Engineering analysis of flight vehicles*, Addison-Wesley, 1974.

[46] R. Bowen and C-C. Wang, *Introduction to vectors and tensors*, Vol. I, Plenum Press, 1976.

[47] J. Oden and J. Reddy, *An introduction to the mathematical theory of finite elements*, Wiley Interscience, 1976.

[48] L. Loomis and S. Sternberg, *Advanced calculus*, Addison-Wesley, 1968.

[49] J. Fromme and M. Golberg, *On the L_2 convergence of collocation for the generalized airfoil equation*, accepted for publication in J. Math. Analysis and Applics.

[50] C. Baker, *The numerical treatment of integral equations*, Oxford University Press, 1977.

[51] K. Atkinson, *A survey of numerical methods for the solution of Fredholm integral equations of the second kind*, SIAM, Philadelphia, Pa., 1976.

[52] M. Landahl, *Pressure loading functions for oscillating wings with control surfaces*, J. AIAA, 6(2), 345-348, 1968.

[53] W. Rowe, J. Sebastian and M. Redman, *Some recent developments in predicting unsteady loadings caused by control surface motions*, AIAA Paper 75-101, 1975.

[54] W. Rowe, M. Redman, F. Ehlers and J. Sebastian, *Prediction of unsteady loadings caused by leading and trailing edge control surface motions in subsonic compressible flow--analysis and results*, NASA CR-2543, 1975.

[55] A. Flax, *Reverse flow and variational theorems for lifting surfaces in nonstationary compressible flow*, J. Aero. Sci., 20 (2), 120-126, 1953.

[56] R. Milne, *Application of integral equations for fluid flows in unbounded domains*, Vol. 2 of Finite Elements in Fluids, John Wiley and Sons, 1975.

[57] E. Nissim and I. Lottati, *Oscillatory subsonic piecewise continuous kernel function method*, J. Aircraft 14(6), 515-516, 1977.

[58] J. Fromme and M. Golberg, *Projection methods for the generalized airfoil equation*, SIAM Fall Meeting, Albuquerque, N.M., 1977.

[59] I. Sloan, B. Burn, and N. Datyner, *A new approach to the numerical solution of integral equations*, J. Computational Physics, 18(1), 92-105, 1975.

[60] I. Sloan, *Error analysis for a class of degerate kernel methods*, Numerische Mathematik, 1975.

[61] J. Phillips, *The use of collocation as a projection method for solving linear operator equations*, SIAM J. Num. Analysis, 9, 14-27, 1972.

[62] M. Williams, *The resolvent of singular integral equations*, Quart. J. Appl. Math. 28, 99-110, 1977.

[63] M. Williams, *Exact solutions in thin oscillating airfoil theory*, AIAA J. 15(6), 875-876, 1977.

[64] G. Strang and G. Fix, *An analysis of the finite element method*, Prentice-Hall, 1976.

[65] B. Noble, *The numerical solution of integral equations* in *The state of the art in numerical analysis*, Academic Press, 1976.

[66] M. Abramowitz and I. Stegun, *Handbook of mathematical functions*, National Bureau of Standards A.M.S. 55, U.S. Government Printing Office, 1964.

[67] H. Runyan and C. Watkins, *Considerations on the effect of wind tunnel walls on oscillating air forces for two dimensional subsonic compressible flow*, NACA Report 1150, 1953.

[68] H. Tidjeman and P. Schippers, *Results of pressure measurements on a lifting airfoil with oscillating flap in two dimensional high subsonic and transonic flow*, NLR TR 73018L, The Netherlands, 1974.

APPENDIX

This appendix provides example TIMESHARE input and output for three problems. Responses by the user are underlined for ease of identification.

The first problem is entirely defaulted and produces results which agree to 6 decimals with the exact Söhngen and Küssner-Schwarz solutions [5] (Problem one is listed to display the initial default values.) The second problem is chosen to verify Bland's results [8] for an airfoil oscillating about the 42.5% chord in a closed wall tunnel at M=.85. The second problem is not listed and another problem is not immediately entered. Computer execution then occurs and the printed output follows.

To demonstrate the modification of old problems into new ones, a new problem one is next defined as the old problem two and then edited. The new problem one utilizes five methods of solution. The first method merely demonstrates checking the airfoil polynomials. Methods 2-4, if extrapolated with (11.51), will show that C_{L_δ} of a thin symmetrical airfoil for a flap hinged at the 75% chord in a ventilated wind tunnel with η=550/180, μ=2.0137, and M=.5 is given by

$$C_{L_\delta} = 3.204, \tag{A-1}$$

which matches experimental results [68, Table 4], and is predicted by method 5 using automatic extrapolation.

```
THIS IS TWODI-III
     FOR DEFAULT TO INITIAL OR MOST RECENTLY DEFINED VALUES
TYPE D FOLLOWED BY CARRIAGE RETURN IF IN TIMESHARE AND ENTER
AN OTHERWISE BLANK CARD WITH A D IN COLUMN 1 IF IN BATCH.
IF IN TIMESHARE TYPE HALT TO STOP.


ARE YOU IN TIMESHARE OR BATCH
? D
ENTER NUMBER OF LINES PER PAGE
? D
ENTER TITLE
? D
ENTER OUTPUT COMBINATION OF FOURIER, SECTION AND WORK
? D
ENTER LIST OF PRESSURE POINTS
? D
ENTER LIST OF MACH NUMBERS
? D
ENTER LIST OF FREQUENCIES
? D
ENTER LIST OF HEIGHT TO CHORD RATIOS
? D
ENTER LIST OF MASS EFFECT VENTILATION COEFFICIENTS
? D
ENTER LIST OF VISCOUS EFFECT VENTILATION COEFFICIENTS
? D
ENTER LIST OF NODES
? D
ENTER NUMBER OF MODE SHAPES
? D
ENTER MODE SHAPE  1
? D
ENTER MODE SHAPE  2
? D
ENTER MODE SHAPE  3
? D
ENTER LIST OF NODE NUMBERS OF HINGES
? D
ENTER NUMBER OF METHODS OF SOLUTION
? D
ENTER SOLUTION PARAMETERS FOR METHOD  1
? D
DO YOU WANT THE INPUT DATA LISTED
? YES
```

```
                                SAMPLE PROBLEM

                              TIMESHARE =   T
                           LINES PER PAGE =  66
                                 FOURIER =   T
                                 SECTION =   T
                                    WORK =   F

                             10 PRESSURE POINTS
    -.800000        -.600000        -.400000        -.200000              0
     .200000         .400000         .600000         .800000       1.000000

                              1 MACH NUMBERS
                                      0

                           2 REDUCED FREQUENCIES
                                      0
                                1.000000

                          1 HEIGHT TO CHORD RATIOS
                                INFINITY

                    1 WIND TUNNEL MASS EFFECT VENTILATION COEFFICIENTS
                                INFINITY

                   1 WIND TUNNEL VISCOUS EFFECT VENTILATION COEFFICIENTS
                                      0

                             3 CHORDWISE NODES
   -1.000000                0        1.000000

                              3 MODE SHAPES
  MODE  1
       .564190         .564190         .564190
  MODE  2
      -.564190         .564190        1.692569
  MODE  3
       .564190        -.564190        2.820948

                             0 HINGE LOCATIONS

                            1 METHODS OF SOLUTION
    SOLUTION PARAMETERS FOR METHOD  1
    I1 =  3   I2 =  5   I3 =  0   R1 =           0       R2 =           0
 DO YOU WANT TO MAKE CHANGES
? NO
 DO YOU WANT TO ENTER ANOTHER PROBLEM
? YES
```

```
 TO MODIFY OR RETAIN AN OLD PROBLEM, ENTER ITS NUMBER
 OTHERWISE TYPE D FOLLOWED BY CARRIAGE RETURN
? D
 ENTER TITLE
? VERIFICATION OF RESULTS IN BLAND SIAM J APPL MATH 18(4) 830-848 1970
 ENTER OUTPUT COMBINATION OF FOURIER, SECTION AND WORK
? SECTION
 ENTER LIST OF PRESSURE POINTS
? 0
 ENTER LIST OF MACH NUMBERS
? 1 .85
 ENTER LIST OF FREQUENCIES
? 3 0 .1 .2
 ENTER LIST OF HEIGHT TO CHORD RATIOS
? 1 7.5
 ENTER LIST OF MASS EFFECT VENTILATION COEFFICIENTS
? D
 ENTER LIST OF VISCOUS EFFECT VENTILATION COEFFICIENTS
? D
 ENTER LIST OF NODES
? 2 -1 1
 ENTER NUMBER OF MODE SHAPES
? 1
 ENTER MODE SHAPE  1
? -.85 1.15
 ENTER LIST OF NODE NUMBERS OF HINGES
? D
 ENTER NUMBER OF METHODS OF SOLUTION
? D
 ENTER SOLUTION PARAMETERS FOR METHOD  1
? D
 DO YOU WANT THE INPUT DATA LISTED
? NO
 DO YOU WANT TO MAKE CHANGES
? NO
 DO YOU WANT TO ENTER ANOTHER PROBLEM
? NO
```

SAMPLE PROBLEM

MACH = 0 REDUCED FREQUENCY = 0 FREE AIR
SOLUTION BY COLLOCATION. NUMBER OF BASIS FUNCTIONS = 5

FOURIER COEFFICIENTS OF PRESSURE DUE TO DISPLACEMENT MODE 1

0	0
0	0
0	0
0	0
0	0

AERODYNAMIC NORM OF PRESSURE FUNCTION = 0

FOURIER COEFFICIENTS OF PRESSURE DUE TO DISPLACEMENT MODE 2

2.00000000	0
0	0
0	0
0	0
0	0

AERODYNAMIC NORM OF PRESSURE FUNCTION = 2.00000000

FOURIER COEFFICIENTS OF PRESSURE DUE TO DISPLACEMENT MODE 3

6.00000000	0
4.00000000	0
.00000000	0
.00000000	0
-.00000000	0

AERODYNAMIC NORM OF PRESSURE FUNCTION = 7.21110255

SECTION AIRLOAD COEFFICIENTS

MODE	COEFF	REAL	IMAGINARY	MAGNITUDE	PHASE ANGLE
1	LIFT	0	0	0	0
1	PITCH	0	0	0	0
1	X CP	.25000000	0	.25000000	0
2	LIFT	7.08981540	0	7.08981540	0
2	PITCH	0	0	0	0
2	X CP	.25000000	-0	.25000000	0
3	LIFT	21.26944621	0	21.26944621	0
3	PITCH	-3.54490770	0	3.54490770	-180.00
3	X CP	.58333333	-0	.58333333	0

PRESSURES

MODE	X	X/C	REAL	IMAGINARY	MAGNITUDE	PHASE ANGLE
1	-.80000	.10000	0	0	0	0
1	-.60000	.20000	0	0	0	0
1	-.40000	.30000	0	0	0	0
1	-.20000	.40000	0	0	0	0
1	0	.50000	0	0	0	0
1	.20000	.60000	0	0	0	0
1	.40000	.70000	0	0	0	0
1	.60000	.80000	0	0	0	0
1	.80000	.90000	0	0	0	0
1	1.00000	1.00000	0	0	0	0
2	-.80000	.10000	13.54055	0	13.54055	0
2	-.60000	.20000	9.02703	0	9.02703	0
2	-.40000	.30000	6.89451	0	6.89451	0
2	-.20000	.40000	5.52791	0	5.52791	0
2	0	.50000	4.51352	0	4.51352	0
2	.20000	.60000	3.68527	0	3.68527	0
2	.40000	.70000	2.95479	0	2.95479	0
2	.60000	.80000	2.25676	0	2.25676	0
2	.80000	.90000	1.50451	0	1.50451	0
2	1.00000	1.00000	0	0	0	0
3	-.80000	.10000	24.37299	0	24.37299	0
3	-.60000	.20000	23.47029	0	23.47029	0
3	-.40000	.30000	23.44134	0	23.44134	0
3	-.20000	.40000	23.21721	0	23.21721	0
3	0	.50000	22.56758	0	22.56758	0
3	.20000	.60000	21.37457	0	21.37457	0
3	.40000	.70000	19.50162	0	19.50162	0
3	.60000	.80000	16.70001	0	16.70001	0
3	.80000	.90000	12.33695	0	12.33695	0
3	1.00000	1.00000	0	0	0	0

SAMPLE PROBLEM

MACH = 0 REDUCED FREQUENCY = 1.00000 FREE AIR
SOLUTION BY COLLOCATION. NUMBER OF BASIS FUNCTIONS = 5

FOURIER COEFFICIENTS OF PRESSURE DUE TO DISPLACEMENT MODE 1

-.39972777	.53943896
-.50000591	-.00000177
.00000577	.00000160
-.00000316	-.00000116
.00000112	.00000056

AERODYNAMIC NORM OF PRESSURE FUNCTION = .83712758

FOURIER COEFFICIENTS OF PRESSURE DUE TO DISPLACEMENT MODE 2

.77942828	1.87833520
-.75001865	2.00001662
-.24998218	-.00001614
-.00001090	.00000834
.00000407	-.00000262

AERODYNAMIC NORM OF PRESSURE FUNCTION = 2.95985423

FOURIER COEFFICIENTS OF PRESSURE DUE TO DISPLACEMENT MODE 3

3.43720243	1.47722619
3.75000126	4.00006962
-.41666717	1.99993338
-.16666885	.00003832
.00000178	-.00001229

AERODYNAMIC NORM OF PRESSURE FUNCTION = 6.94699559

SECTION AIRLOAD COEFFICIENTS

MODE	COEFF	REAL	IMAGINARY	MAGNITUDE	PHASE ANGLE
1	LIFT	-1.41699805	1.91226132	2.38004765	-126.54
1	PITCH	.44311870	.00000157	.44311870	-.00
1	X CP	.47168992	.29917627	.55856765	-32.39
2	LIFT	2.76300130	6.65852491	7.20903115	-67.46
2	PITCH	.66468672	-1.77246858	1.89300114	69.44
2	X CP	.63359860	.35878941	.72805424	-29.53
3	LIFT	12.18456537	5.23663048	13.26219937	-23.26
3	PITCH	-3.32335208	-3.54496940	4.85916424	133.15
3	X CP	.92154087	.29326671	.96707959	-17.65

PRESSURES

MODE	X	X/C	REAL	IMAGINARY	MAGNITUDE	PHASE ANGLE
1	-.80000	.10000	-.67518	3.65215	3.71404	-100.47
1	-.60000	.20000	-1.35286	2.43476	2.78537	-119.06
1	-.40000	.30000	-1.72272	1.85957	2.53491	-132.81
1	-.20000	.40000	-1.93404	1.49098	2.44203	-142.37
1	0	.50000	-2.03048	1.21738	2.36746	-149.06
1	.20000	.60000	-2.02641	.99399	2.25706	-153.87
1	.40000	.70000	-1.92022	.79696	2.07904	-157.46
1	.60000	.80000	-1.69227	.60869	1.79841	-160.22
1	.80000	.90000	-1.27863	.40579	1.34148	-162.39
1	1.00000	1.00000	0	0	0	0
2	-.80000	.10000	8.39126	4.59251	9.56580	-28.69
2	-.60000	.20000	5.05245	6.67258	8.36962	-52.87
2	-.40000	.30000	3.16940	7.85409	8.46947	-68.02
2	-.20000	.40000	1.76728	8.50845	8.69005	-78.27
2	0	.50000	.63055	8.75251	8.77520	-85.88
2	.20000	.60000	-.29591	8.62050	8.62558	-91.97
2	.40000	.70000	-1.00550	8.09369	8.15591	-97.08
2	.60000	.80000	-1.44499	7.08436	7.23022	-101.53
2	.80000	.90000	-1.47486	5.32471	5.52519	-105.48
2	1.00000	1.00000	0	0	0	0
3	-.80000	.10000	7.40125	-6.78906	10.04340	42.53
3	-.60000	.20000	12.72149	-3.80348	13.27791	16.65
3	-.40000	.30000	15.68226	-.14707	15.68295	.54
3	-.20000	.40000	17.19512	3.86216	17.62352	-12.66
3	0	.50000	17.53623	7.84745	19.21203	-24.11
3	.20000	.60000	16.82917	11.41936	20.33772	-34.16
3	.40000	.70000	15.13622	14.11989	20.69967	-43.01
3	.60000	.80000	12.46017	15.29776	19.73011	-50.84
3	.80000	.90000	8.62172	13.68896	16.17781	-57.80
3	1.00000	1.00000	0	0	0	0

VERIFICATION OF RESULTS IN BLAND SIAM J APPL MATH 18(4) 830-848 1970

MACH = .85000 REDUCED FREQUENCY = 0 ETA = 7.5000

CLOSED TUNNEL WALL

SOLUTION BY COLLOCATION. NUMBER OF BASIS FUNCTIONS = 5

SECTION AIRLOAD COEFFICIENTS

MODE	COEFF	REAL	IMAGINARY	MAGNITUDE	PHASE ANGLE
1	LIFT	12.23511824	0	12.23511824	0
1	PITCH	-.03818645	0	.03818645	-180.00
1	X CP	.25624211	-0	.25624211	0

VERIFICATION OF RESULTS IN BLAND SIAM J APPL MATH 18(4) 830-848 1970

MACH = .85000 REDUCED FREQUENCY = .10000 ETA = 7.5000

CLOSED TUNNEL WALL

SOLUTION BY COLLOCATION. NUMBER OF BASIS FUNCTIONS = 5

SECTION AIRLOAD COEFFICIENTS

MODE	COEFF	REAL	IMAGINARY	MAGNITUDE	PHASE ANGLE
1	LIFT	5.89895953	-5.39528821	7.99417653	42.45
1	PITCH	-.39062630	-.35268436	.52628430	137.92
1	X CP	.26256375	.13106613	.29345878	-26.53

VERIFICATION OF RESULTS IN BLAND SIAM J APPL MATH 18(4) 830-848 1970

MACH = .85000 REDUCED FREQUENCY = .20000 ETA = 7.5000

CLOSED TUNNEL WALL

SOLUTION BY COLLOCATION. NUMBER OF BASIS FUNCTIONS = 5

SECTION AIRLOAD COEFFICIENTS

MODE	COEFF	REAL	IMAGINARY	MAGNITUDE	PHASE ANGLE
1	LIFT	5.43100764	-.22007538	5.43546476	2.32
1	PITCH	-.01944215	-.78007066	.78031290	91.43
1	X CP	.24552645	.28708426	.37775734	-49.46

```
 DO YOU WANT TO ENTER ANOTHER PROBLEM
? YES
 YOU MAY MODIFY OR RETAIN OLD PROBLEM N AS NEW PROBLEM M
 PROVIDED N IS GREATER THAN OR EQUAL TO M
 TO MODIFY OR RETAIN AN OLD PROBLEM, ENTER ITS NUMBER
 OTHERWISE TYPE 0 FOLLOWED BY CARRIAGE RETURN
? 2
 DO YOU WANT THE INPUT DATA LISTED
? NO
 DO YOU WANT TO MAKE CHANGES
? YES
 DO YOU WANT TO LINE EDIT
? YES
 NOW OPEN FOR LINE EDITING. WHEN DONE TYPE END
? TITLE
 ENTER TITLE
? COMPARISON WITH TIJDEMAN & SCHIPPERS NLR TR 73018L 1974
? MACH
 ENTER LIST OF MACH NUMBERS
? 1 .5
? FREQUENCY
 ENTER LIST OF FREQUENCIES
? 1 0
? HEIGHT
 ENTER LIST OF HEIGHT TO CHORD RATIOS
? 1 3.0555556
? MASS
 ENTER LIST OF MASS EFFECT VENTILATION COEFFICIENTS
? 1 2.0137
? NODES
 ENTER LIST OF NODES
? 3 -1 .5 1
? MODE
 ENTER NUMBER OF MODE SHAPES
? 1
 ENTER MODE SHAPE  1
? 0 0 .5
? HINGE
 ENTER LIST OF NODE NUMBERS OF HINGES
? 1 2
? METHOD
 ENTER NUMBER OF METHODS OF SOLUTION
? 5
 ENTER SOLUTION PARAMETERS FOR METHOD  1
? 1 9 0 0 0
 ENTER SOLUTION PARAMETERS FOR METHOD  2
? 3 3 0 0 0
 ENTER SOLUTION PARAMETERS FOR METHOD  3
? 3 6 0 0 0
 ENTER SOLUTION PARAMETERS FOR METHOD  4
? 3 12 0 0 0
 ENTER SOLUTION PARAMETERS FOR METHOD  5
? 3 3 2 0 0
? END
 DO YOU WANT THE INPUT DATA LISTED
? YES
```

```
COMPARISON WITH TIJDEMAN & SCHIPPERS NLR TR 73018L 1974

                    TIMESHARE =   T
                LINES PER PAGE =  66
                      FOURIER =   F
                      SECTION =   T
                         WORK =   F

                  0 PRESSURE POINTS

                    1 MACH NUMBERS
                       .500000

                1 REDUCED FREQUENCIES
                             0

              1 HEIGHT TO CHORD RATIOS
                       3.055556

        1 WIND TUNNEL MASS EFFECT VENTILATION COEFFICIENTS
                       2.013700

      1 WIND TUNNEL VISCOUS EFFECT VENTILATION COEFFICIENTS
                             0

                    3 CHORDWISE NODES
   -1.000000          .500000          1.000000

                    1 MODE SHAPES
 MODE  1
            0                0          .500000

                    1 HINGE LOCATIONS
                             2

                  5 METHODS OF SOLUTION
   SOLUTION PARAMETERS FOR METHOD  1
   I1 =  1   I2 =  9   I3 =  0   R1 =          0       R2 =          0
   SOLUTION PARAMETERS FOR METHOD  2
   I1 =  3   I2 =  3   I3 =  0   R1 =          0       R2 =          0
   SOLUTION PARAMETERS FOR METHOD  3
   I1 =  3   I2 =  6   I3 =  0   R1 =          0       R2 =          0
   SOLUTION PARAMETERS FOR METHOD  4
   I1 =  3   I2 = 12   I3 =  0   R1 =          0       R2 =          0
   SOLUTION PARAMETERS FOR METHOD  5
   I1 =  3   I2 =  3   I3 =  2   R1 =          0       R2 =          0
 DO YOU WANT TO MAKE CHANGES
? NO
 DO YOU WANT TO ENTER ANOTHER PROBLEM
? NO
```

```
****COMPUTATIONAL CHECK OF MAJOR SUBROUTINES****
9.1  CHECKING AFP.  CORRECT VALUES, THEN CURRENTLY COMPUTED VALUES.
     .2482434168     .5941373295     -.6544599169     .5508566527
     .2482434168     .5941373295     -.6544599169     .5508566527

        COMPARISON WITH TIJDEMAN & SCHIPPERS NLR TR 73018L 1974

 MACH =   .50000      REDUCED FREQUENCY =        0      ETA =    3.0556
       MASS EFFECT (SLOTTED WALL) VENTILATION COEFFICIENT =    2.0137
     VISCOUS EFFECT (POROUS WALL) VENTILATION COEFFICIENT =         0
          SOLUTION BY COLLOCATION.  NUMBER OF BASIS FUNCTIONS =  3

                        SECTION AIRLOAD COEFFICIENTS
   MODE     COEFF          REAL    IMAGINARY   MAGNITUDE   PHASE ANGLE
      1      LIFT     2.86621003            0 2.86621003             0
      1     PITCH     -.77670622            0  .77670622       -180.00
      1      X CP      .79197439           -0  .79197439             0

        COMPARISON WITH TIJDEMAN & SCHIPPERS NLR TR 73018L 1974

 MACH =   .50000      REDUCED FREQUENCY =        0      ETA =    3.0556
       MASS EFFECT (SLOTTED WALL) VENTILATION COEFFICIENT =    2.0137
     VISCOUS EFFECT (POROUS WALL) VENTILATION COEFFICIENT =         0
          SOLUTION BY COLLOCATION.  NUMBER OF BASIS FUNCTIONS =  6

                        SECTION AIRLOAD COEFFICIENTS
   MODE     COEFF          REAL    IMAGINARY   MAGNITUDE   PHASE ANGLE
      1      LIFT     3.01589975            0 3.01589975             0
      1     PITCH     -.74651846            0  .74651846       -180.00
      1      X CP      .74505522           -0  .74505522             0

        COMPARISON WITH TIJDEMAN & SCHIPPERS NLR TR 73018L 1974

 MACH =   .50000      REDUCED FREQUENCY =        0      ETA =    3.0556
       MASS EFFECT (SLOTTED WALL) VENTILATION COEFFICIENT =    2.0137
     VISCOUS EFFECT (POROUS WALL) VENTILATION COEFFICIENT =         0
          SOLUTION BY COLLOCATION.  NUMBER OF BASIS FUNCTIONS = 12

                        SECTION AIRLOAD COEFFICIENTS
   MODE     COEFF          REAL    IMAGINARY   MAGNITUDE   PHASE ANGLE
      1      LIFT     3.10514470            0 3.10514470             0
      1     PITCH     -.73830865            0  .73830865       -180.00
      1      X CP      .72553897           -0  .72553897             0

        COMPARISON WITH TIJDEMAN & SCHIPPERS NLR TR 73018L 1974

 MACH =   .50000      REDUCED FREQUENCY =        0      ETA =    3.0556
       MASS EFFECT (SLOTTED WALL) VENTILATION COEFFICIENT =    2.0137
     VISCOUS EFFECT (POROUS WALL) VENTILATION COEFFICIENT =         0
          SOLUTION BY EXTRAPOLATION.  ORDER = 2  PERIOD =  3

                        SECTION AIRLOAD COEFFICIENTS
   MODE     COEFF          REAL    IMAGINARY   MAGNITUDE   PHASE ANGLE
      1      LIFT     3.20398970            0 3.20398970             0
      1     PITCH     -.73468821            0  .73468821       -180.00
      1      X CP      .70860835           -0  .70860835             0
 DO YOU WANT TO ENTER ANOTHER PROBLEM
? NO
```

1. Report No.	2. Government Accession No.	3. Recipient's Catalog No.
NASA CR -3210		

4. Title and Subtitle	5. Report Date
TWO DIMENSIONAL AERODYNAMIC INTERFERENCE EFFECTS ON OSCILLATING AIRFOILS WITH FLAPS IN VENTILATED SUBSONIC WIND TUNNELS	December 1979
	6. Performing Organization Code
7. Author(s) Joseph Fromme, Michael Golberg, and John Werth	8. Performing Organization Report No.
	10. Work Unit No. 505-06-31
9. Performing Organization Name and Address University of Nevada Las Vegas, Nevada 89154	11. Contract or Grant No. NSG 2140
	13. Type of Report and Period Covered Contractor Report
12. Sponsoring Agency Name and Address National Aeronautics and Space Administration Washington, D. C. 20546	14. Sponsoring Agency Code

15. Supplementary Notes

16. Abstract

The numerical computation of unsteady airloads acting upon thin airfoils with multiple leading and trailing-edge controls in two-dimensional ventilated subsonic wind tunnels is studied. The foundation of the computational method is strengthened with a new and more powerful mathematical existence and convergence theory for solving Cauchy singular integral equations of the first kind, and the method of convergence acceleration by extrapolation to the limit is introduced to analyze airfoils with flaps. New results are presented for steady and unsteady flow, including the effect of acoustic resonance between ventilated wind-tunnel walls and airfoils with oscillating flaps. The computer program TWODI is available for general use and a complete set of instructions is provided.

17. Key Words (Suggested by Author(s))	18. Distribution Statement
Unsteady aerodynamics, aeroelasticity Ventilated wind tunnels Subsonic flow, structural dynamics Two-dimensional aerodynamics Integral equations Computational fluid mechanics	Unlimited STAR Category - 02

19. Security Classif. (of this report)	20. Security Classif. (of this page)	21. No. of Pages	22. Price*
Unclassified	Unclassified	149	$7.25

*For sale by the National Technical Information Service, Springfield, Virginia 22161

NASA-Langley, 1979

90 %

50 %

END

6-11-81